Study of Impedance Matching in Antenna Arrays

Irfan Ali Tunio

UNIVERSITE BRETAGNE LOIRE / MATHSTIC

UNIVERSITÉ DE NANTES

THESE DE DOCTORAT DE

L'UNIVERSITE DE NANTES

COMUE UNIVERSITE BRETAGNE LOIRE

ECOLE DOCTORALE N° 601
Mathématiques et Sciences et Technologies de l'Information et de la Communication
Spécialité : Sciences de l'Information et de la Communication

Par
Irfan Ali TUNIO

Study of Impedance Matching in Antenna Arrays

Thèse présentée et soutenue à NANTES, le 10 décembre 2020
Unité de recherche : IETR UMR CNRS 6164

Rapporteurs avant soutenance :

Thierry MONEDIERE	Professeur des universités, Université de Limoges
Fabien NDAGIJIMANA	Professeur des universités, Université de Grenoble Alpes

Composition du Jury :

Présidente :	Claire MIGLIACCIO	Professeur des universités, Université Côte d'Azur
Examinateurs :	Thierry MONEDIERE	Professeur des universités, Université de Limoges
	Fabien NDAGIJIMANA	Professeur des universités, Université de Grenoble Alpes
Directeur de thèse :	Tchanguiz RAZBAN	Professeur des universités, Université de Nantes
Co-encadrants :	Bruno FROPPIER	Maître de Conférences, Université de Nantes
	Yann MAHE	Maître de Conférences, Université de Nantes

Résumé

1. Introduction

Pour concevoir une antenne réseau dédiée à un équipement spécifique, il est nécessaire d'en spécifier la technologie, le réseau de distribution ainsi que l'antenne élémentaire qui le composera entre autres choses. Ces éléments de base ne s'avèrent pas suffisants et il est bien souvent nécessaire de bien comprendre la manière dont les champs sont rayonnés par le réseau. C'est alors un point critique pour estimer les effets sous-jacents sur les performances globales de l'antenne telle que l'impédance d'entrée, le diagramme de rayonnement ou encore le gain. L'un des principaux problèmes dans la conception d'an réseau d'antennes est alors la modification de l'impédance d'entrée de chaque antenne élémentaire qui compose le réseau lorsqu'elles sont excitées simultanément. La cause de cette désadaptation de l'impédance d'entrée est liée à plusieurs facteurs tels que les ondes de surfaces, le rayonnement en champ proche ou en champ lointain. Dans ce travail, nous allons particulièrement nous intéresser à la contribution du champ lointain et ses conséquences sur l'impédance d'entrée des antennes élémentaires agencées en réseau.

Il existe deux manières pour évaluer l'impédance d'entrée des antennes : 1) la première est basée sur le calcul de la puissance rayonnée en champ lointain pour une distribution de courant donnée et 2) la seconde par l'utilisation de la matrice de répartition dîtes active. Par exemple, le formalisme le plus simple consiste en le produit de la contribution d'un élément seul avec le facteur de réseau du réseau d'antennes ainsi formé. De nombreux autres formalismes ont aussi été proposés afin de tenir compte du comportement de chaque antenne élémentaire dans le réseau. Malheureusement, dans tous ces formalismes, la matrice de répartition est évaluée dans une approche passive. En d'autres termes, dans le cas d'un réseau d'antennes, les coefficients de la matrice sont évalués en imposant un seul port actif (le reste des accès est alors éteint). Cette situation ne correspond alors pas à la réalité d'un réseau en situation de fonctionnement. D'un point de vue pratique, cela signifie que l'évaluation passive de la matrice de répartition n'est pas rigoureusement juste dans ce contexte. Une analyse des paramètres actifs est alors requise pour caractériser convenablement un tel système.

De plus, dans un réseau d'antennes, il est établi que le couplage inter source est à l'origine de la dégradation des performances globales de l'antenne en impédance d'entrée et rayonnement. Ce phénomène est bien décrit dans la littérature. Cependant, lorsque le réseau est utilisé en condition de fonctionnement opérationnel, les dégradations observées se révèlent plus importantes. C'est pourquoi, dans ce travail, nous souhaitons étudier la contribution du rayonnement champ lointain sur les performances d'un réseau d'antennes en l'absence des autres contributeurs tels que le couplage champ proche et par onde de surface.

2. Analyse théorique

Un modèle théorique a été développé sous Matlab© afin d'évaluer la contribution du champ lointain seul sur l'impédance d'entrée de chaque élément d'un réseau d'antennes. Dans ce modèle, seuls le diagramme de rayonnement de chaque antenne et le facteur de

réseau sont pris en compte. Le couplage mutuel entre les différents éléments, les rayonnements parasites liés à la diffraction aux bords de la structure sont alors supposés négligeables. Le but de cette approche est d'isoler la contribution du rayonnement champ lointain et de vérifier si c'est un contributeur important dans la perte de performance et notamment la désadaptation d'impédance observée.

Dans ce travail, nous avons envisagé trois types d'antennes élémentaires : le dipôle court, le dipôle demi-onde et l'antenne patch. Ces différentes antennes sont alors évaluées seules puis mises en réseau (même taille et distance inter source constante). Nous avons arbitrairement retenue la fréquence de 5GHz afin de répondre aux contraintes matérielles de fabrication et de mesures du laboratoire. La distance inter-élément est choisie d'une demie longueur d'onde dans l'air. Le code Matlab© calcule, dans un premier temps, l'impédance d'entrée de chaque antenne par une approche champ lointain. Les résultats obtenus sont alors confrontés aux formules analytiques de la littérature. Ce premier travail a permis de valider l'approche champ lointain puisque les résultats obtenus sont convergents. Après cette étape, ces différentes antennes canoniques sont disposées en réseaux linéaires et planaires i.e. selon les axes x et y et suivant le plan xy.

Pour ces différentes mises en réseau, le rayonnement en champ lointain est alors évalué par le produit du rayonnement élémentaire de chaque antenne et du facteur de réseau. Enfin, une boucle est exécutée afin de déterminer les impédances individuelles de chaque source pour chaque configuration réseau retenue. Dans cette étude, nous avons fixé les courants d'excitation à 1 Ampère dans le cas des antennes dipôles (court et demi-onde). Dans le cas de l'antenne patch, la tension aux extrémités rayonnantes est considérée égale à 1 Volt.

Dans le cas du dipôle court, la mise en réseau linéaire de 2, 4, 8, 16 et 64 antennes élémentaires est évaluée et comparée avec le cas de l'antenne seule isolée. L'impédance d'entrée de chaque antenne observée pour chacune des configurations vaut respectivement 8.19Ω, 8.43Ω, 8.60Ω, 8.71Ω, 8.81Ω alors que l'antenne seule présente une impédance de 7.89Ω. Dans ce cas, l'impédance d'entrée augmente linéairement mais cette croissance reste modérée et ne peut pas être considérée comme significative. Dans le cas du réseau à deux dimensions, i.e. suivant le plan xy, la croissance est beaucoup plus importante. Pour des réseaux 2×2, 4×4 et 8×8, les impédances calculées valent alors respectivement 9.04Ω, 12.71Ω et 18.45Ω, soit plus du double de l'antenne seule pour la configuration la moins favorable.

La même procédure est appliquée au cas du dipôle demi-onde. Dans le cas de la mise en réseau linéaire de 2, 4, 8, 16 et 64 éléments, l'impédance d'entrée de chaque dipôle est alors respectivement 77.14Ω, 80.47Ω, 82.88Ω, 84.46Ω et 85.86Ω alors qu'il n'était que de 73.13Ω pour le dipôle seul. La variation d'impédance observée pour le réseau linéaire est donc manifeste. Elle devient même critique lors de la mise en réseau suivant les deux axes. En effet, pour des réseaux 2×2, 4×4 et 8×8, l'impédance d'entrée calculée pour chaque antenne est respectivement 86.01Ω, 124.1Ω et 183.12Ω.

Enfin, nous avons traité le cas de l'antenne patch rectangulaire. Le modèle retenu est alors le modèle de la cavité rayonnante. L'antenne est alors modélisée par la mise en réseau de deux fentes rayonnantes séparées l'une de l'autre d'une demie longueur d'onde guidée. Dans un premier temps, une antenne patch est optimisée seule et les résultats obtenus par l'approche rayonnement champ lointain sont comparés avec celle des équations de pertes par rayonnement. L'impédance d'entrée Z_{in}, au niveau d'une fente

rayonnante, est alors de 160.36Ω et 160.91Ω respectivement. L'erreur constatée entre les deux approches est suffisamment faible et permet de valider le modèle champ lointain.

Cette antenne patch élémentaire est alors mise en réseau linéaire de 2, 4, 8, 16 et 64 éléments suivant le plan E. L'approche champ lointain est ainsi utilisée pour calculer l'impédance d'entrée de chaque antenne et les résultats obtenus sont consignés dans le tableau 1.

Nombre d'antennes	**Impédance d'entrée au niveau d'une fente rayonnante pour un réseau suivant le plan E**	**Impédance d'entrée observée au niveau du point 50Ω identifié pour le patch seul**
1×1	160.36 Ω	50.00 Ω
2×1	117.45 Ω	30.31 Ω
4×1	100.14 Ω	28.49 Ω
8×1	91.31 Ω	23.57 Ω
16×1	86.62 Ω	22.01 Ω
64×1	82.64 Ω	21.24 Ω

Tableau 1: Impédance d'entrée d'une antenne patch mise en réseau linéaire suivant le plan E.

L'analyse de ces résultats montre que l'impédance d'entrée diminue fortement en fonction du nombre d'antennes placées dans le réseau comme montré dans les deux dernières colonnes du tableau 1. Bien évidemment, nous sommes conscients que l'approche champ total rayonné en champ lointain n'est pas suffisante pour évaluer convenablement la variation d'impédance observée lors de la mise en réseau de plusieurs antennes. Néanmoins, elle a permis de montrer et de quantifier sur quelques exemples la nécessité de considérer le rayonnement champ lointain sur l'adaptation du réseau.

3. Simulations 3D et mesures

Afin de valider la modélisation Matlab au travers de simulation 3D et de mesures, nous devons prendre en considération les points clés suivants :

- L'analyse au paramètres S lorsque toutes les antennes du réseau sont excitées de manière cohérente simultanément (concept de l'influence du rayonnement champ lointain)
- Les facteurs environnementaux du réseau (couplage mutuel, effets de bords)

Les logiciels de simulation électromagnétique tels que CST MWS© ou Ansys HFSS© évaluent la matrice de répartition aux accès des antennes élémentaires en exploitant la matrice passive de répartition. Cette approche n'est malheureusement pas suffisante pour notre étude. Même l'option paramètres S actifs de la nouvelle version de HFSS© ne répond pas à ce problème puisque, là encore c'est la matrice de répartition passive qui est utilisée. En effet, il est convenu que les paramètres de la matrice de répartition active sont exprimés à partir des paramètres passifs comme le montre l'équation (1)

$$Active\_S_{mn} = \frac{\sum_{i=1}^{N} S_{mi} a_i}{a_n} \quad (1)$$

Où S_{mi} sont les coefficients de couplage passif entre les antennes élémentaires *i* et *m*, a_i et a_n sont les excitations complexes des antennes élémentaires *i* et *n* respectivement et *N* représente le nombre total d'antennes qui composent le réseau.

Bien évidemment, dans un mode de fonctionnement normal du réseau, tous les éléments de ce réseau interagissent les uns avec les autres simultanément. Ce phénomène n'est donc pas correctement pris en compte en ne considérant que les paramètres de la matrice passive. Malgré tout, l'expression de l'équation (1) est largement acceptée dans la communauté mais elle n'est pas rigoureusement juste lorsque tous les éléments du réseau rayonnent de manière concurrente. En d'autres termes, l'équation (1) ne prend en considération que les interactions de premier ordre et néglige ceux des ordres supérieurs. Par conséquent, les paramètres actifs de la matrice de répartition du réseau vont présenter de valeurs différentes de ceux donnés par l'équation (1).

Puisque le modèle que nous avons implémenté sous Matlab© n'intègre pas les effets des couplages mutuels, nous allons chercher à valider le concept pour des réseaux d'antennes présentant des niveaux de couplages relativement faible. Or, une première simulation électromagnétique, portant sur un réseau de dipôles demi-onde espacés les uns des autres d'une demie longueur d'onde dans l'air, a montré un couplage relativement important ($S_{12} = -13.52dB$). Ce type de réseau n'est donc pas approprié à ce que nous souhaitons démontrer. Nous nous sommes donc reportés sur un réseau d'antennes patch rectangulaires.

Une antenne patch optimisée pour fonctionner à une fréquence de $5GHz$ est alors disposée en réseau linéaire suivant son plan E. Un coefficient de couplage de $-20.43dB$ est alors observé. Ce niveau de couplage est alors suffisamment faible pour pouvoir être négligé. Un réseau de 4 antennes patch est alors simulé et sa matrice de répartition analysée. Les résultats obtenus nous ont alors permis la réalisation de ce réseau de 4 antennes distribuées linéairement suivant le plan E. Le problème est alors d'être dans la capacité de mesurer le coefficient de réflexion aux accès des différentes antennes en garantissant l'excitation cohérente et simultanée des autres. Nous avons alors mis en œuvre une procédure exploitant les capacités d'excitation synchrone d'un analyseur de réseau 4 ports VNA Rhodes & Schwartz ZVA 24 afin de mesurer les paramètres actifs vrais du réseau. Ce protocole de mesure est ainsi détaillé en termes de calibration et de mise en œuvre. Il est à noter que ce nouveau protocole de mesure a permis de limiter les incertitudes liées à l'utilisation de coupleurs à directivité finie et de diviseurs de puissance.

Fondamentalement, un diviseur de puissance équilibré permet l'excitation cohérente des antennes. Une mesure préalable de chacun des coefficients d'émission de ce diviseur de puissance et des câbles coaxiaux associés permet de valider l'équilibre des amplitudes et des phases aux accès des antennes. Cette mesure garantit également la compensation de l'amplitude et de la phase relative au niveau de l'antenne à mesurer en contrôlant les paramètres de la source associée à ce port (précision de 0,1 dB en amplitude et 1° en phase).

Une antenne patch optimisée pour fonctionner à une fréquence de $5GHz$ est alors disposée en réseau linéaire suivant sont plan E. Un coefficient de couplage de $-20.43dB$ est alors observé. Ce niveau de couplage est alors suffisamment faible pour pouvoir être négligé. Un réseau de 4 antennes patch est alors simulé et sa matrice de répartition analysée. Les résultats obtenus nous ont alors permis la réalisation de ce réseau de 4 antennes distribuées linéairement suivant le plan E. Le problème est alors d'être dans la

capacité de mesurer le coefficient de réflexion aux accès des différentes antennes en garantissant l'excitation cohérente et simultanée des autres. Nous avons alors mis en œuvre une procédure exploitant les capacités d'excitation synchrone d'un analyseur de réseau 4 ports VNA Rhodes & Schwartz ZVA 24 afin de mesurer les paramètres actifs vrais du réseau. Ce protocole de mesure est ainsi détaillé en termes de calibration et de mise en œuvre. Il est à noter que ce nouveau protocole de mesure a permis de limiter les incertitudes liées à l'utilisation de coupleurs à directivité finie et de diviseurs de puissance.

Fondamentalement, un diviseur de puissance équilibré permet l'excitation cohérente des antennes. Une mesure préalable de chacun des coefficients d'émission de ce diviseur de puissance et des câbles coaxiaux associés permet de valider l'équilibre des amplitudes et des phases aux accès des antennes. Cette mesure garantit également la compensation de l'amplitude et de la phase relative au niveau de l'antenne à mesurer en contrôlant les paramètres de la source associée à ce port (précision de 0,1 dB en amplitude et 1° en phase).

Les mesures sont alors réalisées en deux grandes étapes :

Etape 1 : Chaque antenne est alimentée individuellement par un port de l'analyseur dont la puissance de la source est fixée à 0dBm soit 1mW. Les coefficients de réflexion mesurés à chacun des accès sont alors consignés dans le tableau 2 colonne A. Un comportement symétrique est observé et les impédances d'entrée de toutes les antennes restent très proches de 50Ω à la fréquence de résonance retenue. A cause des tolérances de fabrication, nous observons un léger décalage de la fréquence de résonance (5,07 GHz au lieu de 5GHz). Ce décalage en fréquence reste tout à fait modéré et n'a aucun impact sur l'analyse. Dans le tableau 2 colonne B, les impédances d'entrée actives évaluées par l'équation (1) sont données. Il est à noter que ces impédances d'entrée ont tendance à décroître comparativement à celle mesurée sur les antennes individuellement.

Etape 2 : Les quatre antennes élémentaires sont alimentées simultanément en exploitant le mode cohérent de l'analyseur de réseau. Le premier port de l'analyseur est alors connecté à une antenne seule et le second aux trois autres antennes via un diviseur de puissance équilibré. Les mesures obtenues pour chacune des antennes sont données dans la colonne C du tableau 2.

Impédance d'entrée en Ω @ 5.07GHz	**A) Une seule antenne est alimentée**	**B) Impédance d'entrée active évaluée par (1)**	**C) Toutes les antennes sont alimentées simultanément**
Antenne 1	(46.3-j0.6) Ω	(43.55-j7.41) Ω	(44.85-j9.35) Ω
Antenne 2	(52.2-j1.15) Ω	(45.05-j15.42) Ω	(47.1-j17.7) Ω
Antenne 3	(52.25-j0.4) Ω	(45.25-j13.05) Ω	(46.15-j14.1) Ω
Antenne 4	(49.15-j0.5) Ω	(45.6-j6.31) Ω	(46.7-j8.22) Ω

Tableau 2: Impédances d'entrée de quatre antennes patch mises en réseau évaluée en mesure.

D'après le tableau 2 colonne B, un couplage inter élément de l'ordre de -20dB montre une influence non négligeable dans la mesure où l'impédance d'entrée évaluée par l'équation (1) (colonne B) montre une diminution par rapport aux mesures sur l'antenne seule. La colonne C, quant à elle, montre les impédances d'entrée vraies en situation de fonctionnement normal du réseau. Ces résultats prennent en compte non seulement les effets de couplages mais aussi la contribution en champ lointain. Par conséquent, afin de comparer les résultats de manière objective avec le modèle développé dans la première

partie, il est nécessaire de minimiser les coefficients de couplage à des niveaux tels qu'ils n'ont plus d'effets significatifs sur les impédances d'entrée des antennes (via une évaluation par l'équation (1)). En d'autres termes les impédances d'entrée des colonnes A et B doivent présentées les mêmes valeurs. Les valeurs obtenues en colonne C pourront alors être comparée avec le modèle théorique implémenté.

Dans ce contexte de réduction de couplage, une nouvelle structure DGS (Defected Ground Structure) en forme de μ est introduite. Cette dernière a permis une réduction faible bande du coefficient de couplage (S_{12}) jusqu'à $-33dB$ pour un réseau de deux antennes suivant le plan E. Avec cette méthode la bande de réjection est très faible et la structure reste très sensible aux tolérances de fabrication. Il est alors important de proposer une nouvelle structure plus large bande et moins sensibles aux contraintes de réalisation. Un objectif de $-35dB$ sur la bande est alors envisagé.

Dans le contexte de la réduction du couplage mutuel avec des caractéristiques de rejet à large bande, il a été démontré qu'une antenne patch chargée par des vias surpasse une antenne patch classique en termes de suppression des ondes de surface et de rayonnement dans les directions horizontales. Elle présente par ailleurs une meilleure directivité. De plus lorsque ces vias sont mis en réseau, ils permettent de réduire de 4 à $5\ dB$ (par simulation) le couplage inter éléments comparativement aux réseaux d'antennes patch classiques. Pour réduire encore le couplage, cette technique est associée par l'ajout de murs électriques érigés entre les antennes. Le but est alors de minimiser le couplage champ proche dans l'air. La combinaison de ces deux techniques a montré une réduction de 15 et $19\ dB$ (par la mesure) dans le plan E et dans le plan H respectivement. Il a été aussi montré que, au-delà de la réduction du couplage, la bande de réjection est significativement élargie pour les deux configurations de réseau (suivant les plans E et H).

Un réseau linéaire (suivant le plan E) de 4 antennes patch chargées par des vias avec les murs électriques est alors fabriqué. Un couplage de l'ordre de $-37dB$ est observé entre les antennes 2 et 3. Les impédances dénormalisées des 4 antennes sont alors données dans le tableau 3. A cause des tolérances de fabrications, la fréquence de résonance des antennes est décalée autour de $5.56GHz$. Cet écart n'est cependant pas préjudiciable pour l'analyse.

Impédance d'entrée en Ω @ 5.56GHz	**A) Une seule antenne est alimentée**	**B) Impédance d'entrée active évaluée par (1)**	**C) Toutes les antennes sont alimentées simultanément**
Antenna 1	(49.2+j16.9) Ω	(49.05+j14.75) Ω	(46.5+j19.35) Ω
Antenna 2	(47.8+j11.4) Ω	(48.15+j8.95) Ω	(44.6+j14.17) Ω
Antenna 3	(47.8+j11.4) Ω	(48.15+j8.95) Ω	(44.6+j14.18) Ω
Antenna 4	(44.7+j1.1) Ω	(44.96+j0.4) Ω	(41.7+j5.23) Ω

Tableau 3: Impédance d'entrée de quatre antennes patch chargée par des via avec inclusion de murs électriques mises en réseau évaluée en mesure.

Dans le tableau 3, il est observé que les impédances données dans les colonnes A et B sont très proches. Ce résultat confirme qu'un couplage inférieur à -35dB n'impacte pas l'impédance d'entrée active lorsqu'elle est évaluée par l'équation (1). Par contre, les mesures réalisées en exploitant le mode cohérent de l'analyseur (colonne C), où toutes les antennes rayonnent simultanément, montrent une diminution des impédances actives vraies des antennes qui composent le réseau malgré un coefficient de couplage entre les sources très faibles.

4. Conclusion

Nous pouvons déduire, de la discussion ci-dessus, qu'en dépit d'un couplage négligeable, l'effet du rayonnement champ lointain ne peut être ignoré. Nous observons dans le tableau 3 (colonne C) que lorsque tous les éléments rayonnent simultanément, l'impédance d'entrée des antennes diminue par rapport à celles présentées séparément. Ce changement d'impédance n'est pas aussi important que celui du modèle proposé. Il est tout de même suffisamment significatif et doit être pris en compte lors de la conception de réseaux d'antennes notamment de grandes dimensions.

Ces résultats valident donc l'hypothèse selon laquelle les impédances d'entrée des antennes élémentaires d'un réseau sont affectées par le rayonnement champ lointain du réseau (lié aux recombinaisons constructives et destructives des champs rayonnés). Afin de consolider ces derniers résultats, il est nécessaire de prévoir la modélisation des antennes patch chargées par des vias. Par une approche champs lointain combinée à un modèle circuit permettant de ramener l'impédance d'entrée au niveau du point d'excitation de ces antennes, il sera alors possible de confirmer la diminution de l'impédance d'entrée observée pour un réseau de 4 antennes et de l'étendre par la suite à des configurations plus complexes.

Acknowledgements

During the course of PhD I met a lot of people and experienced a lot of events, inside and outside the campus, which I will always cherish for the rest of my life. Here I feel urge to mention few people who played a key role for my journey to have this prestigious title of PhD to my career.

First of all I would like to thank my thesis supervisor, Tchanguiz RAZBAN, for his exceptional support, time and friendly attitude. I am also highly grateful to my co-supervisor, Yann MAHÉ, who not only mentored me academically but whenever I found myself lost in the worries of life outside the university, he appeared to help me out. I have learned a lot from his mentorship and empathy. I would also like to thank to my other co-supervisor, Bruno FROPPIER, for his support throughout my work. I must say, I would have lost in the early days of my PhD if I would not have had the professional instructions and warm encouragement from them.

I would like to appreciate and extend thanks to CSI committee members, Julien SARRAZIN and Cédric QUENDO, for their valuable comments and thoughtful discussions throughout the years. I am also indebted to Claire MIGLIACCIO, Thierry MONEDIERE and Fabien NDAGIJIMANA for being members of my Jury.

I'm sincerely grateful to all other teachers and staff at IETR Laboratory of Polytechnique de L'Université de Nantes. Special thanks to Sandrine CHARLIER, Marc BRUNET and Guillaume LIRZIN for their aid to carry out administrative and technical works smoothly. Moreover, I am thankful to all my colleagues who have played an important part throughout my research by sharing their knowledge and expertise.

While on the part of private life outside the university, I was lucky to have family friends like Andrew LITTLE, Jéremmy JOUBERT, Mireille MONNET, Sikandar ALI, Ravi GHAEL, Muhammadou SINAYOKO, Hashim RAZZAQ, and many more, who helped and facilitated me to integrate in French society. Specially, their support was the most important one when I was struggling to find an apartment for my family in Nantes. I sincerely pay gratitude to each one of them.

I would like to thank Government of Pakistan (QUEST University) for providing me an opportunity to study in France and sponsored my research work.

Finally, I am thankful to my parents who have supported me throughout my endeavors with selfless love. My younger brother, Kami, has remained a great source of encouragement and help to me throughout. I am extremely grateful for their support.

And last of all, I would like to share equally the credit of this work to my wife Shakeela and kids Umar and Bakhtawar for their immense love, patience, encouragement and time. I dedicate this thesis to them.

Thank you everyone for your support.

Contents

List of Figures

List of Tables

List of Abbreviations

ADS	Advanced Design System
AEP	Active Element Pattern
AEF	Active Element Factor
CST MWS	Computer Simulation Technology Micro Wave Studio
DGS	Defected Ground Structure
EBG	Electromagnetic Band Gap
FDTD	Finite Difference Time Domain Method
FEM	Finite Element Method
FFT	Fast Fourier Transform
FSS	Frequency Selective Surface
HFSS	High Frequency Structure Simulator
MoM	Method of Moments
RADAR	Radio Detection And Ranging
SONAR	Sound Navigation Ranging
TE	Transverse Electric Propagation Mode
TM	Transverse Magnetic Propagation Mode
TEM	Transverse Electromagnetic Propagation Mode
VAEP	Virtual Active Element Pattern
VNA	Vector Network Analyzer

Chapter 1

Introduction

1.1 General Introduction

The year 1860 marked the history of a new beginning in the field of electromagnetism when James Clerk Maxwell introduced his famous Maxwell's equations. Not very late, in 1886, it was Heinrich Hertz who first experimentally verified the Maxwell's theory[1]. Hertz proved that radio waves and light waves were part of the same family, which we call today the electromagnetic spectrum. By the year 1901, it was Guglielmo Marconi who first made a successful transatlantic transmission experiment ranging from Britain to Canada[2]. Since then there has been tremendous research and innovations in the field of electromagnetism and wireless transmission. Antenna, a transducer that converts electromagnetic energy into electrical signals or vice versa, is one of the main inventions in the field of wireless communications.

Nowadays, depending upon applications, these antennas exist in various shapes and sizes. However, some applications require using more than one antenna together in a way to form a cluster of antennas called antenna arrays. Historically, a Nobel Laureate, Luis Walter Alvarez was recognized for inventing multi antenna system for electronic scanning. His system was utilized in RADAR in World War II with the project name EAGLE and received great popularity[3]. Since then the development of antenna arrays has remained an important research and development area in the field of RADAR, SONAR, satellite communication, mobile communication and other commercial applications.

Antenna arrays are utilized in applications when high gain, directivity, beam steering, cancelling interfering signals, determining direction of arrival, maximizing signal to noise ratio etc are required. However, designing an antenna array is a challenging task. Antenna theory requires a broad understanding of different segments related to physical and electrical parameters. The physical parameters like antenna type, number of antenna elements, feed type, inter-element distance and orientation etc are decided depending upon the desired application. A general antenna array design flow is demonstrated in Figure 1.1.

Based upon an application, the electrical parameters like radiation pattern, input impedance, gain, directivity, bandwidth and efficiency of antenna array portray the performance of the array. These electrical parameters show important information regarding the radiated fields from the antenna array. From an antenna array point of view, these electrical parameters are dependent on each other and any change in one parameter will have consequent change in the performance of the antenna.

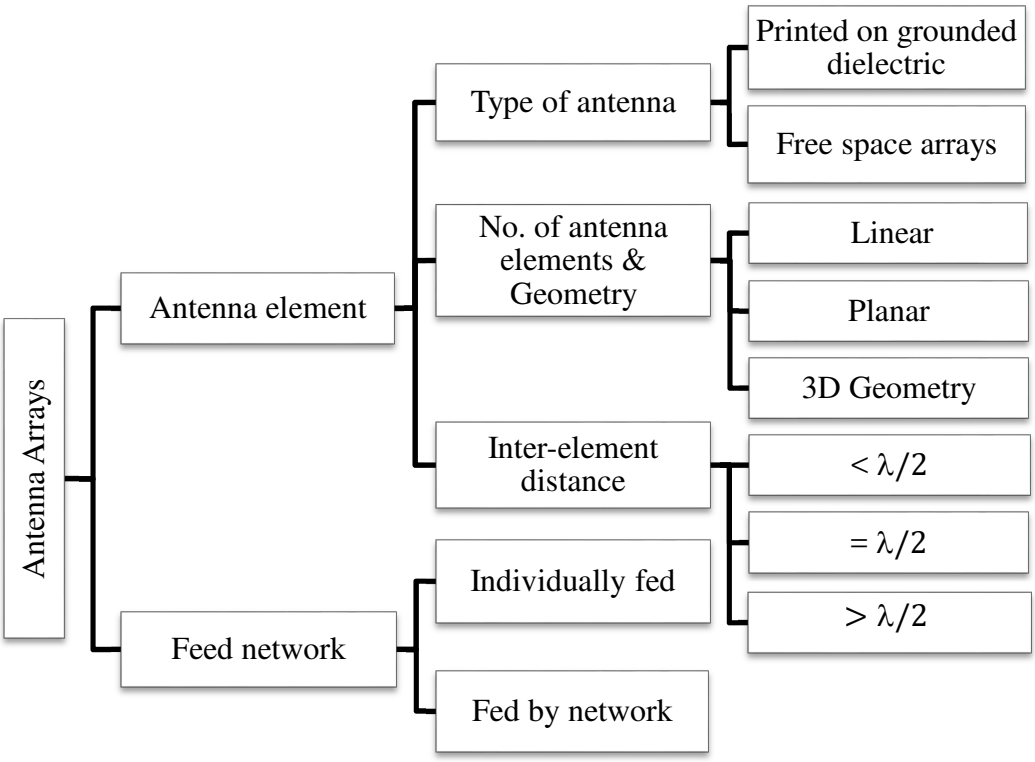

Figure 1.1: Antenna array selection flowchart according to a specified application.

The applications of antennas in different scenarios reveal the fact that there appear to be numerous problems and obstacles that are left to be dealt with. Out of these problems, impedance mismatching is considered to be one of them. This, in short, is the deviation of impedance in the antenna from its original supplied value, leading to shortage in the power radiated by the antenna.

Numerous designs and structures have been designed to overcome the problem of mismatching, and a lot of attempts were successful in achieving so. Yet, a problem still exists when a large number of antenna elements are placed side by side. The impedance of the overall array changes even when each element in the array is well matched.

In all the references the origin of this mismatching is considered as impedance variation because of the phenomenon of coupling among radiating elements. In this context, the first approach is to show that there should be no impedance change if there's no coupling. Therefore, we implemented this approach to calculate the input impedance of antennas in an array without presence of any coupling to show that there's no variation before introducing the coupling to quantify the impedance variation.

As the input impedance of an antenna is calculated from total radiated power, so for an antenna array the same method is used. Surprisingly, the total radiated power shows important impedance variation of each antenna even without any coupling.

Therefore, this thesis is focused on clarifying the phenomenon i.e. “whether the total radiation is what causes the mismatching or there is something missing in the calculation”!

1.2 Back ground study and motivation

In order to design an antenna array, it is important to take into consideration all performance parameters that may get affected when antenna elements are placed in an array arrangement. Radiation pattern and input impedance, being two frequency dependent parameters, are the most discussed in any array performance. In this array context, one of the main problems is the change in input impedance of individual antenna elements when all antennas radiate simultaneously. The cause of such mismatch may be the result of surface waves, near field radiation or far field radiation[4]. In this study, we focus on the far field radiation and its consequent impact over the input impedance of individual antenna elements in an array.

Various modeling methods have been surfaced to put forward solutions that account for the behavior of antennas in an array. Traditionally, there are two ways to evaluate radiation pattern and/or antenna input impedance;1) The far field radiated power over current distribution and 2) Active scattering parametric analysis.

Here, we present a brief overview of different modeling methods and analyze their steady evolution along with their limitations.

1.2.1 Antenna Array Modeling Methods

In order to opt for a specific pattern synthesis method for any array type requires a tradeoff which depend upon: array element type, inter element distance, size of the array, acceptable accuracy level and available computational resources. More specifically, array radiation characteristics are highly dependent on the currents being fed at the terminals of the antennas. The desire to have a pattern in a certain direction and nulls towards undesired directions is highly sought in an adaptive array with sufficiently low side lobe levels[5].

Numerical techniques: Numerical techniques like Method of Moments (MoM), Finite Element Method (FEM) and Finite Difference Time Domain Method (FDTD) are some of the well-known techniques to directly estimate the current distributions over the antenna elements solving through Maxwell’s equations[6]–[8]. The voltage and current expansion coefficients are related in terms of self and mutual impedance matrices. These numerical techniques yield accurate results however, the size of the matrices increases with the array size, and beam scanning. Moreover, these numerical techniques cannot be used for larger arrays and the arrays which are located in highly complex inhomogeneous media. Thus, approximation techniques are rather used to design larger antenna arrays.

Classical element pattern multiplication: The simplest of all methods consists of the product of a single isolated element and its array factor[9]. This method (pattern multiplication) signifies a powerful tool to exhibit first order behavior of antenna pattern. However, it is only valid when all antenna elements are of same size and placed at same distance apart with same orientation. But, in practical arrays, the antenna elements interact with each other. This phenomenon of interaction significantly modifies input impedance

and radiation pattern of individual antenna elements when the elements are placed in close proximity. This is simply the shared microwave power between antenna elements and the phenomenon in literature is known with the term "mutual coupling"[10].

Active element pattern (AEP) method: Kelley and Stutzman [11] proposed several methods based on AEP to include a particular effect of coupling. These are: unit-excitation, phased-adjusted, average and hybrid and compared them. These methods are suited where numerical techniques and classical pattern multiplication method fail. AEP incorporates the radiation of entire array when only one element is excited and the rest of elements are excited parasitically by the active element.

a) Unit-excitation AEP method: In this method the individual element patterns are computed by assuming the elements being excited by unity magnitude of feed voltage with its associated generated impedance (Z_g) and other elements being terminated with their respective generator impedances. The total radiation pattern is given by expression 1.1.

$$E(\theta, \varphi) = \sum_{n=1}^{N} V_n \; g_n^p(\theta, \varphi) \tag{1.1}$$

The term $g_n^p(\theta, \varphi)$ is called unit excitation active element pattern. Here, it represents the pattern radiated by the array by excitation of p^{th} element with unity voltage associated with its generator impedance. V_n is the complex voltage associated to *nth* element and N represents the number of voltage sources applied to array elements. The term $g_n^p(\theta, \varphi)$ contains the coupling effect and since it is measured or calculated only one time that is why it is known as exact active element method.

In other words, these active element patterns represent the pattern of whole array, considering direct excitation with other elements being parasitically excited by the same active element. The pattern of individual antenna elements is computed once only and is valid for both identical and/or non-identical array elements. As disadvantages, the computational complexity of unit-excitation increases with the array size due to the need of the active element pattern data for every array element.

b) Phase Adjusted Unit Excitation AEP method: The unit excitation AEP method does not contain information about the origin of the array coordinate system and this is where phase adjusted unit excitation AEP is preferred with inclusion of spatial phase term. Thus this method computes patterns for any arbitrary array geometries without computing new element patterns. However, phase adjusted element patterns differ for different array geometries, nevertheless this method is useful in the development of other approximate array analysis methods.

c) Average AEP method: As the number of array elements increases to a sufficiently large, a complete array pattern can be expressed in the form of the active element pattern of a typical interior element. Although this method yields better results for very large (equally spaced arrays), but it fails for arrays with smaller size. This is because the individual elemental patterns of a small array vary widely because of array edge effects and mutual coupling.

d) Hybrid AEP method: It can be used for array with moderate number of elements. In this method, the array is divided into two groups, namely, an interior element group and

an edge element group. Thus the total antenna pattern is the sum of the two patterns obtained. This method is advantageous, as it requires less memory than the other methods. Moreover, it yields better results for arrays of any antenna type. Properties of the above AEP methods have been summarized with their merits and demerits in Table 1.1.

The measurement of AEP requires only a large antenna array with each antenna matched loaded except one. Thus, it can be utilized to locate and fix any array design problems and thereby, a costly design failure risk can be avoided.

Analysis method	Merits	Demerits
Unit-excitation AEP method	Exact for any configuration and any type of elements in any scan direction	Needs large computer processing time and memory
Phase-Excitation AEP method	Same characteristics to Unit-Excitation AEP method	Same to Unit-Excitation AEP method
Average AEP method	Fast and requires less computer memory	Requires equally spaced elements, similar elements, and accurate for large arrays
Hybrid AEP method	Requires little computer memory and time, incorporates edge effects.	Similar elements and equally spaced.

Table 1.1: Summary of Active Element Pattern (AEP) methods [11]

In [12] Kelley shows that a combination of two types of active element patterns can be used to find the mutual impedance matrix and relates the element terminal voltages of a phased array to the terminal currents as given below:

Short-circuit active element is found by forcing the terminal voltage of the active element to be unity at zero phase, while the terminals of all the other elements are shorted.

Open-circuit active element pattern is obtained by forcing the terminal current to be unity while the un-driven feed points are open circuited. This approach is useful to find the mutual impedance matrix in situations where it is difficult to make accurate measurements of terminal voltages and currents or S parameters. On the other hand, it has the disadvantage that it is probably not of much practical value. This is because it is difficult to have a perfect short or open circuit termination. Additionally, the terminal voltage or current at the excited element must be maintained at a value of unity with zero relative phase while the element pattern data is being collected. Kelley addressed this in [13] and described a method to obtain the mutual impedance matrix using embedded element patterns obtained using non-zero with finite terminations. This method is potentially more useful than [12] which employ short and open circuit terminations; since

it requires that constant available power to be supplied to every excited element rather than constant voltage or current maintained at the terminals.

Pozar addressed another AEP approach also called embedded element method [14]. In an array, with the pattern taken with a feed at a single element in the array and the rest of elements terminated with matched loads, the pattern obtained is the AEP of the array. In general, this pattern will be different from the isolated element pattern because adjacent elements will radiate some power due to mutual coupling. The paper shows that with this approach the realized gain of the fully excited array at a given scan angle is proportional to the active element pattern gain at this same angle which means that if the measured active element pattern has dips or nulls at particular angles, it can be inferred that the fully excited phased array will have comparable drops in gain when scanned to these same angles. Hence, in [14] the main advantage of the method comes from the fact that the measurement of an AEP is much simpler than the measurement of the scanning characteristics of a large phased array antenna. However, in this paper some assumptions are made: the array must be large enough so that the individual AEP can be approximated as equal, and also each element of the array need to be fed independently. If the array is fed in a series configuration, an additional reflection effect can be observed which are not incorporated in this work and the AEP will not be applicable. Moreover, it is not possible for phased arrays to extract active input impedance with this kind of method.

Consequently, in [15] Pozar found a relation between the active input impedance and the AEP of a phased array. Using the same approach and assumptions that of [14] plus the fact that we need to know the magnitude and phase of the active element pattern, then we can calculate the scattering matrix of the array. Moreover, this data can be used to find the active input impedance of the fully scanned array at the same scan angles from where we get the magnitude and phase of the AEP. These results are applicable to both linear and planar arrays. This relation is interesting in terms of theory, but on the other hand in practice it is easier to measure S-parameters from AEP than obtain their magnitudes and phases.

Later, a method using the active element factor (AEF) is proposed to calculate the radiation pattern considering mutual couplings and array edges [16]. For a continuous source distribution, the total field of the antenna is given by the product of the element and space factors, where the element factor depends on the type of current and its direction of flow while the space factor is a function of the current distribution along the source. The element varying AEF method shows how the array elements can be divided into various sub-arrays which are: edge elements, interior elements and adjacent edge elements. Hence, the main advantage of this method is that it only needs to simulate a small sub-array to obtain the scattering pattern of large arrays. As a result, it is less complex computationally.

Other formalisms have also been developed specially for bigger arrays. The Floquet model analysis is proposed to determine radiation pattern of a neighbored element in an infinite and periodic lattice [17]. In this method, the couplings are considered same for all array elements and the array edge effects are neglected. Other extension to this is proposed to achieve AEP and the array scattering matrix [18]. For unequally spaced antenna arrays, a virtual active element pattern (VAEP) expansion method is proposed [19]. In this, each AEP in an unequally spaced array is considered to be the pattern radiated by a sub-array of equally spaced virtual elements. With the aid of this method, the pattern of an unequally

spaced array including mutual coupling can be efficiently evaluated by fast Fourier transform (FFT).

Numerous modeling methods based on active S-parametric analysis have also been suggested in literature [20]–[23]. A vast literature is available related to antenna array synthesis but it does not sound realistic to provide a fair review of each method.

But however, it is common in all formalisms that antenna array scattering parameters are evaluated under passive conditions. It means the scattering parameters are evaluated when one element is radiating and the rest of elements are powered off which is indeed not the case when an antenna array operates on a given task. It means the passive scattering matrix does not represent the effective power waves over the feeding network when all antenna elements are excited simultaneously.

Nevertheless, the design challenge always persists for an antenna designer in order to decide which method to choose for the best approximation corresponding to array size and complexity of radiating elements.

1.2.2 Motivation

In all above mentioned formalisms, whether it is finite or infinite array, the scattering parameters are evaluated under passive conditions that is to say that in an array of antennas the scattering parameters at each port are evaluated when only one antenna is powered on and the rest of antennas are powered off. This is not the fact when an array is in operating condition. This implies that passive scattering matrix does not represent the effective power waves over the feeding ports. Further, it is assumed in these formalisms that the mutual coupling between antennas elements adds linearly. However, it has been proposed in [24] that the phenomenon of mutual coupling is a reiterative process(multiple scattering effect) and does not qualify for linearity in antenna arrays.

Ideally, if the mutual coupling is relatively negligible then each element in an array should present the same impedance as it was placed alone. However, it is not the case in [25]. In this work, a printed array of 256 patch antennas is designed for satellite communication. The adjacent elements in this array design share -23dB and -30dB of coupling in E and H-plane, respectively. Despite, sharing low coupled power, this design could not witness satisfactory results in terms of radiation pattern and impedance matching. The appearance of grating lobes in radiation pattern and impedance mismatch were blamed on feeding network which was placed on the upper side of the substrate where they could share the spurious radiation with antenna panel and might alter the radiation pattern. Later on, on the same theme of [25] a printed array of 16x16 (Figure 1.2-a) has been proposed in the PhD work of Amal Harrabi [26]. In this work, in order to rule out the effect of spurious radiation from the feed network, the feeding was designed at the opposite side from the ground plane (Figure 1.2-b). But, yet again even after negligible coupling in between antenna elements and avoiding spurious radiation, the active reflection coefficient deteriorated leading towards impedance mismatch issues.

Essentially, the problem lies concerning to the effect of total radiation in the far field. This issue in antenna arrays has not been investigated before and requires a rigorous analysis.

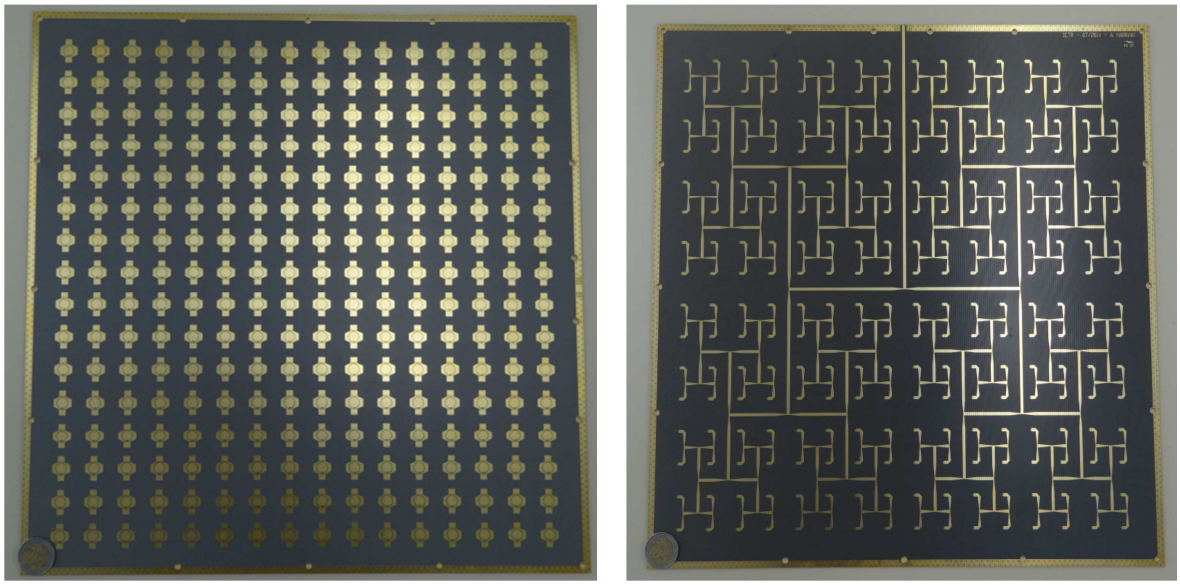

a) b)

Figure 1.2: a) 16x16 Patch Antenna Prototype with front (Patch array) and b) back (feed network).

1.3 Thesis contribution

The main objective of this thesis is the evaluation of input impedance from the effect of total radiation from an antenna array. The main contributions of this thesis involves following aspects:

1. Firstly, a Matlab code is developed to evaluate input impedance of individual antenna elements from an array due to the effect of total radiation. Three different types of antennas namely; short dipole, half wavelength dipole and patch antennas, have been coded in different linear and planar combinations to evaluate their input impedance. It has been demonstrated that by arraying the antennas the input impedance of each element of the antenna array decreases or increases compared to that of the single element which is not arrayed. In other words, the value of the input impedance of individual antenna elements changes versus antenna number and position. This idea has been presented in **EuCAP2019 (European Conference on Antennas & Propagation) held in Poland during 31 March-5 April, 2019**.

2. Secondly, in order to clarify the theoretical aspect of the effect of total radiation, an array of patch antennas has been manufactured. In this part, the problem to address is to excite all antennas simultaneously. This is done with the help of existing four ports VNA. The used VNA (R&S ZVA24) is capable of providing two coherent signals out of four ports. Thus, a novel method of exciting any number of antenna elements is introduced with the help of power splitter. This work further proposes an important aspect of the evaluation of

active S-parameters in antenna arrays. It has been observed that the active S-parameters obtained by using the passive scattering matrix do not correspond to the actual values obtained during a simultaneous excitation of all the elements. This idea has been presented in **JNM, 21èmes Journées Nationales Micro-Ondes, 14-17 mai 2019 Caen (France).**

3. Thirdly, since the theoretical code does not include the effect of mutual coupling, hence to clarify the effect of total radiation, we need to decouple an antenna array to a level where mutual coupling presents no change of Active S-parameters as compared to passive S-parameters. In this context, a novel DGS (**μ** shaped) has been introduced. This work reduced coupling upto -33 dB in two E-plane patch antenna arrays with narrow band rejection characteristics of transmission coefficient (S_{12}). This work is to be presented in **AES 2021, the 8th International Conference on Antennas and Electromagnetic Systems, June 2021, Marrakech, Morocco.**

4. Finally, to have even better rejection in coupled power and wide band rejection characteristics, a method of loaded pins with metallic walls has been introduced. A method of loaded patch antennas with shorting pins and erected walls in between patch antenna arrays is introduced to reduce surface wave and free space wave coupling in both E and H-plane, respectively. This simple technique works equally well in both orientations by reducing coupling upto -39 dB and -44 dB (measured value) in E-plane and H-plane, respectively, as compared to conventional patch antenna array. The scattering parameters are studied and conclusions are made on amounts of mutually coupled power considered negligible and the band width of the rejection band (S_{12}). The simulation results present good agreement with measurements. This work is published in journal **Progress In Electromagnetics Research *(PIER C).***

1.4 Thesis structure

The thesis comprises of 6 chapters including introduction (chapter 1) as covered above. This chapter provides the general introduction to antennas and antenna array with background study and motivation along with contribution of this thesis work.

In chapter 2, an introduction to antenna field regions has been given. Antenna and antenna array basic parameters have been introduced. These basic parameters are frequently used in later chapters as the basic building blocks of the later explanations.

In chapter 3, antenna array theory has been introduced with the aim to develop Matlab code in order to deduce input impedance from the effect of total radiation in an array. In this regard, three types of antenna array (short dipole, half wavelength dipole and patch antenna) have been used in linear and planar combinations.

Chapter 4 involves 3D simulation and measurement of antenna arrays. A simple measurement strategy has been introduced to evaluate active S-parameters with simultaneous excitation of all antenna elements in the array.

Chapter 5 deals with mutual coupling reduction techniques. After introducing mutual coupling and its effects, two decoupling techniques have been developed. DGS and shorting pins along with metallic walls have been introduced. The decoupling techniques aim to reduce coupling in patch antenna arrays to a level where active S-parameters present same values to those of passive S-parameters.

Finally, chapter 6 includes the conclusion and future aspects of the PhD work.

1.5 List of Publications

Journal

1. **Irfan Ali Tunio**, Yann Mahé, Tchanguiz Razban, and Bruno Froppier. "Mutual Coupling Reduction in Patch Antenna Array Using Combination of Shorting Pins and Metallic Walls". *" Progress In Electromagnetic Research C, Vol 107, 157-171, 2021.*

Conference

1. **Irfan Ali Tunio**, Yann Mahé, Tchanguiz Razban, and Bruno Froppier. "Study of Impedance Matching In Antenna Arrays due To Total Radiation," *13th European Conference on Antennas and Propagation* (EuCAP), Krakow, Poland, 2019.

2. **Irfan Ali Tunio,** Yann Mahé, Bruno Froppier, and Tchanguiz Razban. "Analyse de la mesure du TOS actif sur des réseaux d'antennes à l'aide d'un analyseur de réseau vectoriel à quatre ports". *21èmes Journées Nationales Microondes* (JNM 2019), May 2019, Caen, France.

3. **Irfan Ali Tunio,** Yann Mahé, Tchanguiz Razban, and Bruno Froppier. "Measurement Analysis of Active Standing Wave Ratio on Networks with a Four-Port Vector Network Analyzer". *Fifth Sino-French Workshop on Information and Communication Technologies* (SIFWICT 2019), June 2019, Nantes, France.

4. **Irfan Ali Tunio,** Hernan Dellamaggiora, Yann Mahé, Tchanguiz Razban, and Bruno Froppier. "Isolation Enhancement in Microstrip Patch Antenna Arrays". *8^{th} International Conference on Antennas and Electromagnetic Systems (AES 2021), June 2021, Marrakesh, Morocco.(Accepted for conference).*

Chapter 2

Antenna: Theory & Definitions

In this chapter, we develop the basic theoretical concepts related to antenna field regions and antenna parameters. These basics are the building blocks for later chapters in this thesis.

2.1 Antenna field radiation regions

An antenna radiates/receives electromagnetic waves in/from its surrounding. The surroundings have been categorized in three regions, namely[9];

1) Near field or reactive near field region
2) Radiative near field or Fresnel region
3) Far field or Fraunhofer region

Near field region:

The region just in the immediate vicinity of antenna under test is the near field region (Figure 2.1). The outer boundary of this region is generally considered at $R < 0.62\sqrt{D^3/\lambda}$ from antenna surface. Here R is the distance from the antenna under test, D is the maximum dimension of the antenna and λ is wavelength.

Radiative near field

The region in between reactive near field and far field ($0.62\sqrt{D^3/\lambda} \leq R < 2D^2/\lambda$) is radiative near field region (Figure 2.1). In this region, the fields (E and H) are in phase. The wave fronts vary with distance and do not present spherical wave fronts.

Far field region

The region beyond Radiative region is the far field region. This region has electric and magnetic fields in phase. The wave front is spherical and it can be considered as locally plane wave. This means that E, H and k are all together orthogonal. This implies that E and H fields are linked together according to wave impedance equal to 120π or 377Ω in vacuum with real power flow and no stored energy. This region exists at the distances greater than $2D^2/\lambda$.

In this thesis, we are focused to evaluate input impedance from the far field equations of the antennas. Thus, this region is of our focus.

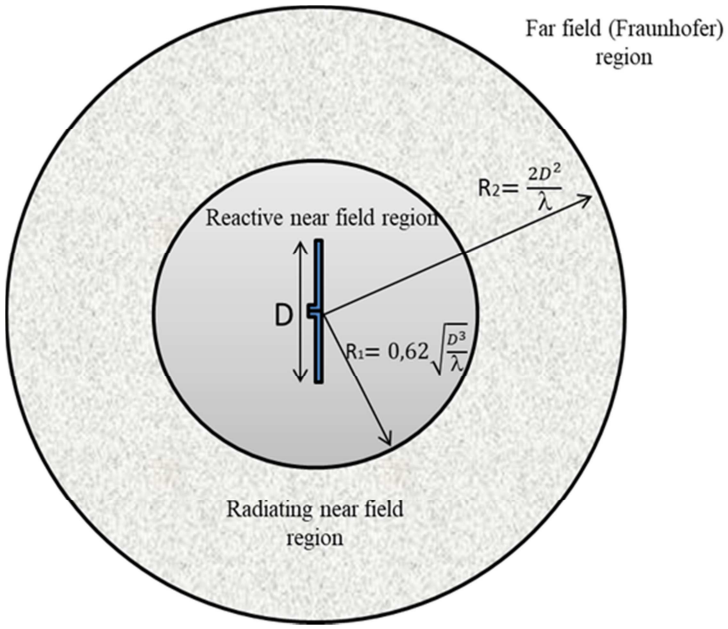

Figure 2.1: Field regions of an antenna[9].

2.2 Polarization

Polarization is defined as the evolution of the direction of the electric field (and therefore the magnetic field) of the electromagnetic wave. It is dependent both on the characteristics of the antenna, its power supply and the wave propagation medium.

Generally, any wave can be defined as an elliptically polarized wave. The cases of circular and linear polarizations can indeed be considered as special cases of elliptical polarization (Figure 2.2). The wave is then characterized by its degree of ellipticity which is described by the parameter, x = arctan(minor - axis/ major - axis) [9].

If the minor axis of the ellipse is zero, the polarization is linear and the coefficient of ellipticity is equal to 0°. If the two axes are equal, then the polarization is circular and the coefficient of ellipticity is equal to ± 45°. If the two axes do not fall under the aforementioned conditions, then the polarization is purely elliptical.

This notion of polarization is important for an antenna. If on reception, the signal arriving on the antenna has a polarization different from that provided for the antenna, there is a polarization mismatch generating additional losses.

In the case of a linear polarization, if the angle made by the direction of the vector E with the ground is equal to 0° then the polarization is said to be horizontal, if it is equal to 90° it is said to be vertical.

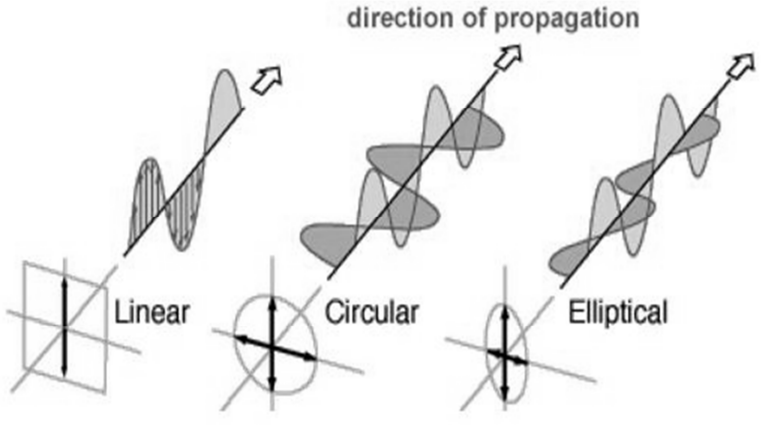

Figure 2.2: Electric field representation for linear, circular and elliptical polarization [27].

2.3 Input Impedance

Input Impedance (opposition to current) can be defined in following simple ways[9]:

- Impedance presented at the terminals of an antenna,
- or the ratio of voltage to current at the pair of terminals,

The input impedance of an antenna can be described generally according to the following model in Cartesian form[9]:

$$Z_{in} = R_{in} + jX_{in} \tag{2.1}$$

Where,

- R_{in} is the resistive part of the antenna (with $R_{in} = R_{radiative} + R_{loss}$)
- X_{in} represents the reactive part of the antenna where X_{in} equals $L\omega$ and represents inductive reactance. X_{in} equals $1/C\omega$ and represents capacitive reactance. Here, ω represents angular frequency ($\omega=2\pi f$). The reactive part represents the stored power in the near field region of the antenna (non-radiated power).

For example, Figure 2.3 represents an antenna connected to a receiver circuit where E_S represents the signal delivered by the source, Z_S the output impedance of the source generally equal to the characteristic impedance and Z_L the load impedance.

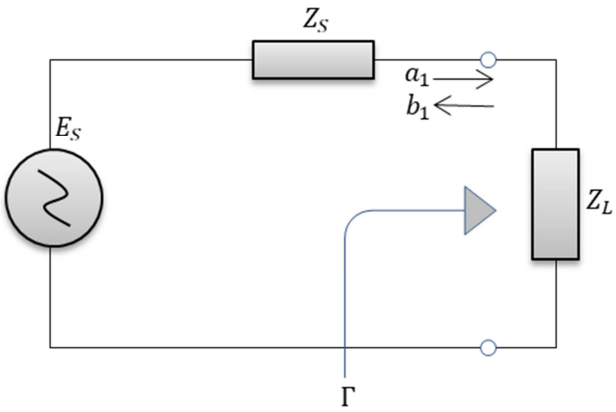

Figure 2.3: Antenna circuit model[28].

When source and load impedances are not well matched, some of the power is reflected back from load to source and is expressed with the term reflection coefficient (Γ) described by following expression;

$$\Gamma = \frac{reflected\ signal}{incident\ signal} = \frac{b_1}{a_1} = \frac{Z_L - Z_S}{Z_L + Z_S} \tag{2.2}$$

The expression 2.2 shows how effectively an antenna receives/transmits energy depending on source and load impedances. Moreover, the impedance is affected with the presence of other voltage and current sources induced on the antenna including those by the effects of mutual coupling. In that case, for example, in a dual antenna system the impedance on the first and second antenna can be visualized with the following expressions;

$$Z_{in\ 1st\ antenna} = Z_{11} + Z_{12}\frac{I_2}{I_1} \tag{2.3}$$

$$Z_{in\ 2nd\ antenna} = Z_{22} + Z_{21}\frac{I_1}{I_2} \tag{2.4}$$

Where;

- Z_{11} and Z_{22} represent self-impedance of antenna 1 and antenna 2 respectively,
- Z_{12} and Z_{21} represent impedance coupling coefficients.

Likewise, the voltage standing wave ratio (VSWR) can be expressed by the expression 2.5.

$$VSWR = \frac{1+|\Gamma|}{1-|\Gamma|} \tag{2.5}$$

VSWR measures radiation potential of an antenna thereby it is usually taken smaller than 2:1. It infers that less than or equal to 10% of the input power is reflected back.

Ideally, the antenna should present a pure resistance to its supply line equal to the characteristic impedance of its line in order to obtain propagation of full progressive wave. By this way, the energy transfer will be maximized and this will ensure the signal transmission without attenuation along the length of the line. In telecommunications standards, this impedance is generally fixed at 50Ω except in special cases.

2.4 Radiation pattern

Antenna radiation pattern (in far field region) is a mathematical or graphical (2D or 3D) representation of radiation characteristics of an antenna in space coordinates (Figure 2.4)[9].

This radiation pattern, commonly expressed in dBi, gives information on how the power is spread around the antenna. It defines the direction along which the power is more efficiently radiated than the other directions. Usually, radiation patterns are normalized field patterns (either gain or power quantities) with respect to the maximum values. In general, radiation properties incorporate radiation intensity, field strength, power flux density, phase and/or polarization, and directivity.

Generally, three common radiation patterns are used to describe radiation properties of an antenna:

- Isotropic – An antenna that radiates/receives electromagnetic power equally in all directions. However, it does not exist in reality but is merely applied to an ideal antenna (lossless) and is often used as a reference to show directive properties of actual antennas.

- Omni- directional – An antenna that receives/radiates electromagnetic power equally in all direction perpendicular (azimuthal directions) to one axis and varying power to other axis (elevation angle), decreasing to zero on the axis[29]. For example, vertically radiating dipole antenna illustrated through Figure (2.4) is one of the Omni-directional antennas. These antennas are generally low gain since power radiates in all directions and are suitable for variety of applications including those of mobile phones[30].

- Directive – An antenna that receives/radiates electromagnetic power more effectively in one direction than in other directions is referred to as directive antenna. These antennas are generally used for point to point communication (like dish antennas, array antennas) because of having high gain as the power is concentrated in one direction[31]. For example, a patch antenna array of four elements produces a directive radiation pattern with 12dBi gain as shown in Figure 2.5.

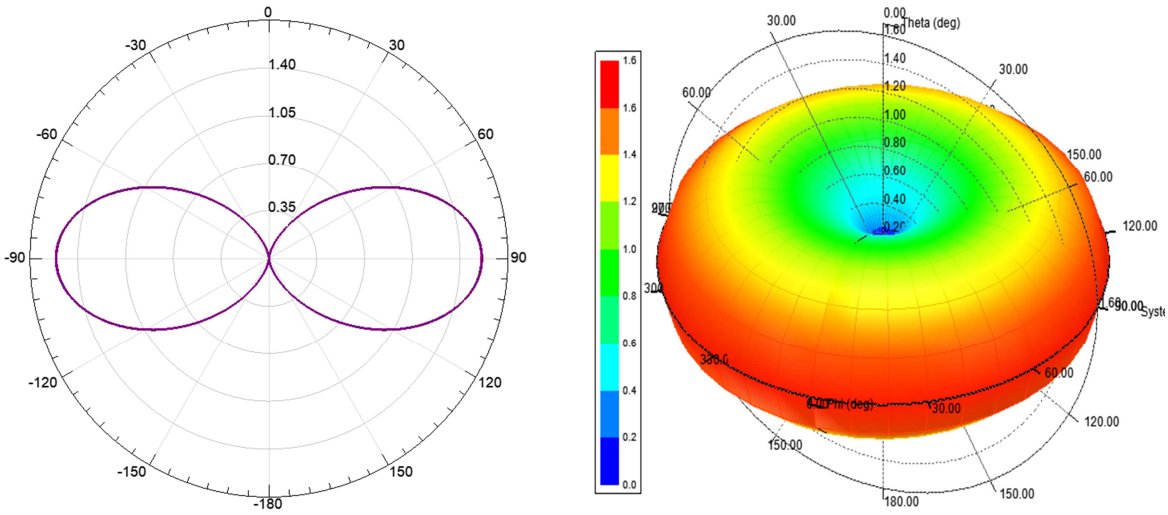

a b

Figure 2.4: Radiation pattern of vertical dipole antenna in polar coordinates; a) 2D radiation pattern, b) 3D radiation pattern.

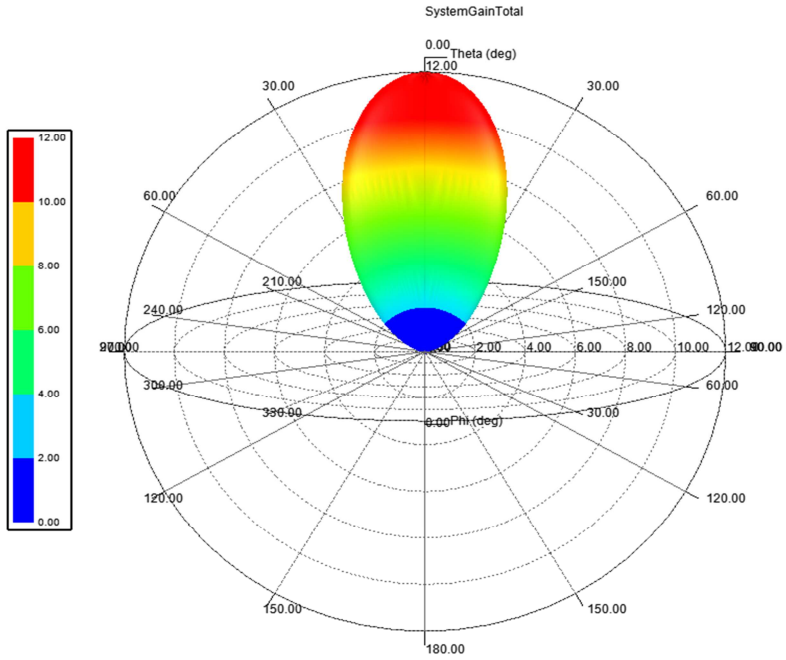

Figure 2.5: Directive 3D radiation pattern of four patch antenna array.

2.5 Directivity and gain

It is the ratio between radiation intensity in a certain direction from an antenna to the averaged radiation radiated in all directions. Mathematically it is given by[9];

$$D = \frac{U}{U_0} = \frac{4\pi U}{P_{rad}} \tag{2.6}$$

If the direction is not specified, the maximum radiation intensity is given then;

$$D_{max} = \frac{U_{max}}{U_0} = \frac{4\pi U_{max}}{P_{rad}} \tag{2.7}$$

Where;

- D is directivity
- U is the radiated power density along direction theta, phi (W/ Ω)
- U_0 is the total radiated power (P_{rad})divided by 4π(W/ Ω)
- D_{max} is maximum directivity
- U_{max} is maximum radiation intensity (W/ Ω)

The efficiency factor of the antenna varies according to $\eta \in (0,1)$, if we call G the gain of the antenna, and using the recently defined directivity D , we can obtain G as follows:

$$G = \eta D \tag{2.8}$$

As a result, gain is always less than directivity, due to losses in the antenna.

2.6 Impedance Bandwidth

Impedance bandwidth (BW) or simply bandwidth is the range of frequencies where an antenna performs optimally. Usually it is considered to be less than 10dB (S11 ≥ -10dB) and often referred as percentage bandwidth (Figure 2.6). For a narrowband antenna, the impedance bandwidth is expressed as:

$$BW = \frac{f_H - f_L}{f_c} \tag{2.9}$$

On the other hand, the bandwidth of the broadband antenna is expressed as the ratio between the higher to lower frequencies at an acceptable performance level:

$$BW = \frac{f_H}{f_L} \tag{2.10}$$

Where,

- f_c is center frequency,
- f_H and f_L are higher and lower frequencies, respectively.

Quality factor (Q) of an antenna defines how well an antenna radiates and is inversely related to bandwidth and is given by the following expression [32]:

$$Q = \frac{stored\ energy}{power\ lost} \tag{2.11}$$

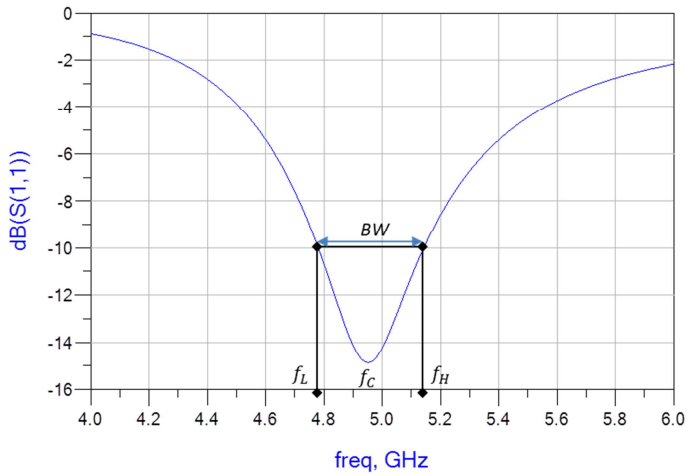

Figure 2.6: Bandwidth measurement through reflection coefficient.

2.7 Scattering parameters

Any two port (or multi-port) linear network can be characterized by a number of equivalent circuit parameters, such as transfer matrix, impedance matrix, admittance matrix, and scattering matrix[33]. Any typical two-port network can be represented by the following figure.

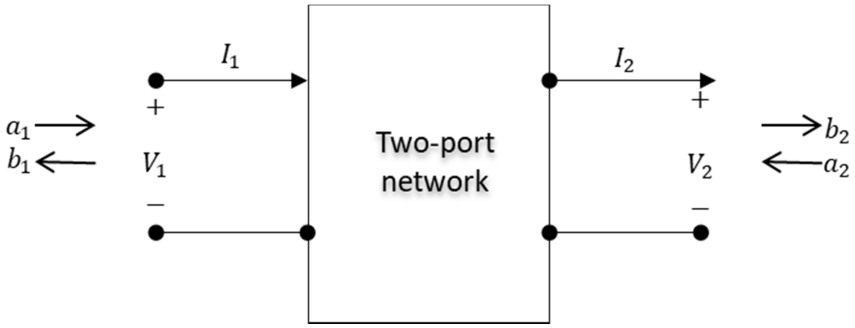

Figure 2.7: Two-port network.

Voltage and current at port1 is related to voltage and current at port2 through transfer matrix also called ABCD matrix, whereas the two voltages (V_1 & V_2) and currents (I_1 & I_2) relates to impedance matrix:

$$\begin{bmatrix} V_1 \\ I_1 \end{bmatrix} = \begin{bmatrix} A & B \\ C & D \end{bmatrix} \begin{bmatrix} V_2 \\ I_2 \end{bmatrix} \qquad \textit{Transfer Matrix} \tag{2.12}$$

$$\begin{bmatrix} V_1 \\ V_2 \end{bmatrix} = \begin{bmatrix} Z_{11} & Z_{12} \\ Z_{21} & Z_{22} \end{bmatrix} \begin{bmatrix} I_1 \\ -I_2 \end{bmatrix} \qquad \textit{Impedance Matrix} \tag{2.13}$$

The transfer and impedance matrices are, therefore, 2x2 matrices:

$$T = \begin{bmatrix} A & B \\ C & D \end{bmatrix}, \quad Z = \begin{bmatrix} Z_{11} & Z_{12} \\ Z_{21} & Z_{22} \end{bmatrix} \tag{2.14}$$

The admittance matrix is inverse of the impedance matrix($Y=Z^{-1}$).

The scattering waves (Kurokawa waves) give the relationship/ratio between outgoing waves (b_1 & b_2) to the incoming waves (a_1 & a_2) that are incident on the ports[34]:

$$\begin{bmatrix} b_1 \\ b_2 \end{bmatrix} = \begin{bmatrix} S_{11} & S_{12} \\ S_{21} & S_{22} \end{bmatrix} \begin{bmatrix} a_1 \\ a_2 \end{bmatrix} \quad , S = \begin{bmatrix} S_{11} & S_{12} \\ S_{21} & S_{22} \end{bmatrix} \textit{ Scattering Matrix} \tag{2.15}$$

The parameters S_{11}, S_{12}, S_{21}, and S_{22} are referred as scattering parameters or simply S-parameters. S_{11} and S_{22} are termed as reflection coefficients and S_{12} and S_{21} are called transmission coefficients.

These travelling wave variables at port1 (a_1 & a_2) and port2 (b_1 & b_2) can be defined in terms of voltages and currents with positive real valued reference impedance Z_0 (Usually 50Ω):

$$a_1 = \frac{V_1 + Z_o I_1}{2\sqrt{Z_o}} \quad , \quad b_1 = \frac{V_1 - Z_o I_1}{2\sqrt{Z_o}} \tag{2.16}$$

$$a_2 = \frac{V_2 - Z_o I_2}{2\sqrt{Z_o}} \quad , \quad b_2 = \frac{V_2 + Z_o I_2}{2\sqrt{Z_o}} \tag{2.17}$$

At lower frequencies, the transfer and impedance matrices can be used, however, at microwave frequencies it becomes difficult to measure through such matrices and therefore, scattering matrix is preferred instead.

The scattering parameters of two port antenna system (Figure 2.8) can be measured as follows:

1) Reflection coefficient (S_{11}): It is the ratio between outgoing waves to incoming waves at the input of a multipole terminal. To measure this, a signal is injected at port1 while port2 is ended with matched impedance. In this case port2 has no signal (a_2=0) as given by equation 2.18.

$$S_{11} = \left.\frac{b_1}{a_1}\right|_{a_2=0} \tag{2.18}$$

2) Forward Transmission coefficient (S_{21}): To measure this, port1 is injected with a signal while port2 is terminated with source load. In this case, a_2=0 and the parameter is defined as the following relation:

$$S_{21} = \left.\frac{b_2}{a_1}\right|_{a_2=0} \tag{2.19}$$

3) Reverse Transmission coefficient (S_{12}): To measure this, a signal is injected at port2 while port1 is terminated with source impedance. In this case, same as previously the parameter is given by the following relation:

$$S_{12} = \left.\frac{b_1}{a_2}\right|_{a_1=0} \tag{2.20}$$

4) Output reflection coefficient (S_{22}): Reflection coefficient on the output represents when port1 is terminated with source load and por2 is injected with a signal. In this case, a_1=0 and relation is represented by following expression:

$$S_{22} = \frac{b_2}{a_2}\Big|_{a_1=0} \tag{2.21}$$

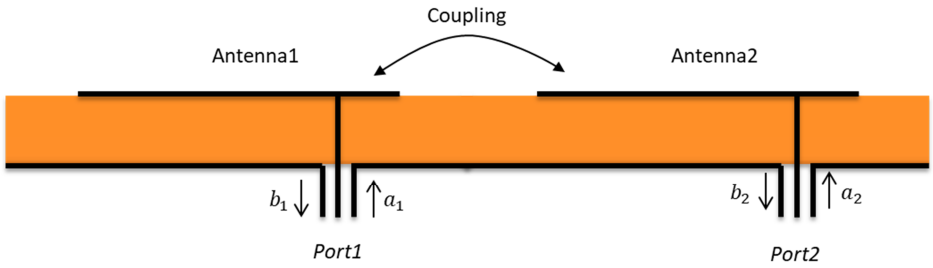

Figure 2.8: Individually fed two elements antenna system.

Reflection coefficient (return loss) and transmission gain of an antenna can be expressed generally with the following expressions:

$$Return\ loss = 10log_{10}(|S_{11}|) \tag{2.22}$$

$$Transmission\ gain = 10log_{10}(|S_{21}|) \tag{2.23}$$

2.8 Conclusion

In this chapter, we have developed the basic concepts related to antenna radiating field regions and antenna analysis parameters. These basic concepts would be used frequently in later chapters to define and characterize antenna and antenna array performance. In the next chapter, we would develop Matlab code to evaluate input impedance of different antenna arrays due to the effect of total radiation.

.

Chapter 3

Antenna array: Theory & Impedance evaluation

3.1 Antenna array

An antenna array is defined as a set of identical or non-identical antennas with the same orientation (or not) in the space which is excited by a feeding circuit which distributes information according to a weighting law on each element. This circuit, called supply network, can be passive (fixed radiation diagram in the network frame), or active (electronic pointing) [4], [9].

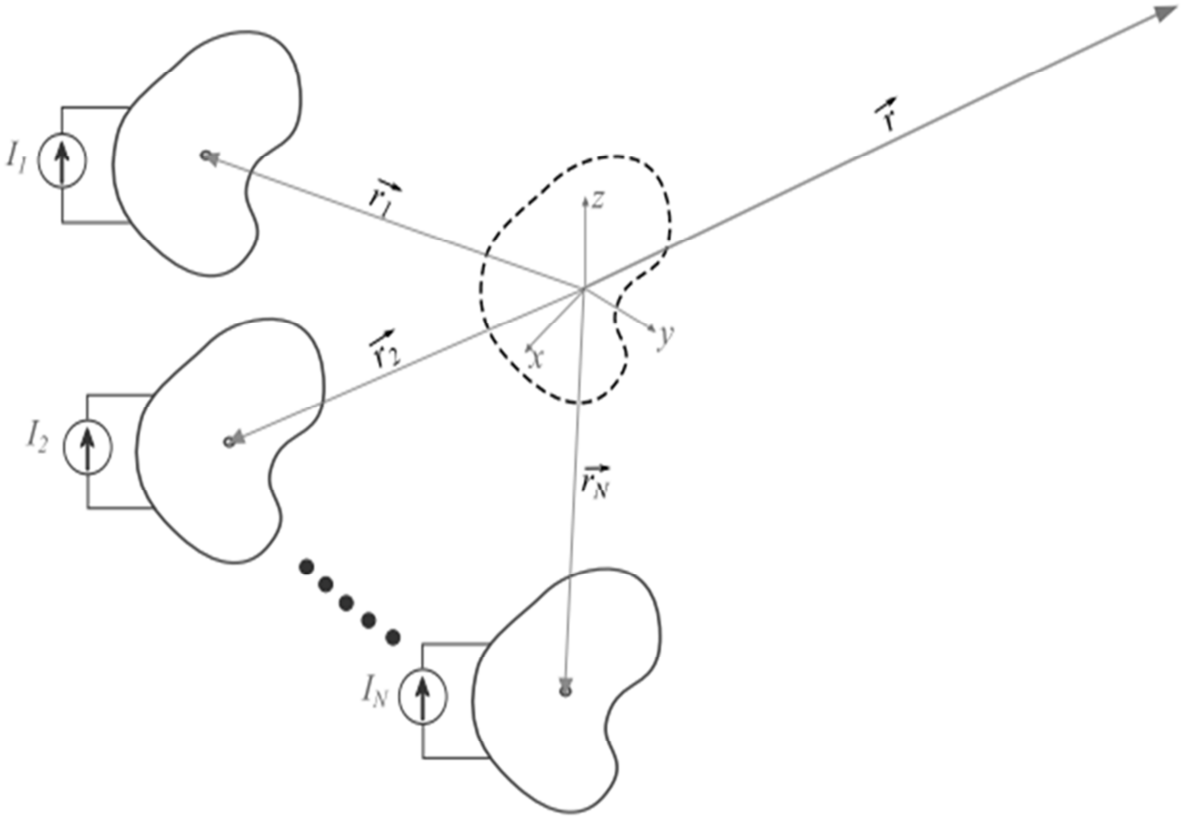

Figure 3.1: A schematic view of an antenna array.

Whether passive or active, it is possible to consider that the excitation current of the element m is written as;

$$I_m = |I_m| e^{j\theta_m} \tag{3.1}$$

According to the antenna theory and at a large distance from the array (far field condition), each of the elements of the array brought back to the origin of an orthonormal reference associated with the network will radiate an electric field proportional to the excitation current, such that:

$$\vec{E}_{m,\ at\ origin}(\theta,\phi) = jk\eta I_m \overrightarrow{l_e}(\theta,\phi)\frac{e^{-jkr}}{4\pi r} \qquad m = 1, 2, \dots\dots, N \tag{3.2}$$

When the element m of the antenna array is moved from a vector $\vec{r}_m$ to a new position (with$|\vec{r}_m| \ll |\vec{r}|$), using the paraxial approximation, the radiated far field is given by the following equation:

$$E_m(\theta,\phi) = jk\eta I_{in}\, l_e(\theta,\phi)\frac{e^{-jkr}}{4\pi r} e^{jk\vec{r}_m.\vec{r}} = E_{e,at\ origin}(\theta,\phi) e^{jk\vec{r}_m.\hat{r}}, \quad m = 1, 2, \dots\dots, N \tag{3.3}$$

With;

$\hat{r} = \sin\theta\, cos\phi\ \hat{x} + sin\theta\ sin\phi\hat{y} + cos\theta\hat{z}$

Using equation above, the total field radiated by the antenna array is then calculated as the vector sum of the fields radiated by the various constituent elements of the array. This total field at a point in space is therefore expressed as:

$$E(\vec{r}) = \sum_{m=1}^{N} E_m = E_e(\vec{r})_{|I_{in}=1} \sum_{m=1}^{N} I_m e^{jk\vec{r}_m.\hat{r}} \tag{3.4}$$

According to equation (3.4), in the case where all the elementary antennas are identical and oriented in the same way, the total radiated field is expressed as the factorization of the intrinsic radiation of each element (un-weighted) $(E_e(\vec{r})_{|I_{in}=1})$ multiplied by a term depending on the geometric and electrical configuration of the network called array factor $(\sum_{m=1}^{N} I_m e^{jk\vec{r}_m.\hat{r}})$.

For an antenna array made up of N elements located in the plane (x, y), equation (3.4) is written as follows:

$$E(\vec{r}) = E_e(\vec{r})_{|I_{in}=1} \sum_{m=1}^{N} |I_m| e^{jk(x_i \sin\theta cos\phi + y_i sin\theta sin\phi) + j\phi_i} \tag{3.5}$$

Where;

$r_m = x_m\vec{x} + y_m\vec{y}$, with (x_m, y_m) , the coordinates of the element m in plane (x, y).

It is noteworthy to mention that to have the maximum of the electric field radiated in any direction (θ_0, ϕ_0) in space, it is necessary to ensure a coherent summation of the contributions along this direction. This condition is met when the electrical phase of each antenna element makes up 2π near the geometric delay linked to the spatial distribution of the elementary antennas, i.e.

$$k(x_i sin\theta_0 cos\phi_0 + y_i sin\theta_0 sin\phi_0) + \phi_i = 2n\pi \qquad n = 0, \pm 1, \pm 2, \ldots \qquad (3.6)$$

Hence, the simplest way to evaluate total radiated fields radiated by the antenna elements in an array is simply the far fields radiated by single antenna multiplied with its array factor. It is the core idea we implement to evaluate input impedance of individual antenna elements from the concept of total radiation in the upcoming sections.

3.2 Antenna array Matlab calculations

In order to understand antennas it is important to know their types, radiation patterns, power and impedance levels, etc. Equations are set to help calculate these properties. Thus, the antenna can be virtually apprehended before designing it or for developing an existing one. Furthermore, for applying these equations and achieving accurate results from the mathematical point of view, some tools exist such as Matlab to analyze different properties of antennas.

In this thesis, Matlab is used to implement theoretical analysis of the input impedance variation from the far field radiation pattern only. In this model, the antenna element radiation pattern and the associated array factor are only considered. The mutual coupling and edge effects are not taken into account. The aim of this approach is to determine if this phenomenon is an important contributor over the impedance mismatching.

In this model, three types of antennas: electric dipole, resonant wire, and rectangular patch antennas are used. Each antenna type and its calculations are discussed thoroughly. As a control experiment, all antennas are tested at frequency of 5GHz.

One antenna element is tested for ensuring the validity of the equations before these antennas are set in arrays of different configurations: along X-axis, Y-axis, and XY-plane, as the objective. The values of the input impedances resulting from calculations are recorded and discussed. The equations in the antenna models have been referenced from the book of C.A Balanis[9].

3.2.1 Short dipole antenna

The dipole antenna is the simplest type of antenna. It is merely an open-circuited, center-fed, small wire with a current of constant amplitude and frequency. The name small or short given to it refers to its size compared to the wavelength which is very small comparatively to the wavelength. Typically, a dipole is called short if its length is less than a tenth of a wavelength [35]. The center-fed short dipole antenna with its radiating coordinates has been shown in Figure 3.2.

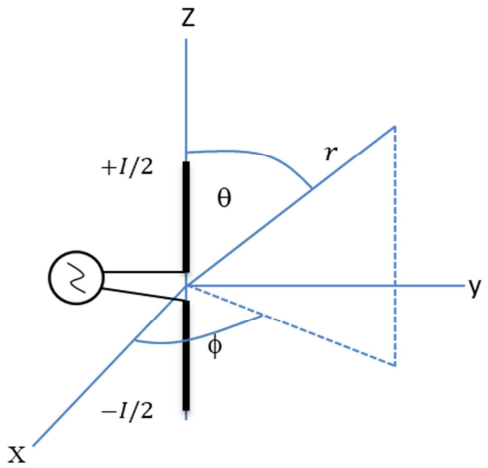

Figure 3.2: The center-fed short dipole antenna with its radiating coordinates.

3.2.1.1 Single element optimization

Before we apply the concept of total radiation in an array and evaluate input impedance, single antenna element should be tested first as per its far field equations so that the validity of equations can later be verified.

The input impedance of the short dipole can be evaluated by the following expression:

$$Z_{in} = \frac{2P}{I^2} \tag{3.7}$$

Where, I represents current (we suppose it as one ampere) and P represents the total radiated power by the antenna in free space and is given by the expression:

$$P = \frac{1}{2} \oiint E \times H^* ds \tag{3.8}$$

On the sphere of radius r: $ds = r^2 d\Omega$ and $d\Omega$ represents space angle ($\sin\theta d\theta d\phi$). E and H fields represent the far field equations for the short dipole. In the general form field equations of short dipole, $E_\emptyset$, H_r and H_θ are zero everywhere and E_r is neglected since r is very large as compared to antenna size (Figure 3.2). Consequently, following equations of short dipole are the far field equations[9]:

$$E_\theta = (i\omega\mu)(I.dl)\ sin\ \theta . \frac{e^{-ikr}}{4\pi r} \tag{3.9}$$

$$H_\emptyset = (i\omega\varepsilon\eta)(I.dl)\ \sin\theta . \frac{e^{-ikr}}{4\pi r} \tag{3.10}$$

In Matlab, integral2, as a built in function, is used (for equation 3.8) with limits set as $0 \leq \theta \leq \pi$ and $0 \leq \emptyset \leq 2\pi$. The variables are of the following values with 5GHz frequency:

$$\lambda_o = \frac{c}{f} = \frac{3x10^8}{5\ x10^9} \tag{3.11}$$

$$dl = \frac{\lambda_o}{10} \tag{3.12}$$

$$k = \frac{2\pi}{\lambda_o} \tag{3.13}$$

$$\eta = 120\pi \tag{3.14}$$

Here,

- λ_o is wavelength in free space,
- c is speed of light in free space,
- f is the frequency of interest,
- dl is short dipole length,
- k is wave number,
- η is wave impedance in free space.

The above variables are used in Matlab code to find the radiated power (equation 3.8) for a single antenna.

The resulting input impedance calculated through equation 3.7 from the Matlab code is **7.8957Ω** which is approximately the same that can be obtained from the radiation resistance formula of short dipole **($Z_{in} = 790(dl/\lambda)^2$).** This ensures that the code is well written and it can be extended to array combinations.

3.2.1.2 Antenna Array Calculation

Each antenna element in the array should be multiplied by a factor that mathematically describes its geometrical position and number in an array. The array factor which can be multiplied to the corresponding far field equations in order to give the resultant far field equation for the entire array i.e:

$$\vec{E}(\textit{total radiated field}) = \overrightarrow{E_o}(\textit{radiated field of a single element}) * \textit{Array Factor}$$

In this case, three different array combinations have been used. The elements are being arranged along X-axis (Figure 3.3(a)) and Y-axis (Figure 3.3(b)) then along XY-axis plane (Figure 3.3(c)).

In case of an array arranged along X-axis or Y-axis, the net far field equations then will be the multiplication of the field equation of one element $\overrightarrow{E_o}(\theta, \phi)$(equations (3.9) and

(3.10)) and the X-axis or Y-axis array factor function as in equation (3.15) or equation (3.16), respectively.

$$\vec{E} = \overrightarrow{E_o} \frac{sin(\frac{n.k.sin\theta cos\phi.dx}{2})}{sin(\frac{k.sin\theta cos\phi.dx}{2})} \tag{3.15}$$

$$\vec{E} = \overrightarrow{E_o} \frac{sin(\frac{n.k.sin\theta sin\phi.dy}{2})}{sin(\frac{k.sin\theta sin\phi.dy}{2})} \tag{3.16}$$

Here, n is number of antenna elements, k is the wave number, dx and dy are the X-axis and Y-axis inter-element distances, respectively.

Moreover, the X-axis and Y-axis array factors along with corresponding far field equations are multiplied to have XY-plane configuration of an array shown in Figure 3.3(c) and given by equation (3.17)

$$\vec{E} = \overrightarrow{E_o} \frac{\sin(\frac{n.k.sin\theta cos\phi.dx}{2})}{\sin(\frac{k.sin\theta cos\phi.dx}{2})} \frac{\sin(\frac{n.k.sin\theta sin\phi.dy}{2})}{\sin(\frac{k.sin\theta sin\phi.dy}{2})} \tag{3.17}$$

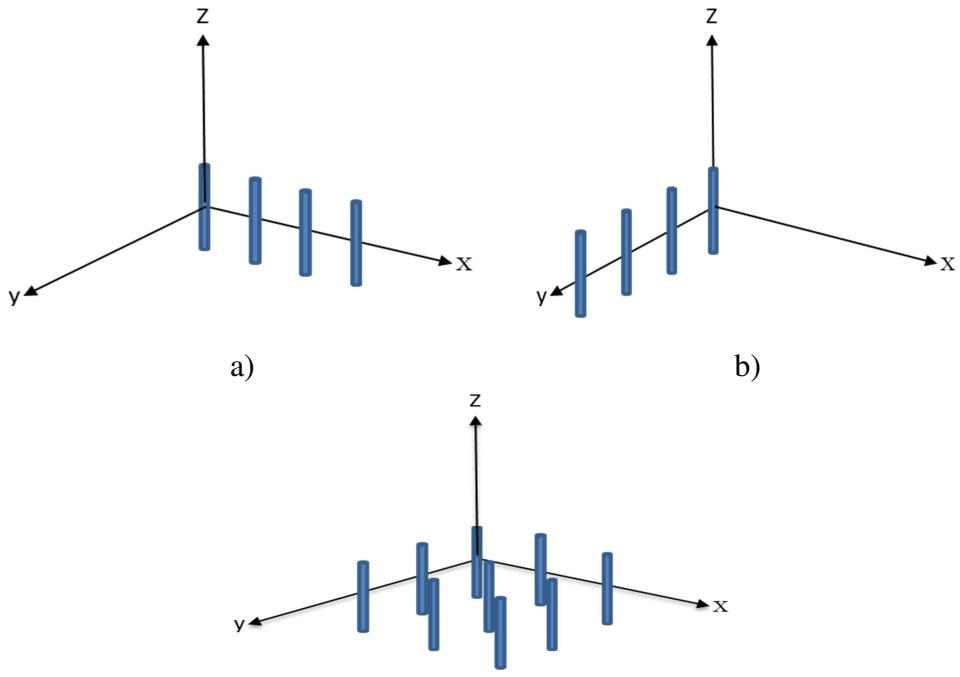

Figure 3.3: Short dipole antenna array combination arranged along; a) X-axis b) Y-axis c) XY-plane (Planar).

Here, the inter element distance(dx and dy) is kept at $0.5\lambda_0$ which is an acceptable trade-off between mutual coupling and side lobes[36]. The equations with the far field are coded. By using equation 3.7 and equation 3.8, the total power due to entire array combination is computed. The power is then divided by the number of antenna elements (n) in the array to yield average input impedance values of individual antenna elements. Here, is the main assumption of the proposed calculation. Indeed, as we assume that there is no coupling phenomenon between elements; all elementary antennas are affected in the same manner. That is why we propose to divide the radiated power over the number of antennas arrayed. Also, we consider an equal phase and equal magnitude being fed to each antenna element.

Finally, a loop is executed in Matlab code for different array combinations and different number of antenna elements. The code achieved the results of input impedance for X-axis and Y-axis and is recorded in Table 3.1. The same is extended for XY-plane configuration and recorded in Table 3.2.

No: of Antennas	A) Input Impedance along X-axis	B) Input Impedance along Y-axis
1X1	7.89Ω	7.89Ω
2X1	8.19Ω	8.19Ω
4X1	8.43Ω	8.43Ω
8X1	8.60Ω	8.60Ω
16X1	8.71Ω	8.71Ω
64X1	8.81Ω	8.82Ω

Table 3.1: Input impedance values of different number of short dipole antennas arranged linearly along: A) X-axis, and B) Y-axis.

No: of Antennas	Input impedance along XY Plane
1X1	7.89Ω
2X2	9.04Ω
4X4	12.7Ω
8X8	18.45Ω

Table 3.2: Input impedance values of different number of short dipole antennas arranged along XY-plane.

It can be concluded from the Table 3.1 that regardless the number of antenna elements along X-axis or Y-axis, the input impedance change is the same except where the number of antennas is 64. Here, due to internal miscalculation of Matlab and complexity of resolution, a little variation is observed. This observation is sensible since the dipole properties allow it to radiate equally in all directions, and therefore, alignment in either X-axis or Y-axis should not differ. However, it can be seen that as the number of antennas increase, the impedance change being observed is not so significant but changes less as the number of elements is increased which can be observed in the graph of Figure 3.4.

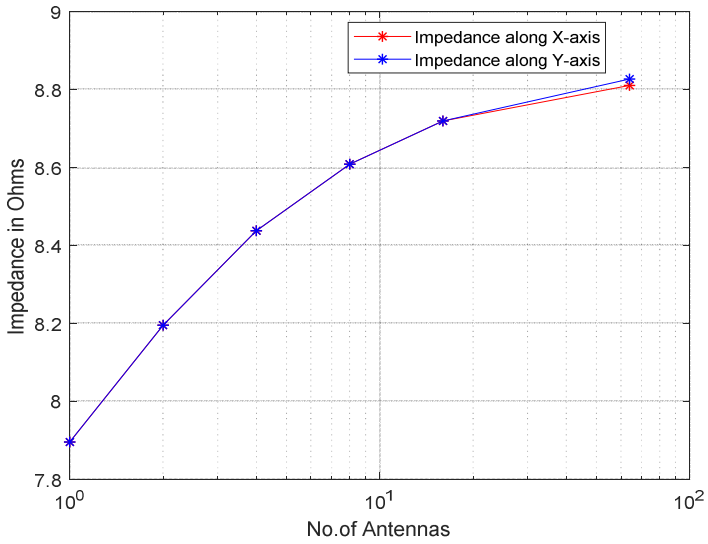

Figure 3.4: Input impedance variation of short dipole in array arranged along X-axis and Y-axis.

However, the change in input impedance along XY-plane as given in Table 3.2 is considerable and cannot be ignored as in the case of linear arrays. When the number of antennas is increased the change also increases with a considerable factor depicted in graph of Figure 3.5.

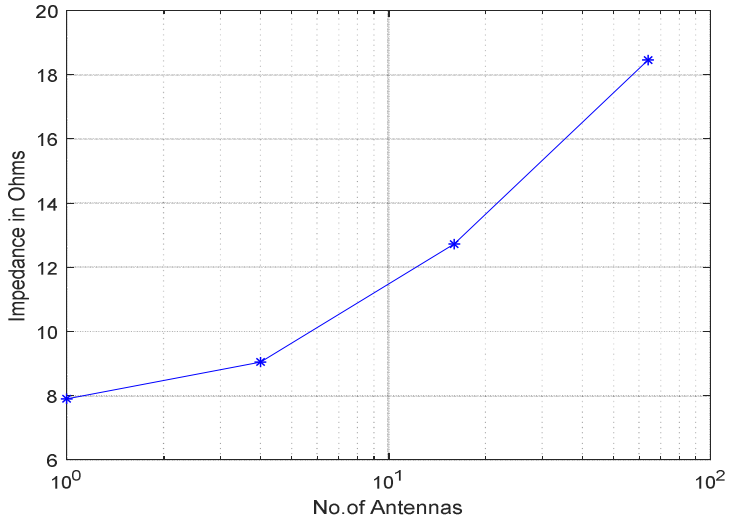

Figure 3.5: Input impedance variation of short dipole in array arranged along XY-plane

3.2.2 Resonant wire antenna

This is the simplest form of any antenna which is considerably larger than the short dipole discussed previously. Dipoles are basically the resonant antennas which resonate at a particular frequency with standing waves of radio current flowing back and forth between their ends. Thus, the length of the dipole elements is determined by the wavelength of the waves used. The most common form is the half wave dipole, in which each of the two rod elements is approximately quarter of the wavelength, so the whole antenna is a half wave length long[9].

As depicted in Figure 3.6, the center point is where the current is maximum and the voltage is at minimum, this makes a suitable point for feeding the antenna as it presents low impedance.

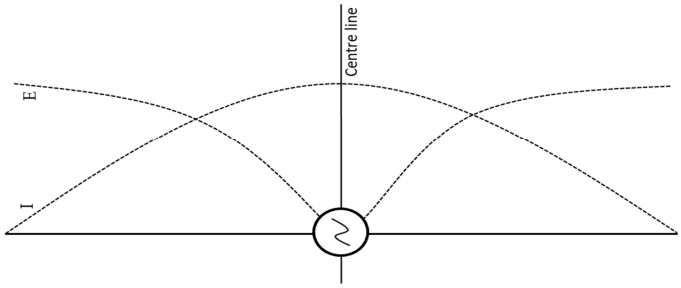

Figure 3.6: Voltage(E) and current(I) relationship in center fed resonant half wavelenght wire antenna.

The far field equations of the resonant dipole antenna are given as below.

$$E_\theta = \frac{i\eta}{2\pi}.I\,\frac{\cos(\frac{\pi}{2}cos\theta)}{sin\theta}\,\frac{e^{-ikr}}{r} \tag{3.18}$$

$$H_\emptyset = \frac{i}{2\pi}.I\,\frac{\cos(\frac{\pi}{2}cos\theta)}{sin\theta}\,\frac{e^{-ikr}}{r} \tag{3.19}$$

The same procedure is followed to first check the input impedance of single resonant wire antenna and then the corresponding array factor is multiplied to get the desired configuration results as in case of short dipole. Table 3.3 and Table 3.4 show input impedance along linear (X-axis and Y-axis) and planar (XY-plane) arrays, respectively.

No: of Antennas	A) Input Impedance along X-axis	B) Input Impedance along Y-axis
1X1	73.13Ω	73.13Ω
2X1	77.14Ω	77.14Ω
4X1	80.47Ω	80.47Ω
8X1	82.88Ω	82.88Ω
16X1	84.46Ω	84.46Ω
64X1	85.86Ω	86.02Ω

Table 3.3: Input impedance variation of resonant half wavelength dipole antennas in array arranged along X-axis and Y-axis.

No: of Antennas	Input impedance along X-Y plane
1X1	73.13Ω
2X2	86.01Ω
4X4	124.10Ω
8X8	183.12Ω

Table 3.4: Input impedance variation of resonant half wavelength dipole antennas in array arranged along XY-plane.

As it can be observed from Table 3.3 that the input impedance increases as the number of elements is being increased in the same manner as that of short dipole antenna. Also the Table 3.4 shows the same variation in XY-plane as that of short dipole. Both the variations can be observed in the graphs of Figure 3.7 and Figure 3.8.

Moreover, in the case of linear arrays, it can be seen that as number of antenna elements is doubled, the graph progresses less steeper. On the other hand, as the number of antennas is doubled in XY-plane, the impedance increases at much higher rate which makes the graph even steeper.

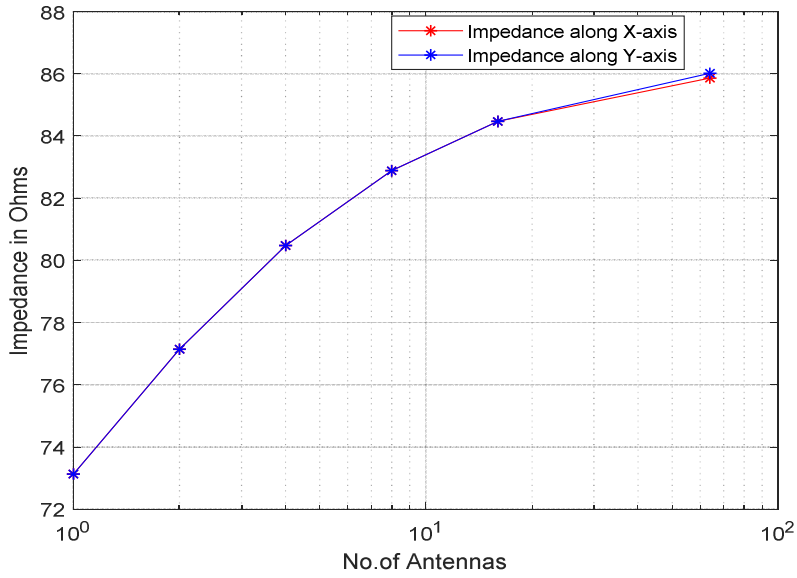

Figure 3.7: Input impedance variation of resonant wire antenna array arranged along X-axis and Y-axis.

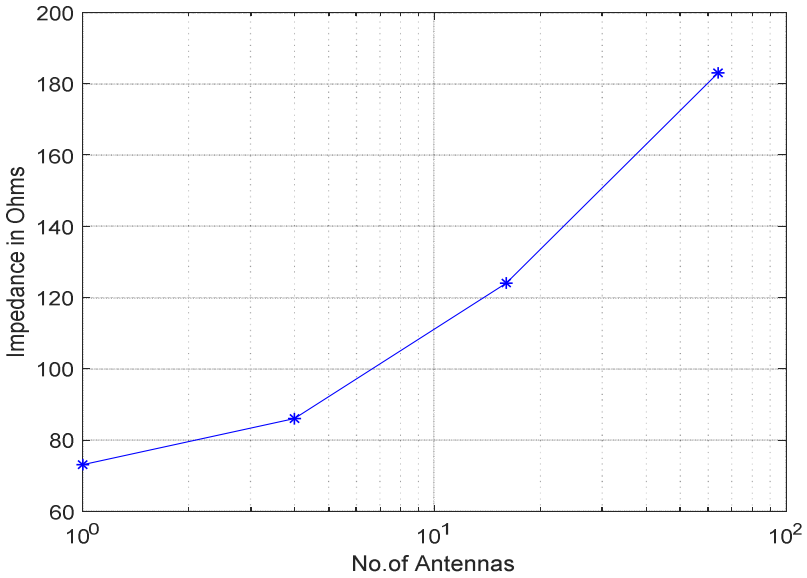

Figure 3.8: Input impedance variation of resonant wire antenna array arranged along XY-plane

Since, short dipole antenna and resonant wire antenna belong to the same class (Resonant and narrow bandwidth antennas), thus, they behave in the same manner. Both have the same radiation patterns and variation of input impedance when they operate in array combination which is evident from the analysis of presented graphs and tables.

3.2.3 Patch Antenna

3.2.3.1 A Brief History

In year 1953, it was G.A Deschamps who first introduced the concept of printed antennas[37]. Initially the development was slow and it took two decades for scientist Robert E. Munson to realize the first printed antenna[38]. The first official conference in 1979 in Mexico attracted the attention of scientists towards such printed antennas[39]. The proceedings of the conference were included in special publication issue of IEEE transactions on antenna and propagation[40]. Later on, the first book written by Bahl and Bhartia became the reference on such antennas[41]. Soon after that Pozar published the first work in the field of coupled aperture Microstrip antennas which helped to draw the attention of scientific community towards such printed antennas[42].

3.2.3.2 General introduction to patch antennas

The patch, usually made of copper, can have various shapes (Figure 3.9), but rectangular and circular patches can cover all the possibilities in terms of radiation pattern, bandwidth and polarization. Regarding the gain, it shows great versatility because this gain can vary from 4 to 10 dBi.

These antennas have many advantages in different applications because of low weight, low volume, low cost and easily manufactured.

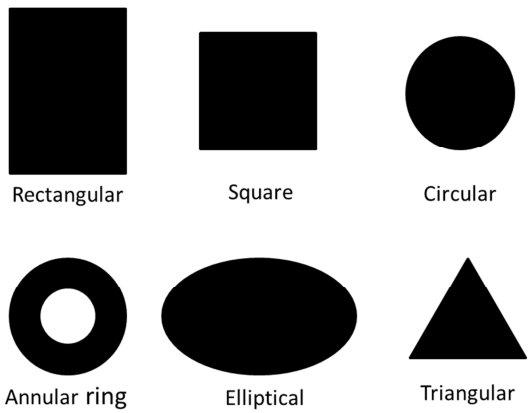

Figure 3.9: Patch antenna in different shapes and forms.

The conventional patch antenna has basically three layers; the patch, the substrate and the ground plane (Figure 3.10). The antenna usually is a highly conductive metal like copper of any shape of size depending upon its use and applicability.

In the Figure 3.10 the patch antenna has simply been shown in which the patch sits on the top of the dielectric substrate material of any thickness. The substrate is grounded by the sheet of metal of the same type of the patch. As shown, the nature of the antenna is such that the electric field appears to be maximum on either of the ends of its lengths and

quite null in the center, due to the standing waves passing through it. So, the radiation from the patch antenna is such that it radiates at both the edges. A convenient radiation model is then two thin apertures located at these both edges.

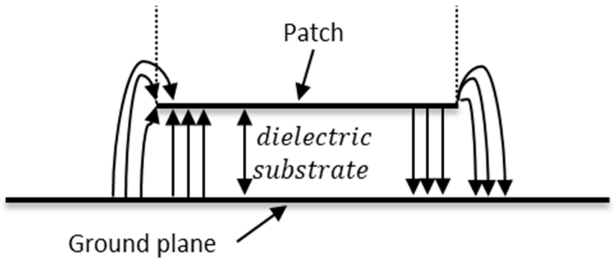

Figure 3.10: Rectangular Patch Antenna structure and its radiation due to fringing fields.

It is then possible to consider that the patch antenna shares two equal sized apertures of length Δ along the width W_p which forms the area of the apertures where radiation takes place as depicted in Figure 3.11. Aperture is merely an extra virtual length on either ends of the patch due to fringing of the electric field. In order to excite primary mode (TM_{10}) in patch antenna, the length of the patch is kept slightly less than the half of the wavelength in the effective medium (quasi-TEM mode approximation) [9].

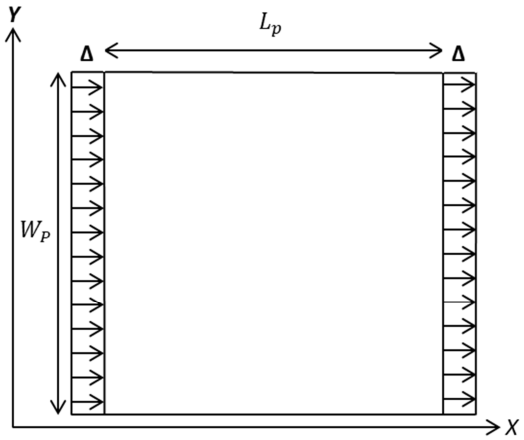

Figure 3.11: Patch antenna with two apertures of length Δ along the width of the patch.

Fringing is basically the sole reason for patch antenna radiation. Since, the patch antenna resembles an open-circuit transmission line from the electric point of view, current at the ends is zero, while maximum at the center of the patch[42]. This explains why the impedance is maximum at the ends, and zero at the center. This has been illustrated through Figure 3.12.

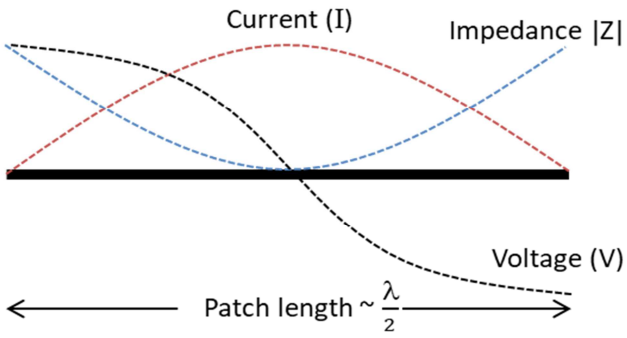

Figure 3.12: Current, voltage and impedance relation w.r.to patch antenna length[43].

Typical patch antenna edge impedance depends upon different factors: substrate permittivity, width and height. The value typically ranges from 150Ω to 300Ω [44].

However, the 50Ω (feeding point) that is required for matching lies at a certain point in between the center and either end of the patch along its length (Figure 3.13). The input impedance can be found by following expression[45].

$$R_i = \frac{1}{2G}\mathrm{Sin}^2\frac{\pi x}{L} \qquad for\ 0 \le x \le \frac{L}{2} \tag{3.20}$$

Where;

R_i is desired feed impedance, x is the distance (along the length) from center of the patch towards the edge and L is the length of the patch.

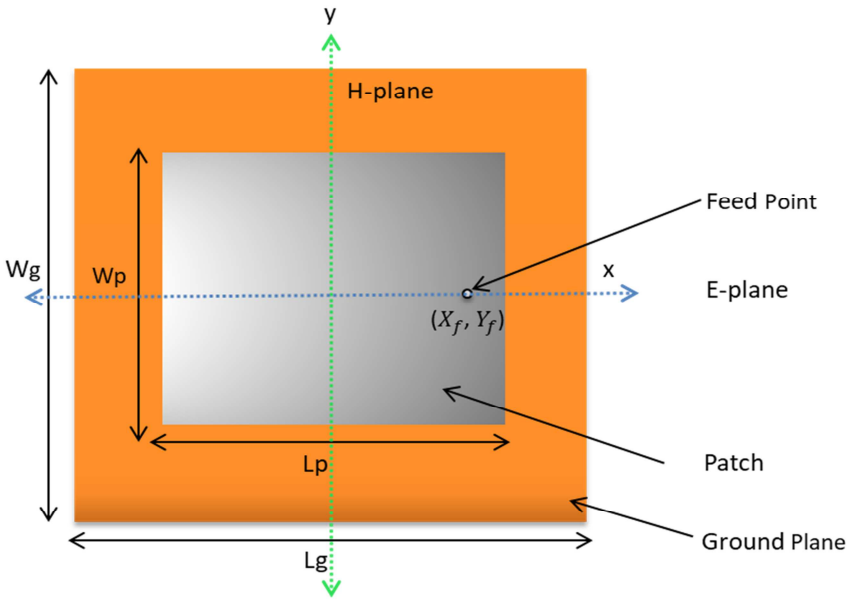

Figure 3.13: Patch antenna showing feed point, width and length and E and H-planes.

3.2.3.3 Impedance evaluation of patch antenna

In order to analyze the effect of total radiation from arrays and consequent impedance evaluation, the same pattern previously done for short dipole antenna and resonant wire antenna is applied to test and verify the efficiency of Matlab code for single patch antenna element then the concept is further extended towards array combinations.

In this context, we first evaluate the impedance of single patch from the total radiated power and then validate it with radiation loss equation. The array impedance evaluation is then carried out.

Here, the following equations of the patch (equation (3.21) – equation (3.24)) are set to size the patch antenna.

$$W = \frac{\lambda_o}{2}\left(\frac{\varepsilon_r+1}{2}\right)^{-1/2} \tag{3.21}$$

$$L = \frac{\lambda_o}{2\sqrt{\varepsilon_{eff}}} - 2\Delta \tag{3.22}$$

$$\varepsilon eff = \frac{\varepsilon_r + 1}{2} + \frac{\varepsilon_r + 1}{2}\left((1 + \frac{10h}{W})^{-1/2}\right) \tag{3.23}$$

$$\Delta = 0.412h.\frac{(\varepsilon_{eff} + 0.3)\left(\frac{W}{h} + 0.262\right)}{(\varepsilon_{eff} - 0.258)\left(\frac{W}{h} + 0.813\right)} \tag{3.24}$$

where W is the width of the patch antenna, L the length, h the height of substrate, ε_r the substrate relative permittivity, ε_{eff} the effective permittivity, and Δ is the added length due to fringing fields

3.2.3.4 One Antenna Element Testing

For a feed point at the radiating edge, the input impedance is at maximum and for a feed point at the center of the patch, the input impedance is at minimum. Knowing the far field expression, one can determine the radiated power, by numerical integration, and the input impedance of the patch at the feed point can be calculated.

The input impedance at the edge of the patch can be evaluated by the following formula:

$$Z_{in} = \frac{V_0^2}{2P} \tag{3.25}$$

Where, V_o represents voltage at the edge of the patch which we suppose one volt and P represents the total radiated power by the antenna in free space and is given by the expression:

$$P = \frac{1}{2}\oiint E \times H^{*} ds \tag{3.26}$$

Where E and H fields in the power equation represents the far field equations for the rectangular aperture (half of a patch antenna) and are given by equation 3.27 and equation 3.28. Here, the length of the patch has been taken along the X-axis which is considered to be the direction of E-plane since electric field lines are parallel to it (Figure 3.13).

$$E_{\phi} = \frac{ie^{-ikr}}{\pi r}\left[-\cos(\phi)\cos(\theta)\,\vec{\theta} + \sin(\phi)\,\vec{\phi}\right]V_o \frac{\sin(\frac{\pi W}{\lambda_o}\sin(\theta)\cos(\phi))}{\sin(\theta)\cos(\phi)} \tag{3.27}$$

$$H_{\theta} = \frac{ie^{-ikr}}{\eta\pi r}\left[-\cos(\phi)\cos(\theta)\,\vec{\theta} + \sin(\phi)\,\vec{\phi}\right]V_o \frac{\sin(\frac{\pi W}{\lambda_o}\sin(\theta)\cos(\phi))}{\sin(\theta)\cos(\phi)} \tag{3.28}$$

Since the radiation from a rectangular patch is equivalent to the radiation of two apertures and thus in order to have entire radiation in half of the space ($0 \leq \theta \leq \pi/2$ and $0 \leq \emptyset \leq 2\pi$), the far field equations should be multiplied by a corresponding two element array factor spaced by half of the wavelength given below (equation 3.29).

$$F_r = 2\cos(\frac{\pi}{2}.\frac{1}{\sqrt{\mathcal{E}eff}}cos\emptyset sin\theta) \tag{3.29}$$

Finally, the far field equations (equation 3.27 and equation 3.28) along with two element factor (equation 3.29) are applied in Matlab code to evaluate total radiated power. Once the radiated power for a single patch is obtained, the input impedance can be evaluated through equation 3.25. In this way, the resultant impedance is $\boldsymbol{Z_{in} = 160.36\Omega}$.

However, in order to ensure the validity of the method, the impedance value is being compared with that obtained from radiation loss equation where we assume, according to cavity model, the feeding point being at the patch edge[46]. Equation 3.30 and equation 3.31 show the way of using this method as they are applied in the Matlab code where G is the radiation loss in admittance equation i.e. $Y_{in} = 2(G + jB)$.

$$G = \frac{\pi W}{\eta\lambda}\left[1 - \frac{(kh)^2}{24}\right] \tag{3.30}$$

$$Z_{in} = \frac{1}{2G} \tag{3.31}$$

The input impedance obtained from this method is **160.91Ω** which is almost the same obtained from the far field equations. It shows that the far field equations are valid and can be further applied to array concept.

3.2.3.5 Antenna Array Calculation

A patch antenna with two apertures on either ends has been tested earlier but now the same is what we are going to do with antenna arrays. Here, by X-axis and Y-axis we refer to patch antennas oriented along E-plane and H-plane respectively as shown in Figure 3.14(a-b). The Figure 3.14(c) shows the planar array combination (XY-plane).

The far field equations of patch antenna (equation 3.27 and equation 3.28) with corresponding two element factor (equation 3.29) is multiplied with X-axis array factor (equation 3.32), Y-axis array factor (equation 3.33) and XY-array factor (multiplication of equation 3.32 and 3.33) to yield total radiated power (by using equation 3.26) in E-plane oriented array, H-plane oriented array and XY-plane array, respectively.

$$\vec{E} = \overrightarrow{E_o} \frac{sin(\frac{n.k.sin\theta cos\phi.dx}{2})}{sin(\frac{k.sin\theta cos\phi.dx}{2})} \tag{3.32}$$

$$\vec{E} = \overrightarrow{E_o} \frac{sin(\frac{n.k.sin\theta sin\phi.dy}{2})}{sin(\frac{k.sin\theta sin\phi.dy}{2})} \tag{3.33}$$

Here, n is number of antenna elements, k is the wave number, dx and dy are the X-axis and Y-axis inter-element distances, respectively.

Here, the equations are coded with a separation distance of half of the wavelength in vacuum. Once the total radiated power due to entire array combination is computed, the total power is then divided by the number of antenna elements (n) in each configuration of the array to yield average input impedance values of individual antenna elements by using equation 3.25. Here, is the main assumption of the proposed calculation. Indeed, as we assume that there is no coupling phenomenon between elements; all elementary antennas are affected in the same manner. This is why we propose to divide the radiated power over the number of antennas arrayed. Also, we consider an equal phase and equal magnitude being fed to each antenna element.

In this way, a number of 1, 2, 4, 8, 16 and 64 (Table 3.5, column 1) patch antenna elements arranged collinearly (along E-plane) has been coded. The input impedance evaluated for each combination of antenna elements has been presented in Table 3.5, column 2. Column 3 shows the input impedance evaluated at 50 Ω feed point.

For an analysis, the values of input impedance in E-plane drop at considerable rate as the number of antenna elements increases in the array as depicted in Table 3.5 and Figure 3.15.

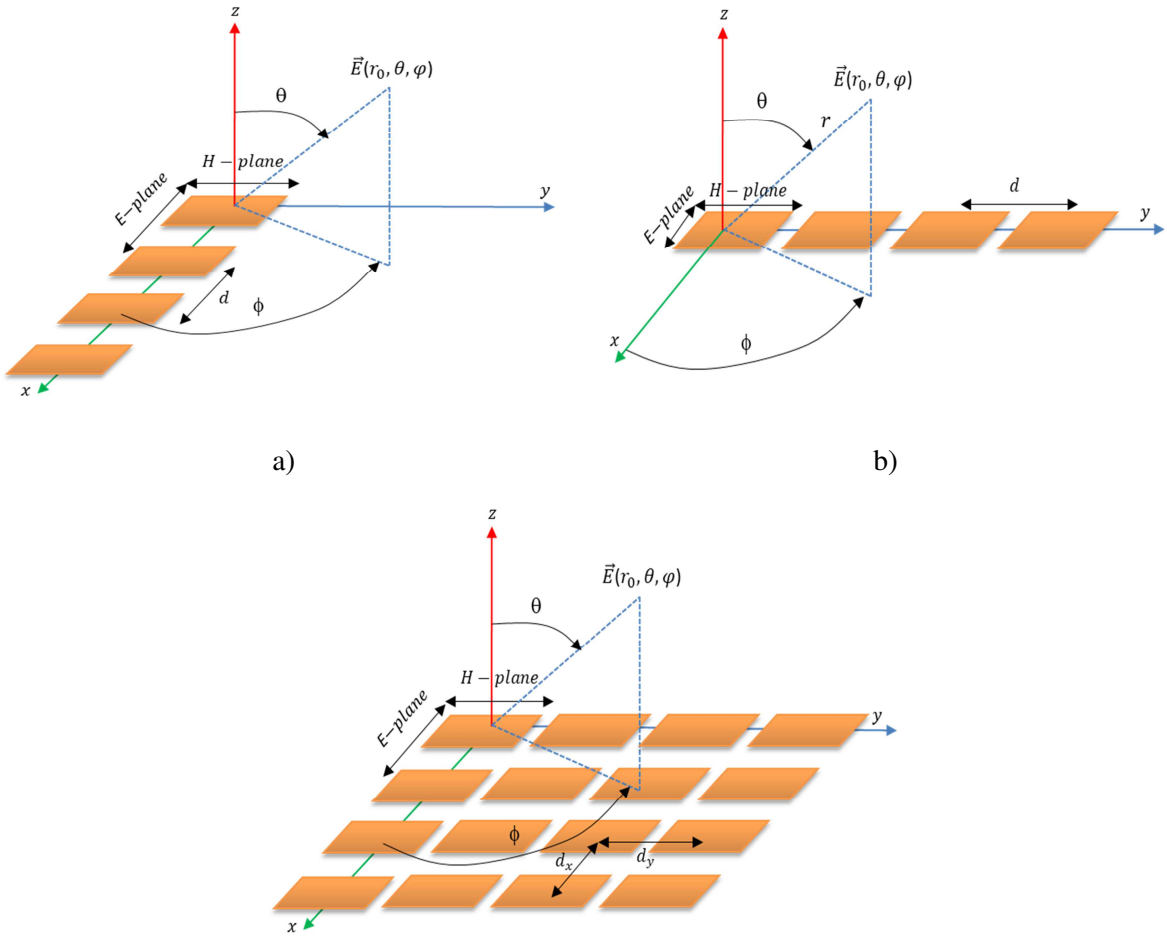

Figure 3.14: Patch antenna array arranged along: a) X-axis (E-plane), b) Y-axis (H-plane), c) XY-plane

No: of Antennas	Input Impedance at the edge of the Patch arranged along X-axis (E-plane)	Input Impedance at 50Ω point of the Patch arranged along X-axis (E-plane)
1X1	160.36 Ω	50.00 Ω
2X1	117.45 Ω	30.31 Ω
4X1	100.14 Ω	28.49 Ω
8X1	91.31 Ω	23.57 Ω
16X1	86.62 Ω	22.01 Ω
64X1	82.64 Ω	21.24 Ω

Table 3.5: Input impedance of patch antenna elements arranged collinearly along x-axis (E-plane).

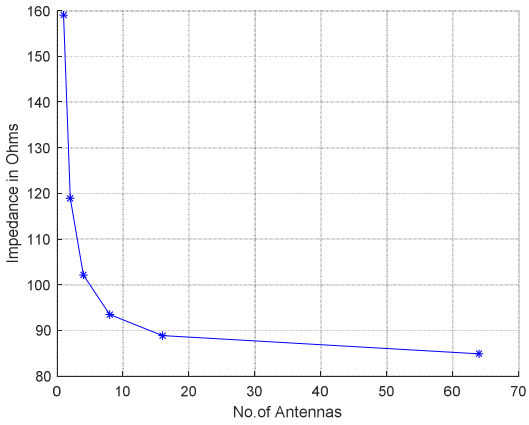

Figure 3.15: Input impedance variation due to total radiation versus number of antenna elements arranged along E-plane.

In the same manner, the input impedance along H-plane and XY-plane has been coded. Table 3.6 and Table 3.7 show the input impedance values due to total radiation arranged along H-plane and XY-plane, respectively. We observe that the input impedance in H-plane increases in drastic manner as shown in Table 3.6(column 2) and Figure 3.16(a). In case of XY-plane array, the impedance increases and decreases in an unpredictable manner as shown through Table 3.7 and Figure 3.16(b).

Of course, we are aware that the total radiation approach is not enough by itself to compute the input impedance of each element. In this approach, we do not take into account mutual coupling. Here, we have considered free space combination as a probable contributor so we tried to investigate this part by isolating this contributor considering the others as null. Nevertheless, it will be interesting to have a deeper approach of all other possible contributors which in terms could explain the impedance shift on antenna array. However, the results suggest that even though there is no mutual coupling, the input impedance of individual antenna elements varies in an array inferring the cause being the total radiation. We are also aware that this approach is not sufficient by itself to justify the active impedance but can be considered.

No: of Antennas	**Input Impedance at the edge of the Patch arranged along Y-axis (H-plane)**
1X1	160.36 Ω
2X1	300.43 Ω
4X1	371.06 Ω
8X1	480.31 Ω
16X1	601.62 Ω
64X1	797.78 Ω

Table 3.6: Input impedance variation of patch antenna elements arranged collinearly along Y-axis (H-plane).

No: of Antennas	Input impedance at the edge of the patch arranged along XY-plane
1X1	160.36 Ω
2X2	238.26 Ω
4X4	222.94 Ω
8X8	245.48 Ω

Table 3.7: Input impedance variation of patch antenna elements arranged along XY-plane.

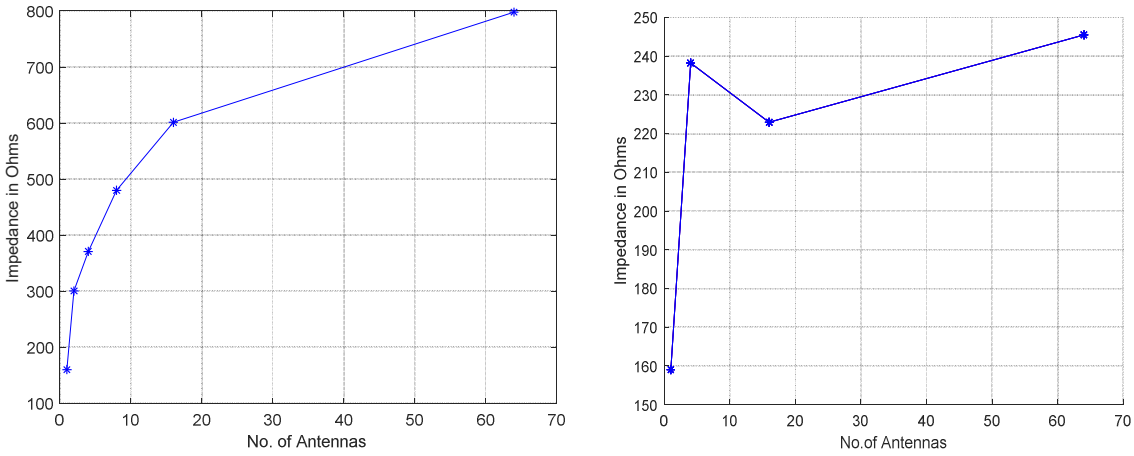

a) b)

Figure 3.16: Input impedance variation due to total radiation versus number of antenna elements arranged along: a) H-plane, b) XY-plane.

3.3 Conclusion

In this chapter, we have proposed theoretical model to evaluate input impedance of short dipole, half wavelength resonant antenna and rectangular patch antenna from their far field equations. After validation of the input impedance evaluation of single antenna, the concept is further extended to array antennas. In this approach, we do not take into account mutual coupling. Here in our approach, we have considered free space combination as a probable contributor so we tried to investigate this part by isolating this contributor considering the others as null. Nevertheless, it will be interesting to have a deeper approach of all other possible contributors which in terms could explain the impedance shift on antenna array. However, the results suggest that even though there is no mutual coupling, the input impedance of individual antenna elements varies in an array inferring the cause being the total radiation. We are also aware that this approach is not sufficient by itself to justify the active impedance but can be considered.

In the next chapter, we would develop 3D simulation models and carry out measurement analysis to further clarify theoretical results proposed in this chapter.

Chapter 4

Active S-parametric analysis

Matlab is a tool to solve problems numerically, that is, in finite-precision arithmetic. Therefore it produces approximate rather than exact solutions, and should not be confused that it only takes inputs and codes supplied to it and only generates the outputs depending upon the codes assigned to it. In other words, it does not take into consideration the environment surrounding radio frequency components like antennas. Therefore, the reliability on its results might not be that much accurate when compared to real life measurements.

For the purpose of radio frequency characterization, there exists 3D simulation softwares purposefully designed for creating accurate results and solutions for electromagnetic design. These softwares take into account all internal and external factors affecting the unit under test. Therefore, such softwares are reliable and user friendly as compared to Matlab.

After characterization radio frequency components in 3D simulation softwares, the same can be manufactured and tested through real time instruments in the laboratory. This is what we develop in this chapter, that is, to validate results of theory (MATLAB coded results) of Chapter 3 through 3D simulations and measurement.

In order to clarify Matlab code through 3D simulations and measurement we have to take into considering following key points;

- S-parametric analysis of simultaneously excited antenna elements in an array (the concept of total radiation).

- Considering environment factors (Mutual coupling, array edge effects) in arrays.

From a circuit point of view, an antenna is characterized from its scattering matrix, commonly called S-parameter matrix. The procedure to evaluate such parameters like return loss or reflection coefficient for a single antenna does not pose any issues. However, in the case of an array, the evaluation of S-parameters becomes more complicated. By definition, the reflection coefficient of an antenna is evaluated when all other sources in the network are powered off:

$$S_{ii} = \left.\frac{b_i}{a_i}\right|_{a_j=0,\quad for\ all\ j\ different\ from\ i} \tag{4.1}$$

S-parameters evaluated through equation (4.1) are called passive S-parameters. However, in case of an array networking, all elements are excited simultaneously by a single source, possibly out of phase and attenuated at the level of the unit radiators, depending on the desired radiation pattern.

Thus, in an array, each element interacts with each other (proximity coupling, radiation coupling etc) and the observed reflection coefficient at each port evaluated by passive approach is no longer representative of the reality.

It is therefore necessary to implement a rigorous method for evaluating these so-called active S-parameters (equation (4.2)). That is to say, in such a way that all antennas are fed simultaneously with synchronous waves, i.e:

$$S_{ii} = \left.\frac{b_i}{a_i}\right|_{a_j \neq 0} \tag{4.2}$$

Electromagnetic simulation softwares (CST MWS or HFSS Ansys) evaluate array scattering parameters ($S_{i,j}$) based on passive scatterings. This is not sufficient to what we require. Even option of active S-parameters in latest versions of HFSS Ansys does not answer to the problem since these are also based on passive scatterings. As defined in [47], [48], active S-parameters are expressed in terms of passive scatterings as given by equation 4.3:

$$Active\_S_{mn} = \frac{\sum_{i=1}^{N} S_{mi} a_i}{a_n} \tag{4.3}$$

Where S_{mi} is passive coupling coefficient between antenna element i and m, a_i and a_n are the excitations of radiating element i and n respectively and N represents total number of antenna elements in the array.

It is believed that the mutual coupling in the mentioned formula (equation 4.3) caters all the couplings in the array when the array radiate simultaneously (based on passive scatterings). As a reminder, in this case, one antenna at a time is powered on and the rest of antennas are matched loaded. However, when all antennas radiate at the same time, the scattering analysis essentially becomes a multiple scattering process where a simple linear combination of coupled power (as in case of equation 4.3) cannot be considered. Due to multiple scattering, here, coupling becomes essentially a non-linear process which invalidates the principle of superposition in highly coupled arrays [24]. That is why we propose, that the passive scattering matrix to evaluate active S-parameters perhaps does not represent the reality when all antennas radiates simultaneously (with coherent mode of excitation). Thus, the actual active S-parameters (equation (4.2) should present different values as compared to so called active S-parameters of equation (4.3).

To do this, we have to develop a new way to evaluate through measurement the true active S matrix of an array when all antennas radiate simultaneously. To be consistent, these results have to be compared with the results obtained through typical approach using the passive scattering matrix as given in the equation 4.3.

4.1 3D simulation & measurement

In order to be consistent, 3D simulation with HFSS Ansys is used to simulate resonant antenna arrays and to observe their S-parameters (input impedance) according to equation (4.1) and equation (4.3). First, resonant half wavelength dipole linear arrays are analyzed.

4.1.1 3D Simulation of $0.5\lambda_0$ resonant wire dipole antenna

A single dipole is first designed and optimized at 5GHz for the verification in HFSS Ansys for input impedance in such a way that it resonates well enough. Table 4.1 shows the geometry parameters of the optimized dipole antenna.

DESCRIPTION	VALUES
Wave Length of the dipole (λ_o)	60 *mm*
Radius of the dipole	0.01 *mm*
Resonant length of the dipole	0.475 λ_o
Feeding gap between the two poles	0.125 *mm*

Table 4.1: Geometry parameters of single half wavelength resonant wire dipole antenna.

Radiation box distance is so designed such that it does not reflect back any radiation from its boundary. Thus, Radiation box is kept at $\frac{\lambda_o}{4}$ and $\frac{\lambda_o}{10}$ in width and height respectively from both sides from the dipole. It is generally recommended to be the minimum distance so that it does not reflect back any radiation from a dipole shown in Figure 4.1.

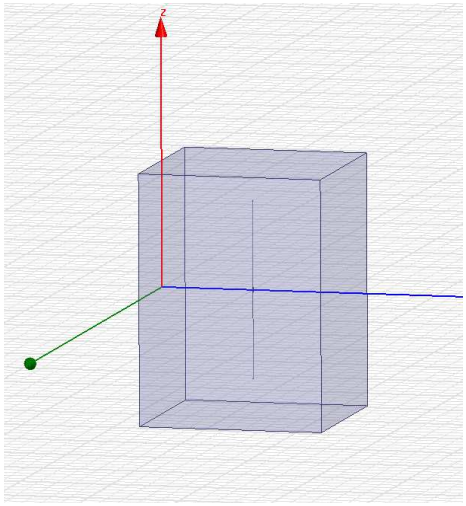

Figure 4.1: Single dipole screen shot with radiation box.

Figure 4.2(a) shows the optimized return loss of the dipole antenna. In viewing the impedance as a function of the dipole length, it can be noted that by reducing the length slightly by $0.475\lambda_o$, the input impedance of the dipole antenna becomes $Z_{in} \simeq 73.7\ \Omega$ with

no reactive part which can be observed in Figure 4.2(b) by de-normalizing the impedance of smith chart. This is only valid if the dipole radius is very thin which in this case is $0.01mm$.

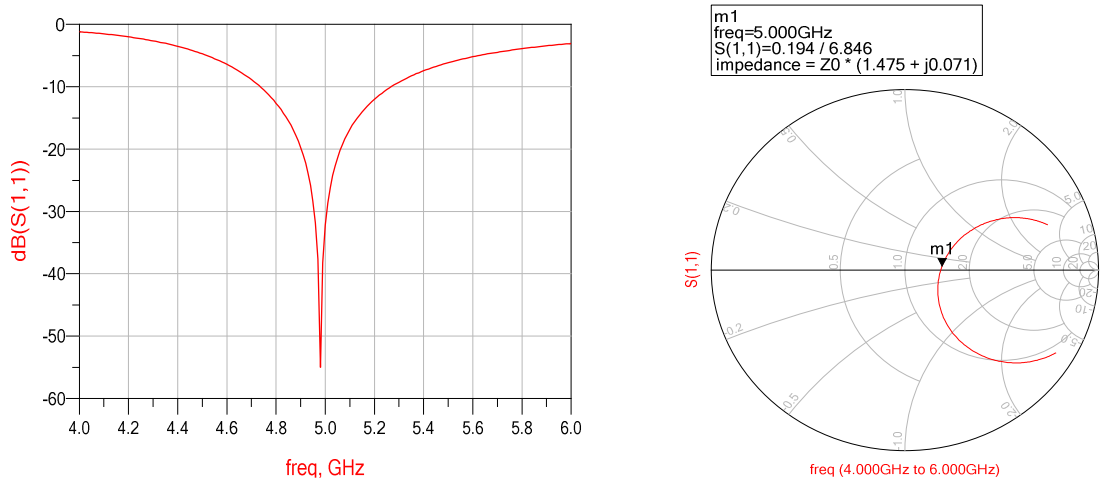

a) b)

Figure 4.2: Single dipole antenna: a) optimized return loss, b) Smith chart.

Thus, the input impedance observed from the Smith chart by HFSS simulation is about 73.7 Ω and from the Matlab it is 73.13 Ω. Here, the difference is of about 0.5 Ω between the Matlab and HFSS results which is quite negligible. Therefore, we can now extent towards array combinations.

4.1.2 3D Simulation of half wavelength resonant wire dipole antenna array

Mutual coupling between the antenna elements is a phenomenon which is due to an exchange of energy between antennas. Since Matlab code is designed in such a way that it does not take into account the effect of mutual coupling. Therefore, HFSS does consider and calculates practical parameters including mutual coupling. In this regard, it is essential first to test the level of mutual coupling between two dipole antenna elements to check whether they present negligible coupling (below 20 dB) when the dipoles are half of the wavelength apart.

– **Mutual coupling test between two elements distanced half wavelength apart**:

The antenna elements are spaced at half of the wavelength so that mutual coupling can be observed by running the simulation results of S_{12}. It can be observed from Figure 4.3 that S_{12} is about $-13.52dB$ which implies that mutual coupling at distance of half of the wavelength between antenna elements is quite considerable.

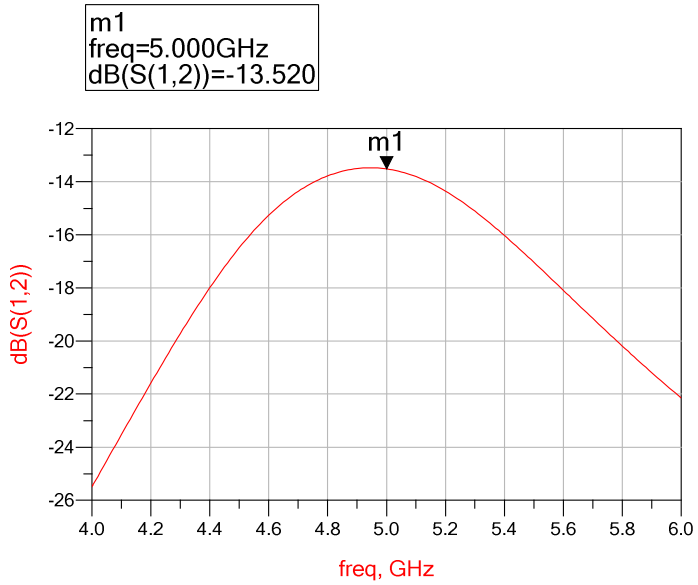

Figure 4.3: Mutual coupling test between two elements distanced half wavelength apart.

Therefore, here, we abandon further 3D analysis of dipole antenna arrays due to high coupling between them. We next, therefore, proceed to test patch antenna arrays in linear combinations to observe the level of coupling.

4.1.3 3D Simulation of rectangular patch antenna

First we design and optimize a single patch antenna at a resonant frequency of 5GHz. Once the antenna is optimized then the same will be inserted in collinear (E-plane) arrays. Table 4.2 shows the optimized parameters of a patch antenna.

DESCRIPTION	VALUES
Targeted Frequency	5 GHz
Patch and ground material	copper (35μm Thick)
Patch antenna length	13.185 *mm*
Patch antenna width	17.38 *mm*
Substrate material	FR4 epoxy (ξr = 4.4,tan δ = 0.02)
Height of the Substrate	1.6 *mm*
Substrate and ground length	73.13 *mm*
Substrate and ground width	77.38 *mm*
Feed point distance from the edge (X_f)	3.392 *mm*

Table 4.2: Geometry parameters of a single patch antenna element.

The S-parameters of the antenna prototype (Figure 4.4-a) show a good matching at 5GHz with return loss (S_{11}) of -35dB (Figure 4.4-b). At 5GHz the denormalized impedance

is 48.85+j1.3 Ω (Figure 4.5). Here, radiation box around the antenna is kept at $\frac{\lambda_0}{2}$ away from antenna geometry.

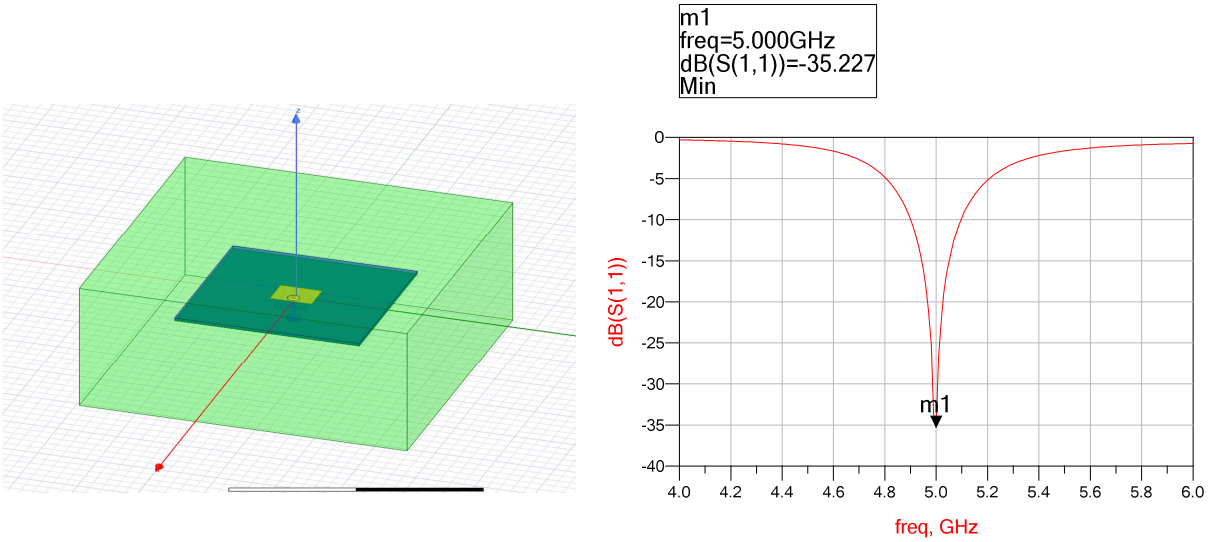

a) b)

Figure 4.4: a) Simulated Patch antenna model in HFSS, b) return loss of the optimized patch.

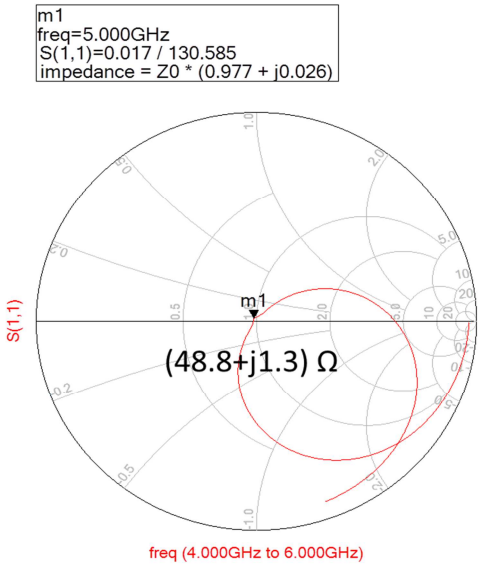

Figure 4.5: Smith chart of an optimized patch antenna.

4.1.3.1 3D simulation of rectangular patch antenna array and measurement

After optimizing a single patch antenna, the same can be inserted with other antenna element. Here, it is important to observe the level of coupling in between the antennas. In patch antenna arrays, mutual coupling may exist due to surface waves, near field coupling and far field coupling[49]. However, the level of coupling depends on the geometry of the antenna elements, inter-element distance, orientation and the dielectric substrate etc. Here,

in this particular case, we can observe that the width of the optimized patch is greater than its length. Hence in E-plane the level of coupling should be less than the level of coupling in H-plane due to their geometry[50]. Thus, first we would test two patch antennas (E-plane) for level of mutual coupling (under 20dB).

– **Mutual coupling test between two elements distanced half wavelength apart**:

Two patch antenna elements arranged along E-plane (Figure 4.6(a)) has been simulated. Figure 4.6(b) shows the return loss of each well matched antenna. In this case, it is observed that the mutual coupling (S_{12}) remains under 20dB (Figure 4.7).

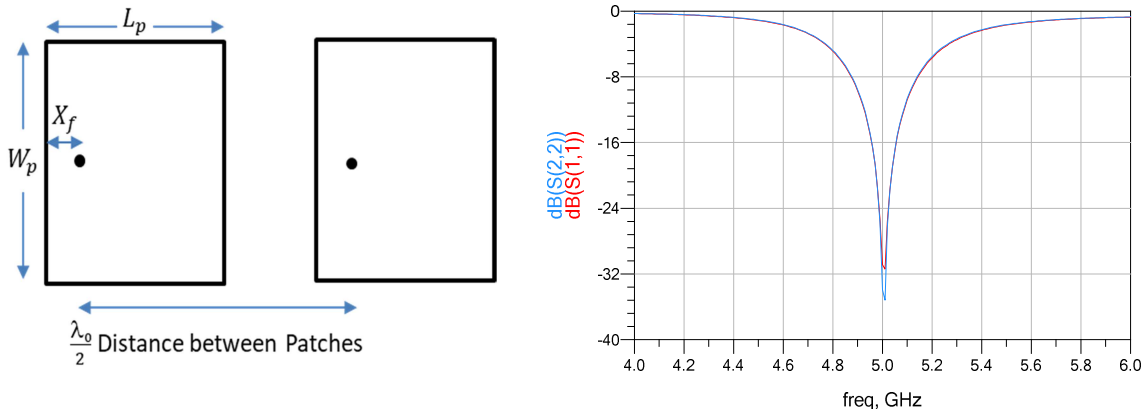

a) b)

Figure 4.6: Simulated two patch antenna elements: a) arranged along E-plane, b) return loss.

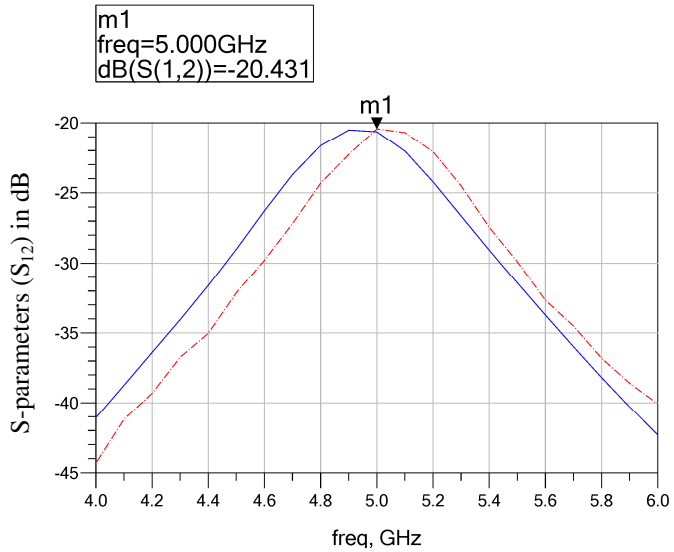

Figure 4.7: Mutual coupling between two E-plane antenna elements through: 3D simulation (solid curve), measurement (dashed curve).

Here, coupling remains under 20dB and we can extent antenna array combinations and can read corresponding S-parameters.

In Table 4.3 (Column A), input impedance of each antenna is extracted by a passive scattering matrix approach while column B gives the values of the input impedance when the two elements are excited according to equation (4.3). Despite the fact that both antennas are modeled with the same dimensions, we observe a slight difference for these two situations. This is mainly related to the mesh process which introduces a different mesh on the two antennas. Anyway, we observe a decrease in the impedance seen at the entrance of the two antennas in active mode. This reflects the importance of active S-parameters in antenna networks.

Input impedance in Ω @ 5GHz	**A) Zin passive**	**B) Zin active**
Antenna 1	(52.72-j0.50) Ω	(43.62-j6.75) Ω
Antenna 2	(51.67+j0.39) Ω	(42.86-j5.81) Ω

Table 4.3: Denormalized input impedance values via HFSS; A) Passive input impedance, B) Active input impedance

4.1.3.2 Measurement analysis of two elements

A lab prototype of two elements arranged along E-plane is fabricated and shown in Figure 4.8. The measurement procedure is then carried out using Rohde & Schwarz ZVA 24 vector network analyzer (Product Id: 1145-111OK26-100326-TU) [51] previously calibrated with SOLT(Short-Open-Load-Thru) calibration in the antenna access plan. Here the calibration kit utilized is Rohde & Schwarz kit ZV-Z135.

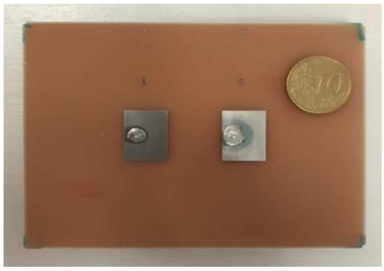

Figure 4.8: Two patch antenna elements arranged along E-plane configuration.

After setting up the equipment, the measurement procedure is carried out in two steps:

Step1: The passive S-parameters are determined using two VNA ports and the corresponding denormalized impedance is recorded in Table 4.4 (column A). The value of the impedance is extracted directly by observing the associated Sii parameter on the Smith chart (Figure 4.9-a) at the optimum operating frequency of the antenna. In our case, due to inaccuracy of etching, the antennas resonate at a slightly higher frequency i.e 5.06GHz. This error is minimal and does not affect the relevance of the observed results. The mutual

coupling is also under 20dB (Figure 4.7). The denormalized input impedance (column B) is extracted from Smith chart (Figure 4.9-b) according to equation (4.3).

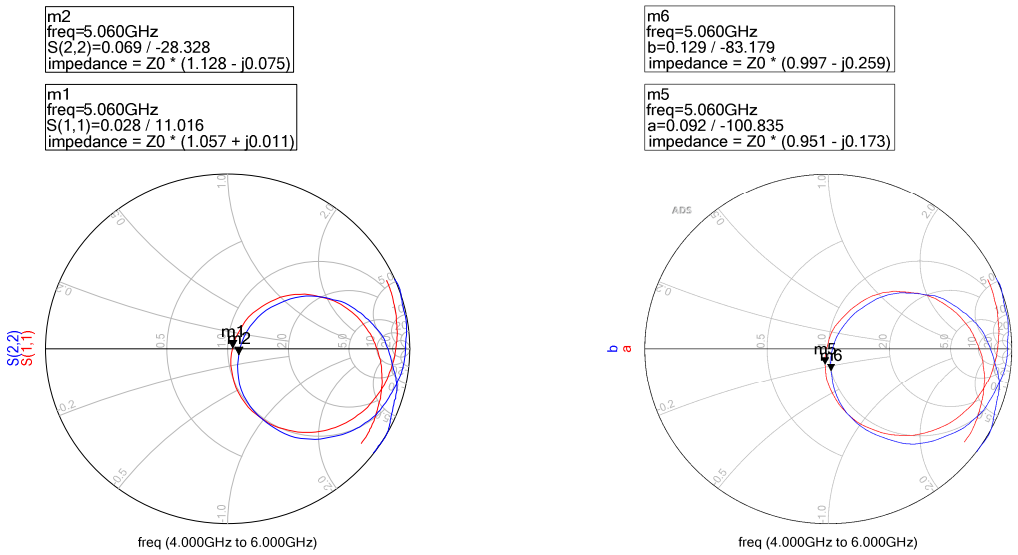

a) b)

Figure 4.9: Smith chart of two antennas according to; a) Passive S-parameters, b) Active S-parameters according to equation 4.3.

Step2: In a second step, the network analyzer is set to coherent mode. In this mode of operation, the input impedance is extracted from the observation of the fraction $\frac{b_1}{a_1}\Big|_{a_2 \neq 0}$ on the Smith chart and is recorded in Table 4.4 (column C). Table 4.4(column C) shows that when both antennas are lit simultaneously, the measured input impedance of the two antennas decreases. This decrease in impedance is close enough to the values obtained in column B.

Input Impedance in Ω @ 5.06 GHz	**A) One antenna is powered on**	**B) Zin active according to equation (4.3)**	**C) All antennas are powered on according to equation (4.2)**
Antenna 1	(52.8+j0.5)Ω	(47.5-j8.60)Ω	(46.9-j8.81)Ω
Antenna 2	(56.4-j3.7) Ω	(49.8-j12.9) Ω	(50.1-j12.7)Ω

Table 4.4: Input impedance of two patch antennas evaluated through measurement.

These preliminary results show that measurement of active S-parameters does not pose any problem with two antennas, however, when it comes to significant number of antenna array elements then the effect can be more noticeable. Therefore, in order to demonstrate the effect of active S-parameters, we next proceed to more than two elements.

4.1.3.3 3D simulation of four patch antenna array

The same procedure is now extended to four antenna elements arranged along E-plane formation and the 3D simulation results are recorded in Table 4.5.

Table 4.5 (column A) shows the values obtained through equation 4.1. Here, the antennas present a different value than 50Ω and it is probably due to the proximity of the other antenna elements. The antennas (1 and 4) and antennas (2 and 3) present also a slightly different value which is due to the introduced mesh. Column B shows the results of active S-parameters (equation 4.3) where the impedance is observed to decrease.

Input impedance in Ω @ 5GHz	A) Zin passive	B) Zin active
Antenna 1	(54.75-j0.07)Ω	(48.96-j3.84)Ω
Antenna 2	(52.89-j1.11)Ω	(40.89-j5.05)Ω
Antenna 3	(52.58-j0.90)Ω	(41.24-j6.91)Ω
Antenna 4	(53.80+j1.6)Ω	(48.47-j2.71)Ω

Table 4.5: Input impedance evaluated via HFSS for four patch antenna elements.

4.1.3.4 Measurement analysis of four elements

Measurement procedure can now be extended to four antenna elements. A patch antenna array of four elements along E-plane is fabricated (Figure 4.10). The problem here is to be able to excite all four antennas together using two ports of existing VNA!

Figure 4.10: Four patch antenna elements arranged along E-plane configuration.

The procedure to excite all antennas together and to measure true active S-parameters using two port VNA has been proposed in [47]. This is based on the measurement of a transmission coefficient in a configuration using a coupler and a balanced power divider (Figure 4.11). Calibration is first necessary in order to compensate for some of the errors introduced in the measurement procedure. However, the accuracy of the measurement depends intrinsically to the quality of the directional coupler which theoretically must present infinite directivity. Moreover, the use of the balanced power

divider introduces an imprecision as to the control of the phase at the level of the excited elements, which can pose problems of its validity.

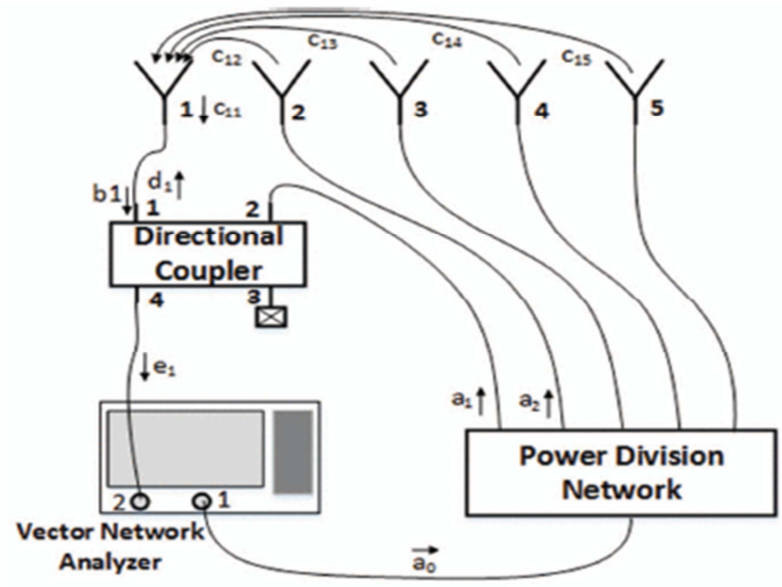

Figure 4.11: Measurement scheme using two port VNA [47].

Keeping in view the ambiguity concerning to directivity and calibration plane involved in previous method, we propose a measurement methodology based on the use of a four-port network analyzer to evaluate true active S-parameters of an antenna array (Figure 4.12). The measurement protocol is thus explained in terms of calibration and avoids the uncertainty of the use of the coupler and the power divider.

Basically, a balanced power divider allows the coherent excitation of the antennas. A prior measurement of each of the transmission coefficients of this power divider and the associated coaxial cables make it possible to validate the equilibrium of the amplitudes and phases at the accesses of the antennas ((Figure 4.12 -Terminal d). This measurement also guarantees to compensate the amplitude and the relative phase at the level of the antenna to be measured by controlling the parameters of the source associated with this port (having accuracy of 0.1dB in magnitude and 1° in phase).

Measurements are carried out again in two steps:

Step1: Each antenna is powered on individually by single port of VNA with 1 milliwatt power and corresponding passive input impedances are recorded in Table 4.6 (Column A). It can be observed that, as for simulation, a symmetrical behavior is observed and the input impedance of all antennas remains quite close to 50Ω at the chosen frequency. Here, due to manufacturing tolerance, we observe a frequency shift (5.07GHz). Table 4.6 (Column B) shows the input impedance evaluated according to equation 4.3 where the impedance shows a decrease in the value.

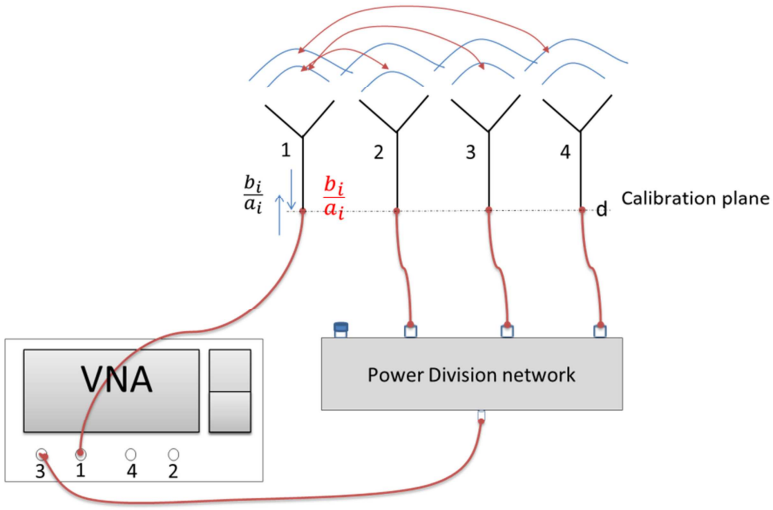

Figure 4.12: Measurement scheme.

Step2: All four antenna elements are powered together simultaneously according to coherent mode. In accordance with measurement scheme of Figure 4.12, both ports of VNA are set to coherent mode. One port of the VNA excites a single antenna and the other excites the rest of the antennas simultaneously through the splitter. In this way, each antenna impedance is recorded from their respective Smith charts (Figure 4.13, a-d) and recorded in column C of Table 4.6. The screen shot of the measurement setup is shown in Figure 4.14.

Input impedance in Ω @ 5.07GHz	**A) One antenna is powered on**	**B) Zin active according to equation 4.3**	**C) All antennas are powered on simultaneously**
Antenna 1	(46.3-j0.6) Ω	(43.55-j7.41) Ω	(44.85-j9.35)Ω
Antenna 2	(52.2-j1.15) Ω	(45.05-j15.42)Ω	(47.1-j17.7) Ω
Antenna 3	(52.25-j0.4) Ω	(45.25-j13.05)Ω	(46.15-j14.1)Ω
Antenna 4	(49.15-j0.5) Ω	(45.6-j6.31) Ω	(46.7-j8.22) Ω

Table 4.6: Input impedance of four patch antennas evaluated through measurement.

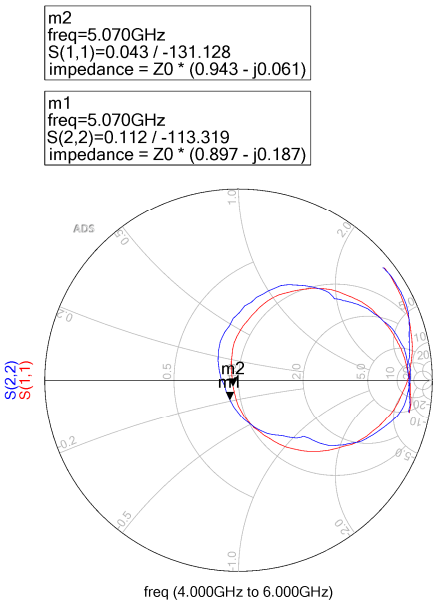

a) Smith chart of antenna 1

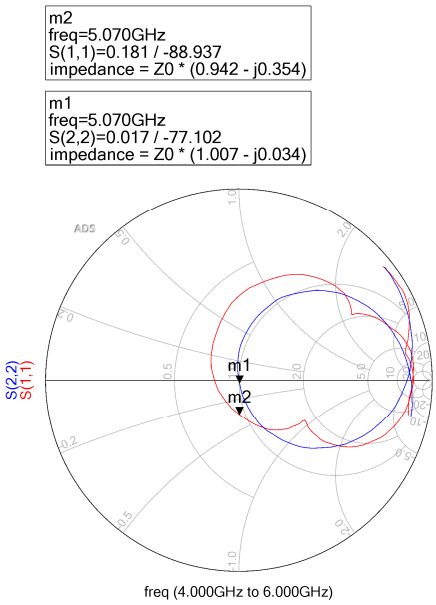

b) Smith chart of antenna 2

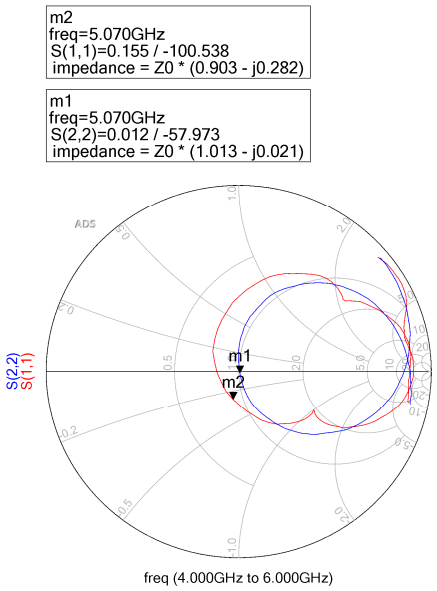

c) Smith chart of antenna 3

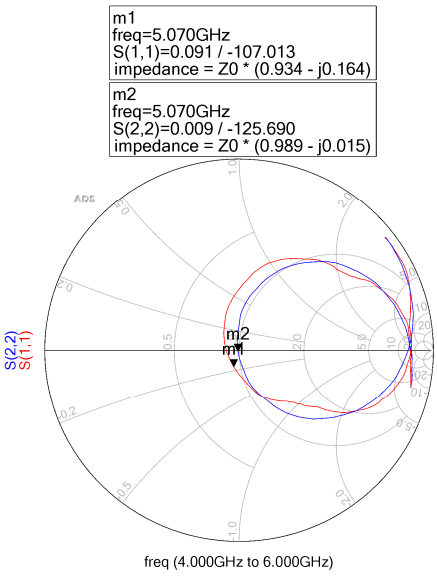

d) Smith chart of antenna 4

Figure 4.13: Smith chart of all four antennas; a) When one antenna is powered on (Red curve) and when all antennas are powered on(Blue curve), b) When one antenna is powered on (Blue curve) and when all antennas are powered on(Red curve), c) When one antenna is powered on (Blue curve) and when all antennas are powered on(Red curve), d) When one antenna is powered on (Blue curve) and when all antennas are powered on(Red curve).

It can be observed that the obtained results (Table 4.6 (Column C)) present decreased impedance which is slightly different than the values obtained via equation 4.3 (Column B). This slight change in impedance is due to higher order interaction of power waves

unlike that of equation 4.3 where there is only first order interaction being involved. However, the change in impedance can be more considerable if higher number of antenna elements operates simultaneously.

Moreover, it can be noticed that when two antennas are set to observe their impedance in coherent mode, they show very minute change in impedance according to Table 4.4 (Column B&C), and this change in case of four antennas increases even a bit further (Table 4.6 (Column B&C)). It can be inferred that this change may drastically increase if the number of antenna elements in an array is quite large. Thus, it is important to take into account the simultaneous excitation of antenna array for better realization of its active S-parameters.

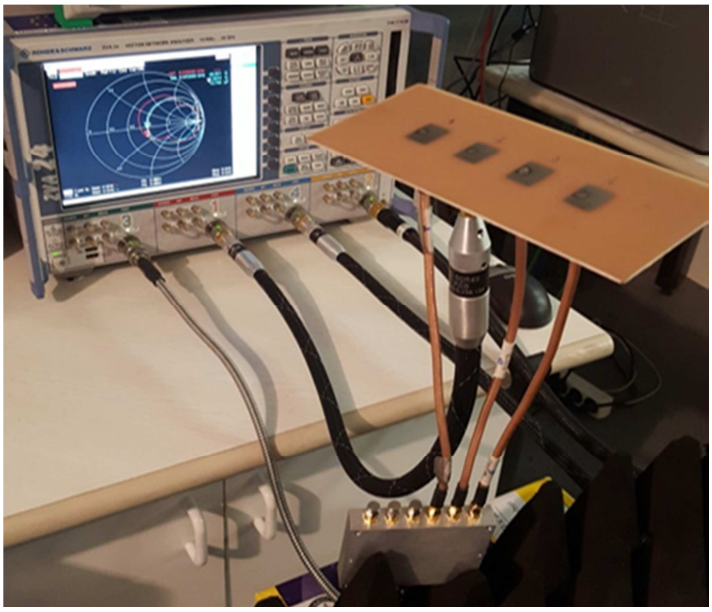

Figure 4.14: Screen shot of measurement setup.

Also it is significant to note that the decreased value of impedance in Table 4.6 (column B) shows that -20dB addition of pure coupling causes the decrease in impedance of individual antenna elements while the decreased impedance in Table 4.6 (column C) shows the combination of coupling as well as simultaneous excitation (the effect of total radiation).

Therefore, in order to compare the results obtained through theory (MATLAB code) and measurement, we need to first reduce coupling to a level where adding coupling power does not affect impedance of individual antenna elements. In other words, the excitation of elements, according to equation 4.1 & equation 4.3 should present same values. The values obtained by simultaneous excitation according to equation 4.2 can then be compared with theoretical results obtained via Matlab code.

Hence, in the next chapters we would explore novel methods of decoupling in between antenna elements in an array.

4.2 Conclusion

In this chapter, a new method to measure active S-parameters has been proposed. This method is based on the simultaneous excitation of all elements of an antenna array by exploiting the capabilities of the vector network analyzer having two synchronizing sources. The advantage of this method is that it does not require any particular calibration. Moreover, this chapter has made it possible to highlight that the evaluation of the active S-parameters by a passive scattering matrix approach is perhaps no longer sufficient to translate the reality.

In the next chapter, we would propose novel methods to reduce mutual coupling in between antenna elements.

Chapter 5

Mutual Coupling Reduction

5.1 Introduction

When two antennas are close to each other, and one of them is transmitting, the other will receive some of the power transmitted by the first antenna. How much of that power gets into the other antenna, is determined by a number of factors like[9]:

- Geometrical configuration of antenna elements in an array environment (linear, planar, circular, substrate height etc),
- Inter-element distance,
- Signal excitation amplitude of each element,
- Signal excitation phase of each element,
- Relative pattern of each element.

In antenna arrays, the elements that compose the array might receive the radiated fields from another array element while radiating and also that signal received might get reflected, reradiated, or scattered. Moreover, this reciprocal action between the antenna elements directs to coupling effect and in that way modifies the array characteristics. Being said that, it is clear that the fields generated by a particular antenna element reach the other elements in the same way as this antenna is reached by the fields generated by the elements in the proximity. So this presence of coupling in an array changes the terminal impedances of the antennas, reflection coefficients, array gain, beam width, etc [52], and the measure on how much this coupling phenomenon affects the array is up to the power of the signal, reflection coefficients, and the additional electrical phase introduced due to the propagation delay from one element to the other, as depicted in Figure 5.1.

In other words, performance characteristics of individual elements in an array are greatly influenced by mutual coupling in presence of the other elements of the array. Since the analysis of isolated elements is useful for predicting some parameters of them (polarization, pattern shape, resonant frequency), we can say that the behavior of the elements is quite different if we take them isolated in array geometry.

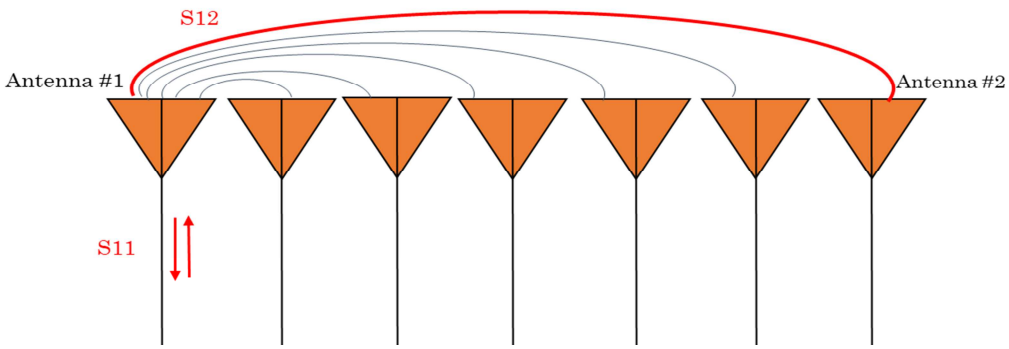

Figure 5.1: Mutual coupling phenomenon.

Mostly this coupling in arrays is unwanted except in certain cases where authors have shown that the presence of coupling actually is beneficial. It is claimed that the mutual coupling can enhance channel capacity and increase efficiency by decreasing bit error rate[53], improves in transfer of power in wireless transmission[54], improves conversion of adaptive algorithm in self-calibrating arrays[55], controls bandwidth of the array through patch sharing technique and shows that the phase gradient needed for beam steer direction is less than classical array[56], and can improve impedance matching[57].

In the case where both antennas are transmitting, each one will receive at the same time part of each other's transmitted energy. According to reciprocity theorem this is the same in case where both antennas are in receiving mode. However, authors in [58] propose that the coupling phenomenon of transmitting and receiving arrays are different in general, and hence different mutual impedance algorithms should be used for the analysis and compensation of mutual impedance.

In any case, however, to achieve independence of the signals that are received or transmitted from the antennas, the coupling between the antennas has to be removed or at least reduced. For this reason, different methods to reduce coupling between array elements have been studied and developed since the early deployment of antenna arrays.

5.2 Mutual coupling reduction in Patch antenna arrays by using DGS

Ubiquitous use of patch antennas in wireless industry reveals the importance of such antennas in terms of their being low profile, light weight, less costly, easily manufactured, conformal, and easily integrated to microwave circuits. When such patch antennas are aimed for arrays on a thick and lossy substrate, the design becomes even more critical. In such a case, the issue of mutual coupling starts to dominate in two different ways as follows[59], [60]:

- Coupling through surface waves,
- Coupling through free space waves.

Depending on many factors like substrate material thickness, ground plane, and type of modes that are excited by the patch antenna, one of the coupling mechanisms mentioned may dominate over the other.

However, the domination of surface wave coupling occurs when the patch antennas are printed on high permittivity dielectric substrates and becomes more dominant when the thickness of the substrate increases in accordance with condition (5.1) [49];

$$\text{Substrate thickness(h)} \geq \frac{0.3\lambda_0}{(2\pi\sqrt{\epsilon_r})} \tag{5.1}$$

Where;

- λ_0 is the wavelength in free space,
- ϵ_r is the relative permittivity of substrate.

These surface waves are sustained in the dielectric substrate and when they reach the ground plane edges, they diffract and propagate (Figure 5.2).

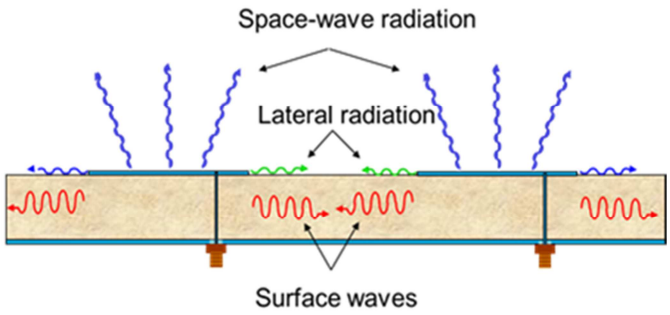

Figure 5.2: Mutual coupling mechanism in patch antennas.

Different methods have been proposed to reduce mutual coupling due to such surface waves in microstrip patch antennas. Some of them are based on:

- Optimizing the antenna design[29],[30] ,
- Adding dielectric layers to cover the patch[63],
- Scratching the dielectric material[64],
- Inserting shorting pins in the substrate to cancel polarization currents[49],
- Usage of meta materials called wave absorbents that cause magnetic resonance and a band gap that improve the insulation between the patch elements[33],[34],
- Using dielectric structures as band gaps between antenna elements called electromagnetic bandgap (EBG) structures[67]–[70],
- Using the techniques called defected ground structure (DGS)[71], [72].

DGS is basically a technique to carve out some shapes (symmetrical or asymmetrical) in the ground plane in between antenna elements. These are used in order to alter the course of surface waves or change the effective dielectric constant of the substrate

(changing its capacitance and inductance) which produces a frequency band elimination effect. DGS carries similar characteristics with that of EBG structures but of simpler manufacturing and also requires little surface to implement. Due to this characteristic of band rejection and ease of implementation, DGS technique has been used in a wide number of microwave circuits and antenna array design applications. DGS may exist in various shapes and sizes as some of them have been illustrated through Figure 5.3.

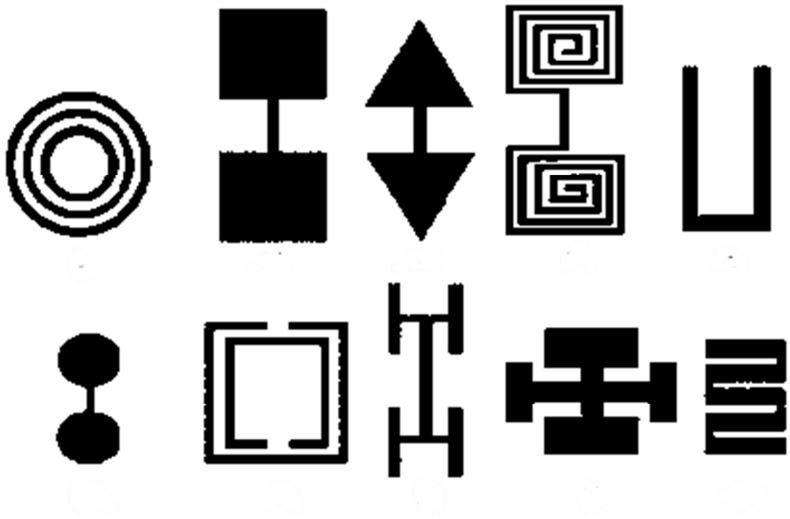

Figure 5.3: Different examples of etched shapes geometries[73].

An etched DGS (we call it **μ** for its similarity to the Greek letter **mu**) is introduced here to increase isolation between two E-plane oriented patch antenna array elements. This novel structure not only reduces mutual coupling (transmission coefficient) but also improves return loss of the antennas with improved bandwidth.

We simulate two patch antenna elements (without and with DGS) arranged collinearly (E-plane) and show their S-parametric analysis.

5.2.1 Patch antenna array without μ-shaped DGS

Two antenna elements, resonating at 5GHz, arranged along E-plane has been simulated at a separation distance of $0.4\lambda_0$. The ground plane is extended $\lambda_0/2$ away in all directions from the antenna elements with epoxy FR-4 as substrate. The antenna array is illustrated through Figure 5.4 with all dimensional parameters.

The array is simulated and its corresponding S-parameters are shown in Figure 5.5. The conventional antennas show a mutual coupling ($S_{12\text{-}21}$) of approximately -18 dB mainly due to the presence of surface waves within the substrate (Condition 5.1). An impedance bandwidth ($|S_{11}$ & $S_{22}| < 10$ dB) of approximately ~200 MHz is observed. It can be seen that both antennas exhibit almost -34 dB return loss at the resonant frequency. Despite having same parameters of both antennas, one of the antennas resonates around

4.99 GHz which is a slight variation and this may have resulted due to the introduced mesh on the antennas.

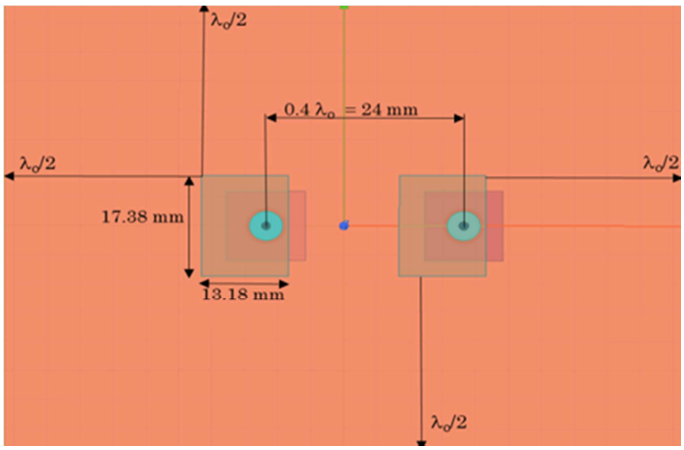

Figure 5.4: Array of two patch antenna elements without DGS arranged along E-plane.

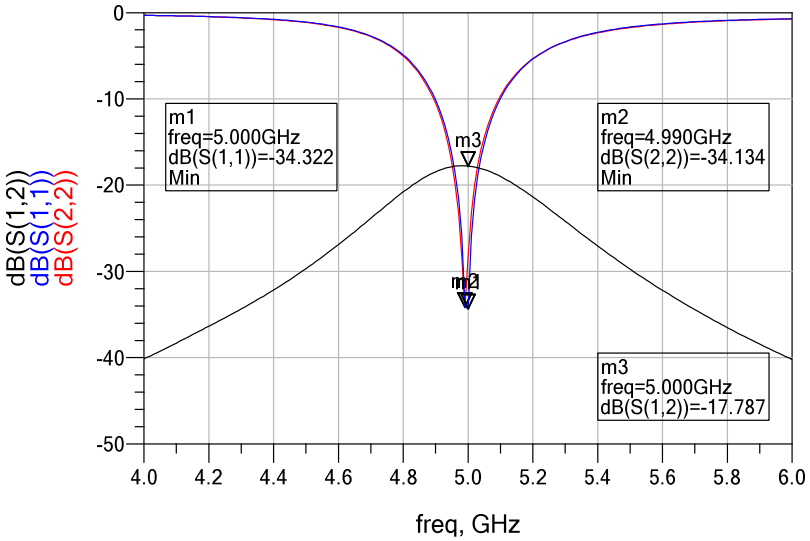

Figure 5.5: Simulated S-parameters without DGS.

5.2.2 Patch antenna array with μ-shape DGS

In order to suppress the strong surface waves a defected ground structure is carved in between the adjacent E-plane coupled elements in the array. The DGS proposed in this work is based on rectangular slots, forming a **μ**-shape and its image, as shown in the Figure 5.6(a). The structure is centered between two antenna elements and optimized in

dimensions, relative position and relative distance to reduce the mutual coupling on a desired frequency band as shown in Figure 5.6(b).

The optimization process is carried out on the proposed design by carefully adjusting the key parameters. The optimized parameters for the DGS are;

L1 = 11.5*mm*, L2 = 10*mm*, L3 = 5.7*mm*, L4 = 5.3*mm*, W1= 3.5925*mm*, D1 = 0.2*mm*, D2 = 1*mm*, D3 = D4 = 0.5*mm*. The total etched area is = 36.5925mm^2.

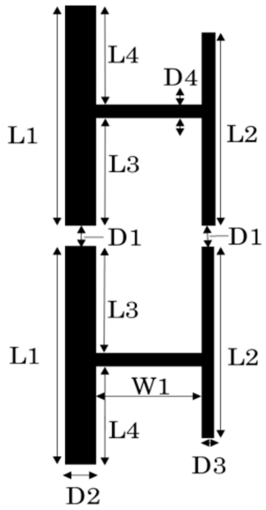

a)

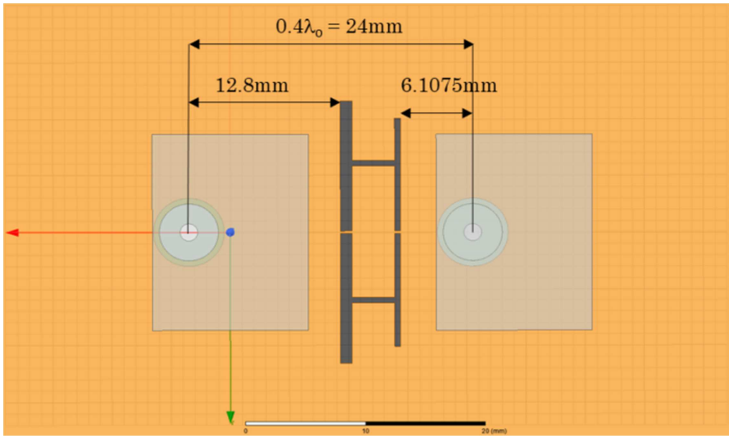

b)

Figure 5.6: a) Proposed DGS design structure, b) Array of two collinearly arranged patch antenna elements with carved **μ** shaped DGS.

Scattering parameters of the decoupled antenna array show -33.4 dB amount of mutual coupling which is about 16 dB lower than the conventional antenna array (Figure 5.7). Here, the filtering slots with the proper position and dimensions exhibit rejection band at 5.07 GHz. This frequency shift may have been caused by the slow wave effect of the DGS. The DGS presents a band-stop effect because of the combination of equivalent inductance and capacitance, which depends on several parameters: length (Lx), width (Wx), spacing & thickness of slots (Dx) and the relative position in the array. Also, it can be observed that the antennas exhibit better return loss response in DGS with an impedance bandwidth (~300MHz) which is slightly over than the conventional antenna array at the rejection band.

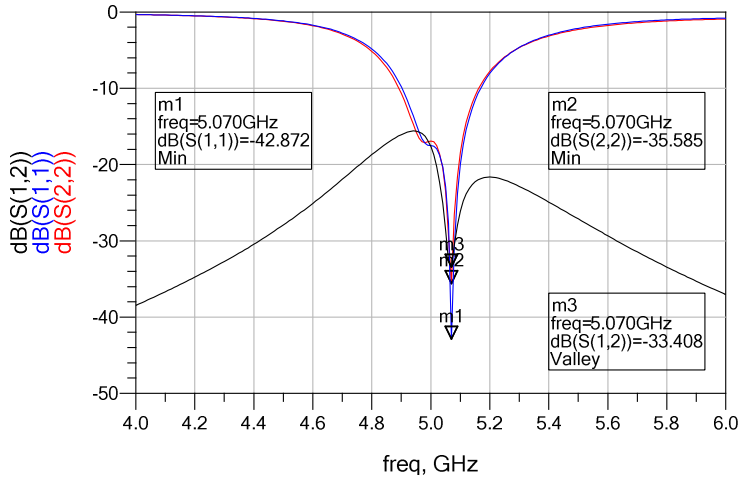

Figure 5.7: Simulated S-parameters with DGS.

As expressed in the theoretical approach, surface waves can be associated to the surface current distribution in the ground plane of the antenna elements. The simulated surface current distributions on the common ground plane for the cases (with and without the proposed DGS slots) are presented in Figure 5.8 & 5.9 at 90° phase. It can be observed from Figure 5.8 that some part of the surface current generated by one antenna circulate around the slots and affect less the second antenna than in the case without slots where surface currents gets easily coupled by the adjacent antenna (Figure 5.9). The slots prevent part of the fields from crossing over to the other element, which decrease the mutual coupling between array elements.

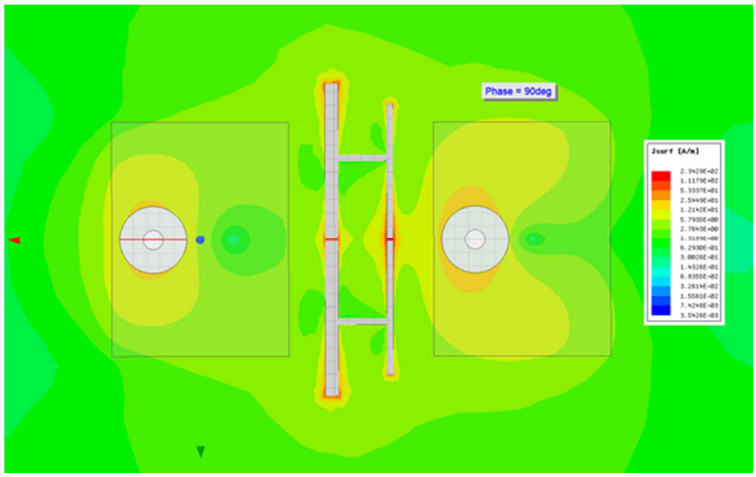

Figure 5.8: A screen shot of Surface current distribution with DGS at 90^0 phase during animation.

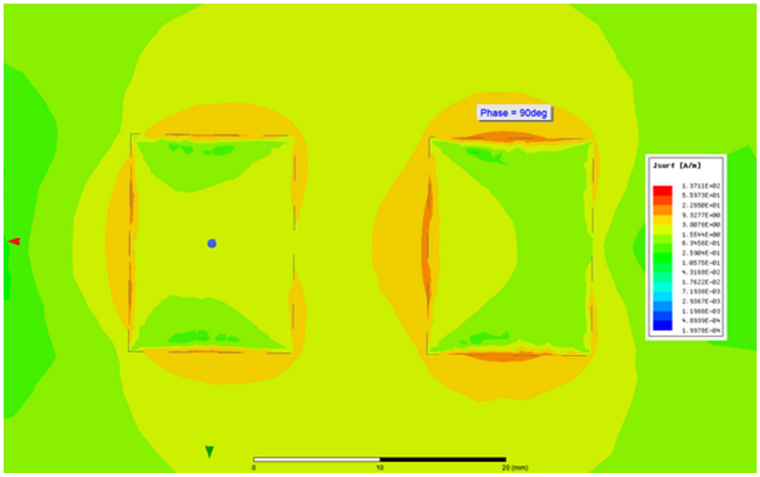

Figure 5.9: Screen shot of Surface current distribution without DGS at 90^0 phase during animation.

It is also observed that when L1 and L2 have unequal lengths, a satisfactory isolation within the matching bandwidth can be achieved. There is an important relationship between the ratio L1/L2 and the rejected bandwidth in this design. The rejected bandwidth is also sensitive to the width of the slots (W1), which in this design is proportional to the resonance frequency of the rejection band. Other crucial parameter, in this design, is the position of the slots. The most appropriate position is in the middle of the ground plane.

5.2.2.1 Parametric analysis

A parametric analysis of the variation of the cutoff frequency in terms of different dimensions of the slots was carried out. It was found that a variation in width (W1 in our design, Figure 5.6(a)) produces a linear shift in the cutoff frequency for this particular

design. As the width of DGS is reduced and increased, a tendency of a higher and lower cut off frequency respectively is observed in S_{12} as illustrated in Figure 5.10.

Here, it can be observed that the bandwidth of the rejection band (S_{12}) is quite narrow and any minor manufacturing tolerance might shift the rejection band from the resonant frequency. Therefore, it is important to make sure that any manufacturing tolerance should not affect this rejection band, we would like to implement mutual coupling reduction in such a way so that the entire band of rejection remains quite low.

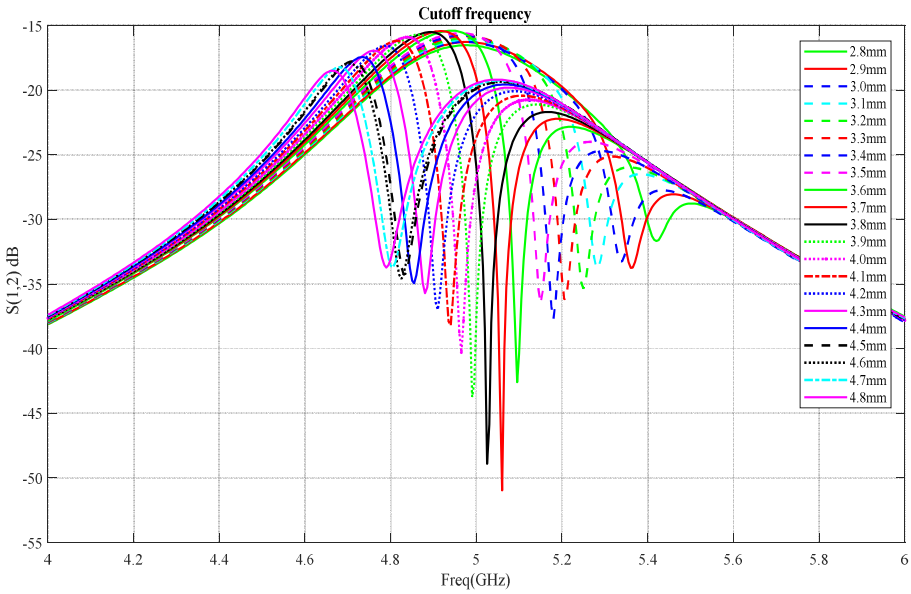

Figure 5.10: Parametric analysis of mutual coupling cutoff frequency shift with respect to the width (W1) of the DGS.

5.3 Mutual coupling reduction through shorting pins and Metallic walls

In the last section, we introduced a novel DGS structure to enhance isolation between E-plane oriented antenna elements. The DGS effectively suppressed dominant surface waves, enhanced return loss and improved bandwidth of antenna elements. However, this method could not attain broader bandwidth of rejection band and was limited to only E-plane orientation.

In this section, we propose a decoupling method to reduce surface wave coupling and free space wave coupling through insertion of metallic pins and metallic walls, respectively in both E and H-plane orientations in patch antenna arrays. This method exhibits a wide band of rejection band (S_{12}).

Various techniques have been proposed to eliminate or reduce the effect of coupling in antenna arrays. Most of these techniques are designed either to reduce coupling in E-plane [67], [74]–[78] or in H-plane orientation [79]–[81] . The techniques which work well in E-plane orientation, do not work in H-plane. The same is true for reduction techniques in H-plane orientation. In addition, there are some examples where authors have shown to reduce coupling in both E and H-plane orientations[82], [83]. However, they have used altogether different techniques to achieve so because of the nature of the coupling. Moreover, some of these approaches demonstrate narrow bandwidth of rejection band (S_{12}) which do not cover the operational bandwidth of the antennas. Table 5.1 provides a summarized comparative analysis between different decoupling methods.

In this section, we propose a simple technique to reduce coupling by using combination of metallic pins and metallic wall barriers. Metallic pins are shorted in between the patch and the ground plane in order to suppress surface waves and radiations in horizontal directions. Later, in arrays, metallic barriers are inserted to reduce further the effect of free space wave coupling. This technique works equally well in both E and H-plane orientations. Apart from coupling suppression better than -40 dB (required in most applications) at the resonant frequency, this technique has an advantage of wide band rejection characteristics.

In next section, single conventional and pin loaded patch antenna are designed which are used in later sections to build antenna arrays in E-plane and H-plane orientations with decoupling mechanism.

Paper	Technique	Orientation E/H-plane	Center to Center distance	Mutual Coupling (S_{12}) in dB	Bandwidth of rejection band (S_{12})	Design complexity
[74]	DGS	E	0.75 λ_o	-27	Narrow	Moderate
[75]	DGS	E	0.5 λ_o	-33	Narrow	Low
[67]	EBG	E	0.5 λ_o	-25.03	Wide	Low
[76]	EBG	E	0.75 λ_o	-40	Wide	Low
[77]	FSS	E	0.75 λ_o	-45	Wide	Moderate
[78]	Choke + EBG walls	E	0.92 λ_o	-90	Wide	High
[79]	U-section	H	0.6 λ_o	-39	Narrow	Moderate
[80]	Wall	H	0.25 λ_o	-40	Wide	Low
[81]	Wall	H	0.28 λ_o	-54.3	Wide	Low
[82]	Wall	E-H	0.6 λ_o	-32	Wide	Moderate
[83]	Rectangular slot	E-H	0.5 λ_o	-37	Narrow	Moderate
This work	Pins + Wall	E-H	0.7 λ_o	-40	Wide	Low

Table 5.1: Comparison between different mutual coupling reduction techniques.

5.4 Single patch antenna design

5.4.1 Conventional patch antenna design

We design and optimize a single patch antenna at operating frequency of 5.69 GHz. Once it is optimized, the same is then put in array combinations. The optimized parameters of the single patch antenna (Figure 5.11) are given in Table 5.2.

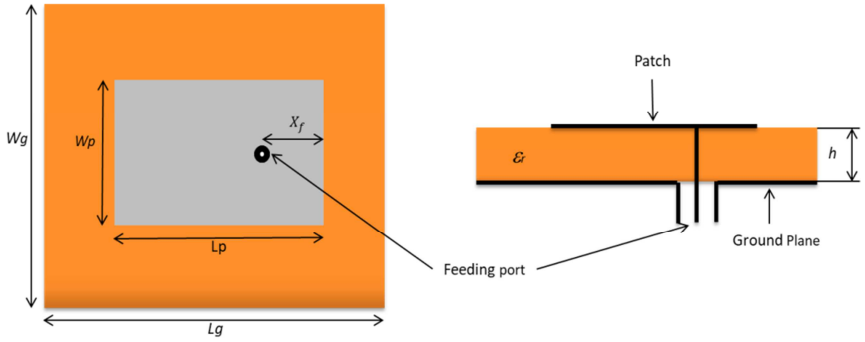

a) b)

Figure 5.11: Conventional single patch antenna: a) top view, b) side view.

DESCRIPTION	VALUES
Targeted Frequency	5.69 GHz
Patch and ground material	copper (35μm Thick)
Patch antenna length (Lp)	11.4 mm
Patch antenna width (Wp)	9.5 mm
Substrate material	FR4 epoxy (ξr = 4.4,tan δ = 0.02)
Height of the Substrate (h)	1.6 mm
Substrate and ground length (Lg)	65.4 mm
Substrate and ground width (Wg)	63.5 mm
Feed point distance from the edge (X_f)	3.9 mm
Antenna feed	Coaxial feed

Table 5.2: Optimized parameters of conventional patch antenna.

The antenna has been simulated with optimized return loss of -28.44 dB as shown in Figure 5.12.

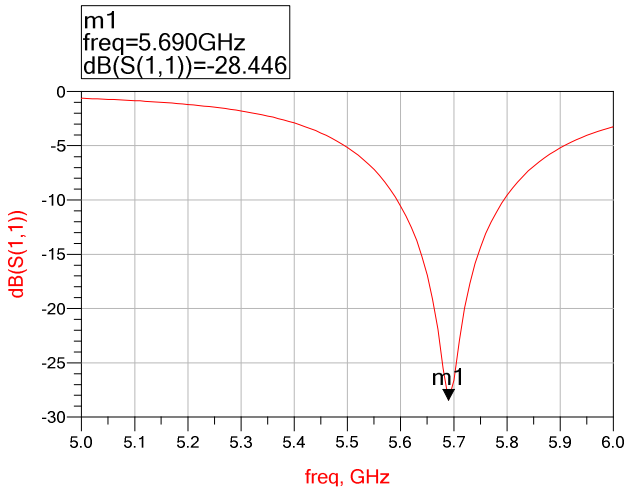

Figure 5.12: Simulated return loss of conventional patch antenna.

Figure 5.13 shows that the radiation pattern of conventional patch antenna presenting around 4.9 dBi of directivity in 2D and 3D radiation pattern in the broad side direction (θ=0°).

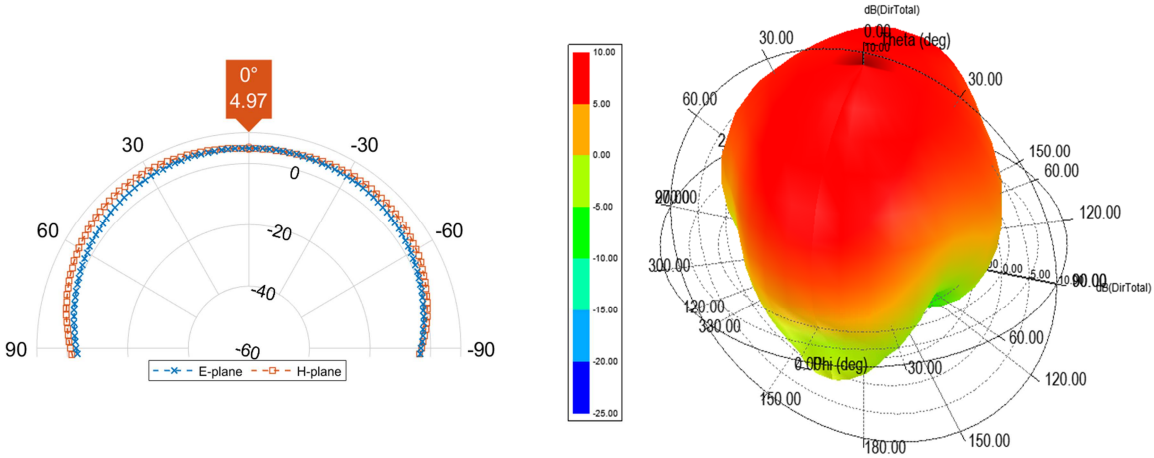

a) b)

Figure 5.13: Simulated radiation pattern of conventional path antenna: a) 2D radiation pattern showing directivity in E and H-plane, b) directivity in 3D radiation pattern.

5.4.2 Pin loaded patch antenna design at 5.69GHz

We design another single patch antenna loaded with shorting pins to resonate at the same frequency as previously. The idea behind this technique is to modify the characteristics of the substrate so that it does not excite sufficient surface waves such that the patch can later be used in array combinations.

Shorting pins in Microstrip patch antenna can be preferred to chip inductors and capacitors due to their lower losses and ease of implementation. Therefore the use of

shorting pins in patch antennas has revealed variety of applications. For instance, shorting pins can be used to enhance gain[84], reduce cross polarization[85], reduce resonant frequency in order to make antenna more compact[86], making antenna dual band[87]–[89], increase impedance bandwidth[90], cancel out polarization currents in substrates[49], suppresses specific modes for isolation enhancement[91] and cancel out harmonic radiations[92].

In patch antennas, polarization currents are initiated due to the presence of surface waves which are guided by the substrate to the air interface. Due to these polarization currents, a strong resonant electrical field exists in the dielectric which is radiated in the vertical direction causing strong surface wave propagation. In order to cancel out the effect of polarization current, a counter phased mechanism is required. In our design, this has been achieved through shorting pins placed at proper locations in between the patch and the ground. This mechanism introduces extra inductive polarization currents which compensate existing capacitive polarization currents in the dielectric. In this way, strong surface waves can be suppressed[49].

Figure 5.14 shows the proposed patch antenna with compensated shorting pins. The position and dimensions of the pins is obtained through trial and error method (from literature and optimization). In this particular case, the length and width of the patch are enlarged in order to compensate the effect of shorting pins. In order to have same frequency that of conventional patch antenna, the new dimensions of the patch become almost $\sqrt{\varepsilon_r}$ times bigger than the conventional antenna printed on FR-4. Here, effective permittivity is close enough to relative permittivity making dielectric behave more like air cavity. In this way, the pin loaded patch antenna behaves as though there is air dielectric as a new dielectric medium and hence eliminating surface waves. The optimized parameters of the pin loaded patch antenna are:

Length of the patch (Lp) =31 *mm*, width of the patch (Wp) =25 *mm*, co-axial feed point distance from the edge of the patch (X_f) = 4.3 *mm*, Height of the substrate(h) = 1.6 *mm,* diameter of the pin (D) = 1*mm*, Inter distance between the pins (dx and dy) = 9*mm*, the distance of pins from the patch edge to pins along X-axis (P_x)=2.5*mm* and along Y-axis(P_y)=3.5 *mm,* total number of pins = 12(4x3).

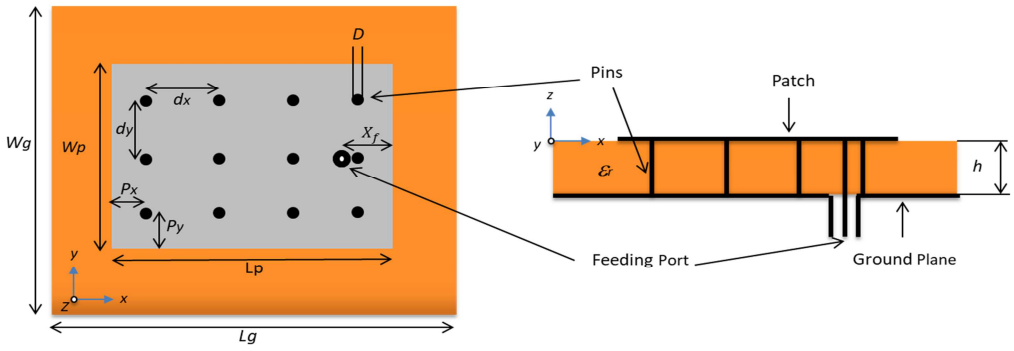

a) b)

Figure 5.14: Pin loaded single patch antenna: a) top view, b) side view.

The pin loaded patch antenna has been simulated. The Figure 5.15 shows the optimized return loss of the antenna. Here, the pin loaded patch antenna presents -35.3 dB at the same resonant frequency as that of conventional patch antenna. It can be observed through radiation pattern (Figure 5.16) that the pin loaded patch antenna presents a directivity of 10.25 dBi which is almost 5.3 dB bigger than conventional patch antenna.

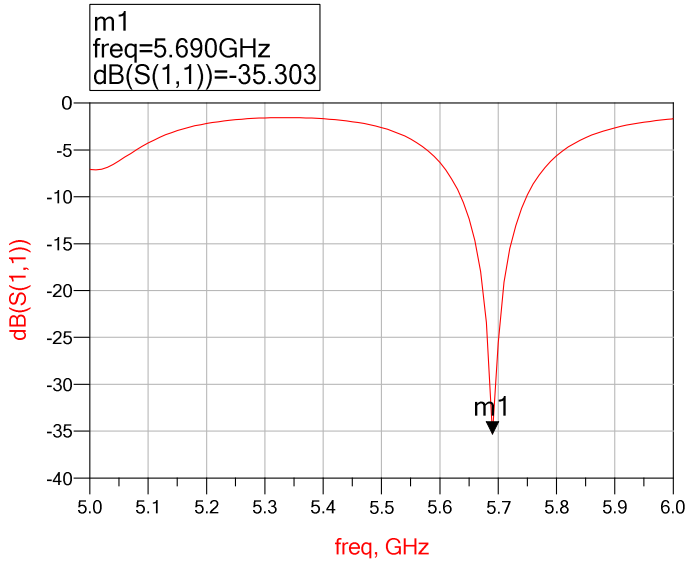

Figure 5.15: Simulated return loss of optimized pin loaded patch antenna.

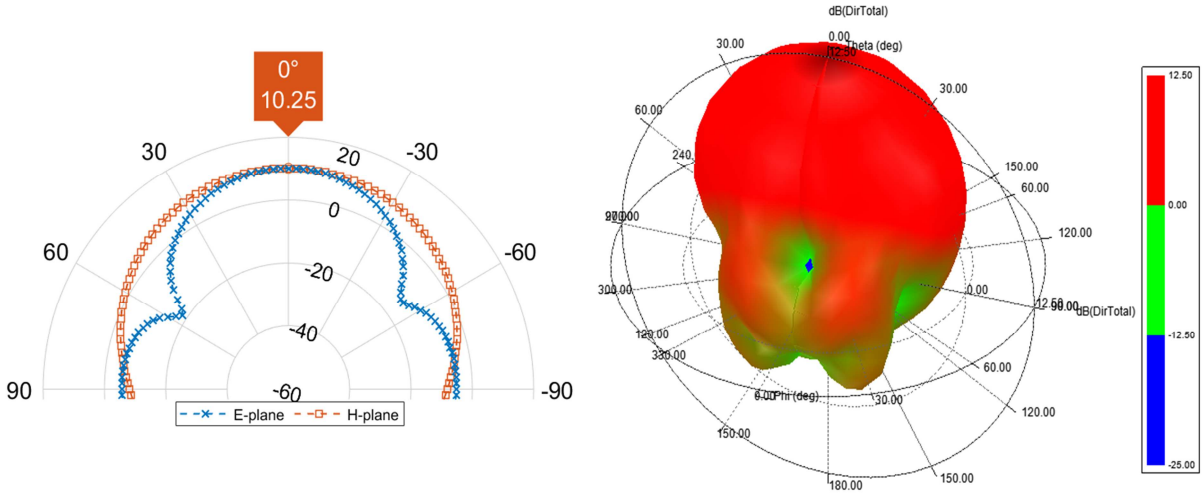

a) b)

Figure 5.16: Simulated radiation pattern of pin loaded path antenna: a) 2D radiation pattern showing directivity in E and H-plane, b) directivity in 3D radiation pattern.

5.5 Realization of conventional and pin loaded patch antenna

In order to validate simulations results, conventional and pin loaded antennas have been manufactured (Figure 5.17). The measured S-parameters of both antennas have been shown in Figure 5.18. It can be observed that both manufactured antennas resonate slightly at different frequencies because of the inherent manufacturing tolerance. Conventional patch antenna resonate around 5.73 GHz with return loss of -21.5 dB and the pin loaded patch antenna resonate at 5.8 GHz with return loss of -23.32 dB. This small variation of the resonant frequency will not affect the observance of our results in terms of reduction of mutual coupling in antenna arrays. Therefore, we would build arrays (both in E and H-planes) with conventional and pin loaded patch antennas so that a comparison can be given.

a) b)

Figure 5.17: Laboratory prototypes: a) conventional patch antenna a) pin loaded patch antenna

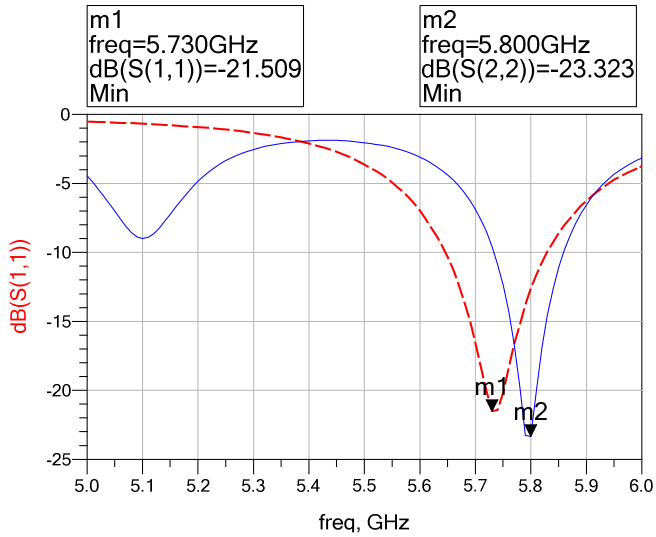

Figure 5.18: Return loss through measurement: Conventional patch antenna (dashed curve) and Pin loaded patch antenna (solid curve).

5.6 Conventional patch antenna array analysis

After optimizing a single conventional patch antenna, an array with it can be constructed in both E and H-planes so that, later on, we can compare them with those of pin loaded patch antennas.

5.6.1 3D simulation of conventional patch antenna array oriented along E and H-planes

Two antenna elements arranged along E and H-plane have been simulated at a feed point separation of $0.7\lambda_0$. The ground plane is extended $\lambda_0/2$ away in all directions from the antenna elements. The antenna array oriented along E-plane and H-plane is illustrated through Figure 5.19(a) and Figure 5.19(b), respectively.

The array is simulated and its corresponding S-parameters are shown in Figure 5.20. The conventional antennas oriented along E and H-plane show a mutual coupling ($S_{12\text{-}21}$) of approximately -21.03 dB and -27.45 dB, respectively. An impedance bandwidth ($|S_{11}$ & $S_{22}| < 10$ dB) of approximately ~180 MHz and ~200 MHz is observed in E and H-planes, respectively.

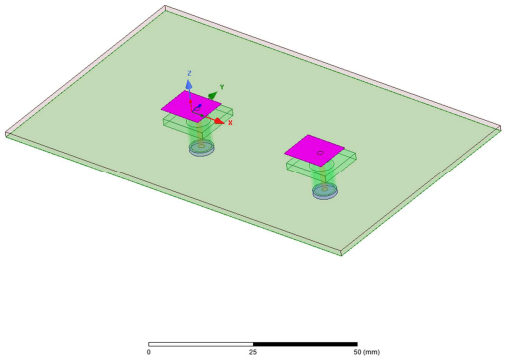

a)

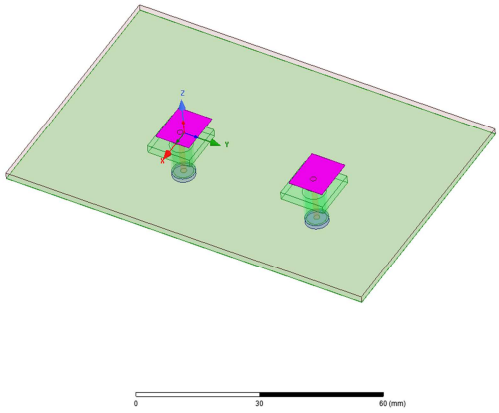

b)

Figure 5.19: Two element conventional antenna array oriented along: a) E-plane, b) H-plane.

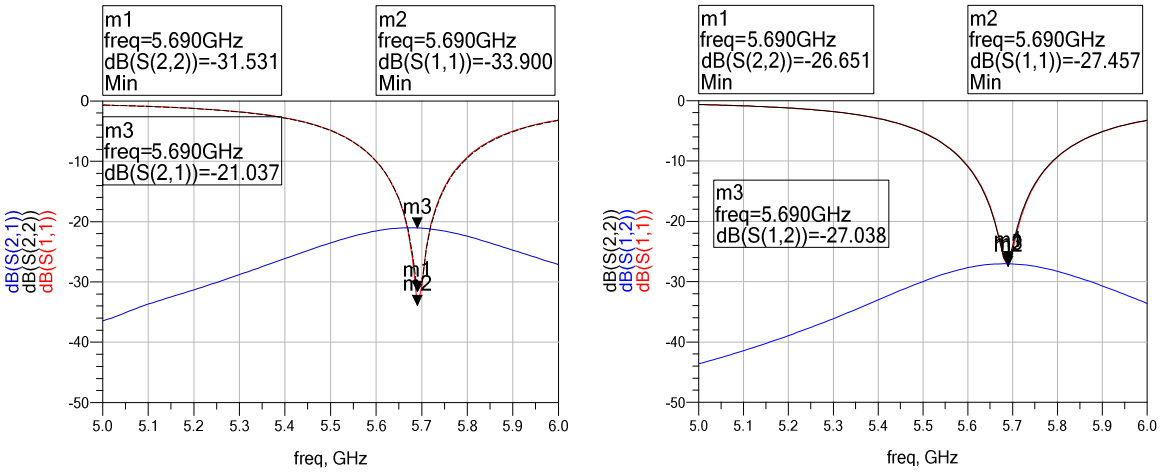

a) b)

Figure 5.20: Simulated S-parameters of two conventional antennas oriented along: a) E-plane, b) H-plane.

5.6.2 Realization of conventional patch antenna array oriented along E and H-planes

Conventional patch antenna array arranged in E and H-plane has been manufactured to validate 3D simulation results. Figure 5.21 shows the manufactured antenna array in both orientations. The conventional antennas oriented along E and H-plane show a mutual coupling ($S_{12\text{-}21}$) of approximately -21.564 dB and -29.503 dB (Figure 5.22), respectively which is almost the same obtained through simulations. It can be observed that the antennas in E-plane resonate slightly at higher frequencies than the reference antenna which is due to the manufacturing tolerance. Also in H-plane one of the antennas resonates slightly lower (5.68 GHz) than the reference antenna which is again due to manufacturing tolerance. It can be seen that both simulation and realized results show similarities in both E and H-plane configurations in terms of transmission coefficients and return losses. Table 5.3 provides the summarized results.

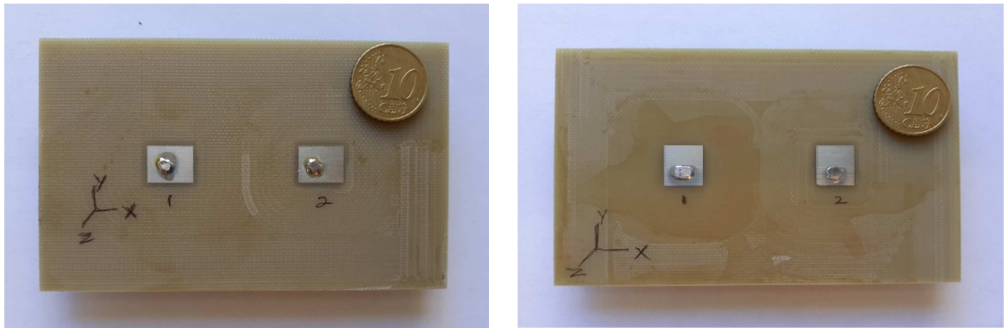

a) b)

Figure 5.21: Two element conventional fabricated antenna array oriented along: a) E-plane, b) H-plane.

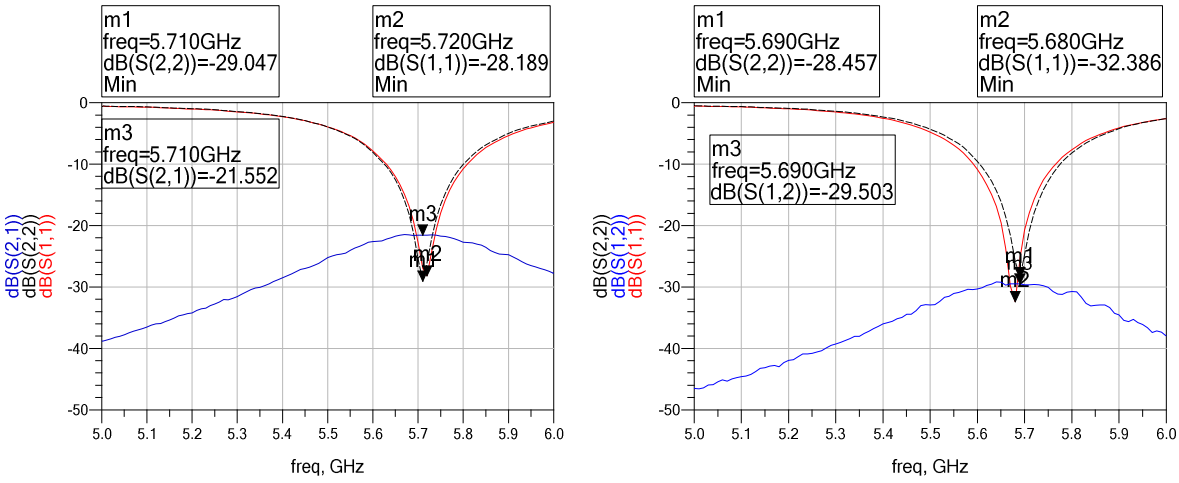

a) b)

Figure 5.22: Measured S-parameters of two conventional antennas oriented along: a) E-plane, b) H-plane.

Two element conventional patch antenna array	**3D Simulation (S_{12})**	**Realization (S_{12})**
E-plane(Coupling coefficient)	-21.03dB	-21.55dB
H-plane(Coupling coefficient)	-27.45dB	-29.50dB

Table 5.3: Coupling coefficient in 3D simulation and realization in both E and H-plane orientation of two element conventional patch antenna array.

5.7 Pin loaded patch antenna array

After optimizing a single pin loaded patch antenna, an array with it can be constructed in both E and H-planes so that, later on, we can compare them with those of conventional patch antenna and pin loaded patch antenna arrays with walls.

5.7.1 3D simulation of pin loaded patch antenna array oriented along E and H-planes

Two element Pin loaded patch antennas have been arranged according to E and H-plane configurations as shown in Figure 5.23(a) and Figure 5.23(b), respectively.

Both E and H-plane configurations have been simulated and their corresponding S-parameters are presented in Figure 5.24(a) and Figure 5.24(b), respectively. The pin loaded antennas oriented along E and H-plane show a mutual coupling ($S_{12\text{-}21}$) of approximately -

26.04 dB and -31.64 dB, respectively. It can be seen that both antenna#1 and 2 resonate slightly at different frequencies in E and H-planes. Despite having same parameters of both antennas, a slight variation in their resonant frequencies may have resulted due to the introduced mesh during simulation.

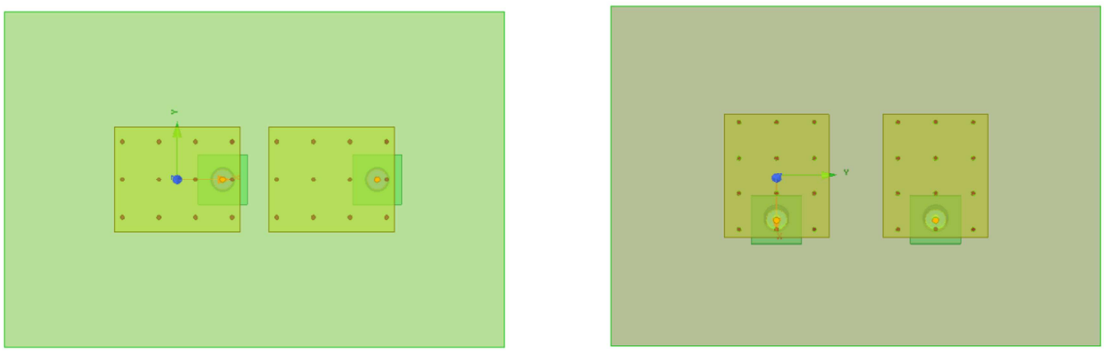

a) b)

Figure 5.23: Pin loaded two element antenna array through 3D simulation: a) oriented along E-plane, b) oriented along H-plane.

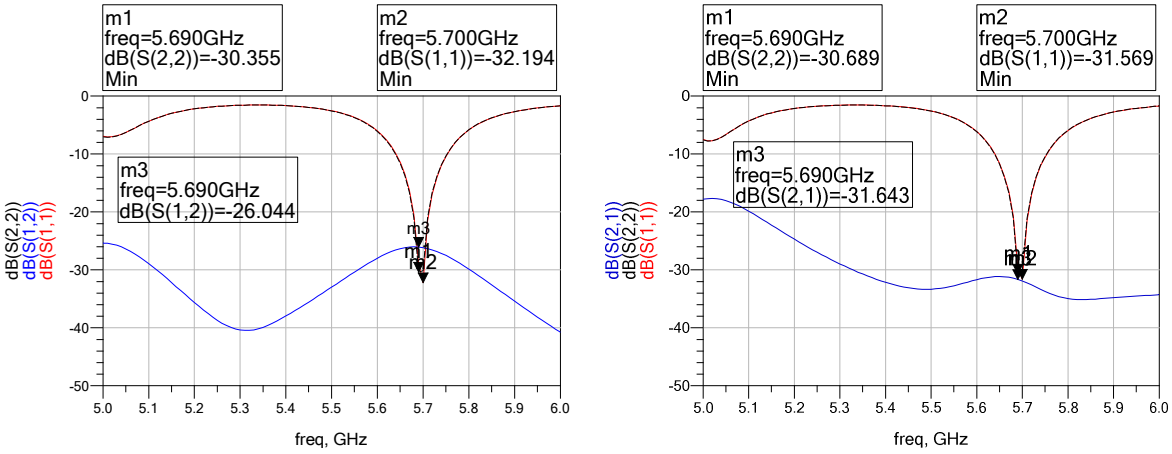

a) b)

Figure 5.24: Simulated S-parameters of pin loaded two antennas through 3D simulation oriented along: a) E-plane, b) H-plane.

At the resonant frequency, it can be observed that patch antennas loaded with pins present almost -5 dB and -4 dB less coupling as compared to conventional antenna array in E-plane and H-planes, respectively.

In order to reduce coupling further, we introduce metallic walls barriers in between antenna elements to suppress free space wave coupling among such pin loaded antenna elements.

5.8 3D simulation and realization of patch antenna array oriented along E and H-planes with combination of shorting pins and metallic walls

After optimizing conventional and pin loaded patch antenna arrays, now an array with pin loaded patch antennas is complemented with metallic wall barriers so that later on a comparison can be made.

5.8.1 3D simulation of pin loaded patch antenna array with metallic wall oriented along E-plane

In order to suppress free space wave coupling a wall is erected in between the adjacent E-plane coupled elements in the array. The wall structure proposed in this work is based on copper sheet with thickness (W_w) of $1mm$, and height (W_h) of $25mm$, as shown in the Figure 5.25. The wall structure is centered between two antenna elements and optimized in height and relative distance (d) of 3mm to reduce the mutual coupling on a desired frequency band.

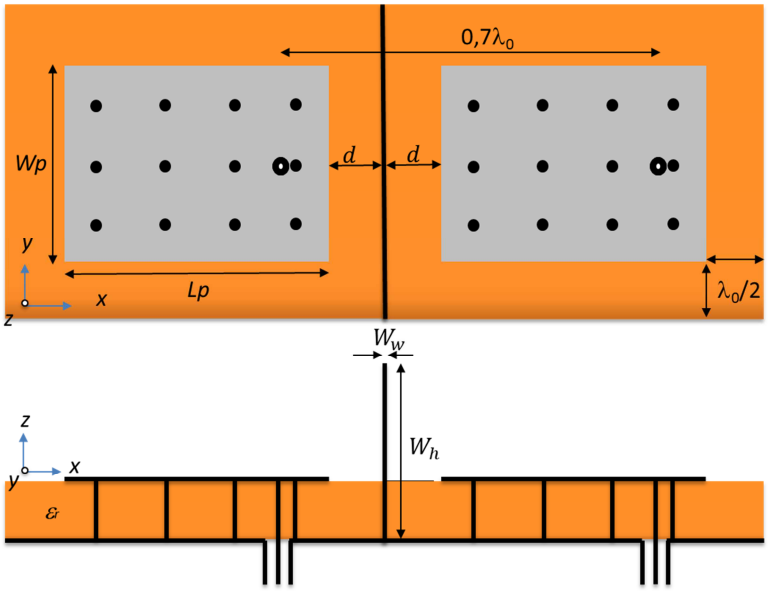

Figure 5.25: Top and side view of two E-plane pin loaded patch antennas with metallic wall barrier.

Figure 5.26 shows the corresponding S-parameters in E-plane. It can be observed that the rejection band presents wide band characteristics with -44.89 dB of coupled power at the resonant frequency. Here, combination of pin loaded patch antennas with metallic wall presents almost 23 dB less coupling as compared to conventional patch antenna array arranged along E-plane.

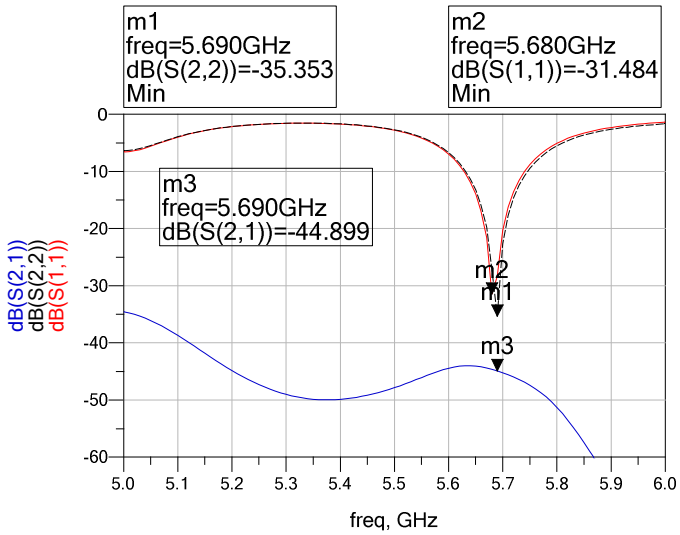

Figure 5.26: Simulated S-parameters of two E-plane pin loaded patch antennas with metallic wall barrier.

5.8.2 3D simulation of pin loaded patch antenna array with metallic wall oriented along H-plane

Similarly, a wall is inserted in between two H-plane oriented pin loaded patch antennas as shown in Figure 5.27. The wall is again placed in the center position in between two antennas and the height of the wall is kept 25mm. The wall structure is centered between two antenna elements with relative distance (d) of 7mm to reduce the mutual coupling on a desired frequency band. The structure is simulated and its corresponding S-parameters are shown in Figure 5.28.

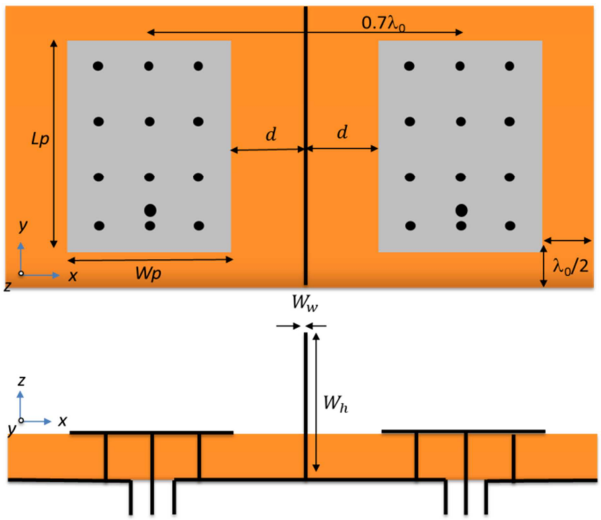

Figure 5.27: Two H-plane pin loaded patch antennas with metallic wall barrier.

S-parameters show that the antennas present -42.14 dB coupling at the resonant frequency with wide band rejection characteristics. Here, combination of pin loaded patch

antennas with metallic wall presents almost -15 dB less coupling as compared to conventional patch antenna array arranged along H-plane.

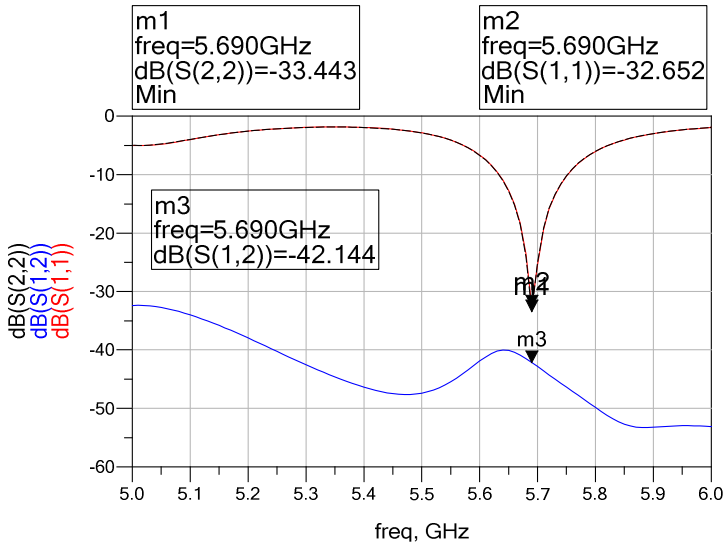

Figure 5.28: Simulated S-parameters of two H-plane pin loaded patch antennas with metallic wall barrier.

5.8.3 Realization of pin loaded patch antenna array with metallic wall oriented along E and H-plane

Pin loaded patch antenna array with metallic walls barriers arranged along E and H-plane have been manufactured to validate 3D simulation results (Figure 5.29). The pin loaded antennas with metallic walls oriented along E and H-plane show a mutual coupling ($S_{12\text{-}21}$) of approximately -39.188 dB and -44.059 dB, respectively with wide band rejection characteristics (Figure 5.30(a-b)). It can be observed that the antennas in both planes resonate slightly at lower frequencies (5.56 GHz) than the reference pin loaded antenna (5.69 GHz) due to manufacturing tolerance. Anyway, slight variations in resonant frequencies do not affect the observance of our results. Table 5.4 provides the summarized results between simulated and realized pin loaded patch antenna elements with walls in both configuration of E and H-plane.

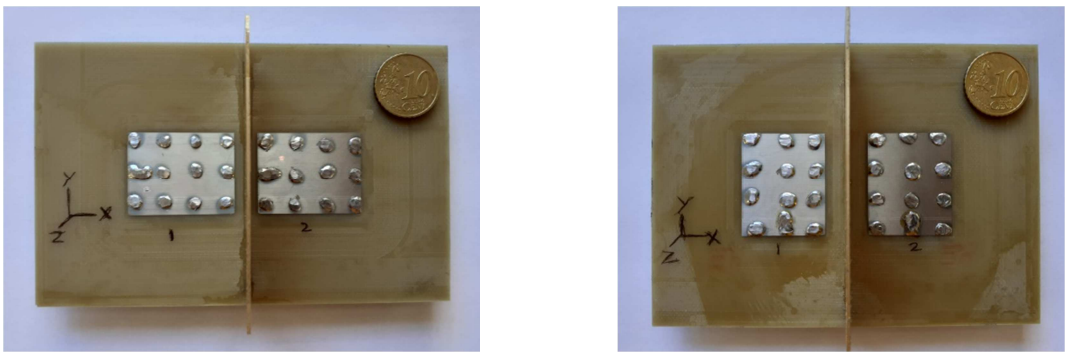

a) b)

Figure 5.29: Fabricated Pin loaded two element antenna arrays with metallic wall barrier oriented along: a) E-plane, b) H-plane.

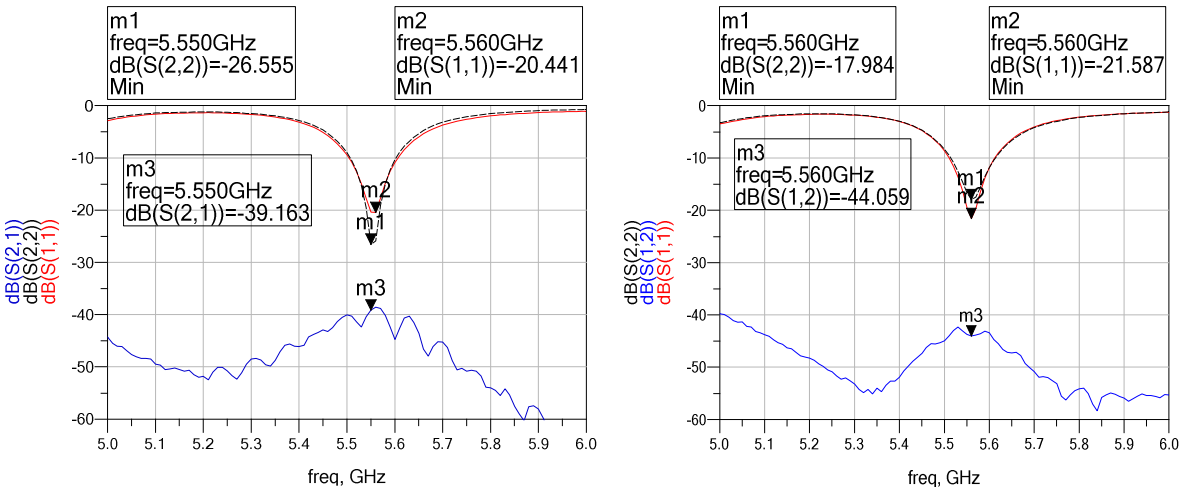

a) b)

Figure 5.30: Measured S-parameters of pin loaded two antennas with metallic wall barrier through realization oriented along: a) E-plane, b) H-plane.

Two element pin loaded patch antenna array with metallic walls	**3D Simulation (S_{12})**	**Realization (S_{12})**
E-plane(Coupling coefficient)	-44.89dB	-39.18dB
H-plane(Coupling coefficient)	-42.14dB	-44.06dB

Table 5.4: Coupling coefficient through 3D simulation and realization in both E and H-plane orientation of two element pin loaded patch antenna elements with metallic walls.

It can be observed that the realized array shows almost 5 dB more coupled power as compare to simulation in E-plane and almost 2 dB less coupled power in H-plane. This little variation of coupled power in simulation and realization is the result of manufacturing tolerance and measurement setup in realized arrays. Figure 5.31(a) and Figure 5.31(b) provides a comparative analysis between E and H-plane respectively, in both simulation and realization. It can also be observed that the rejection band (S_{12}) in both orientations is quite wide and remains almost less than -40 dB in entire frequency band (measured value).

Table 5.5 provides the comparative analysis of the mutual coupling through 3D simulation and realization among conventional patch antenna arrays, pin loaded patch antenna arrays and combination of pins and metallic wall barrier patch antenna arrays in both planes of orientations.

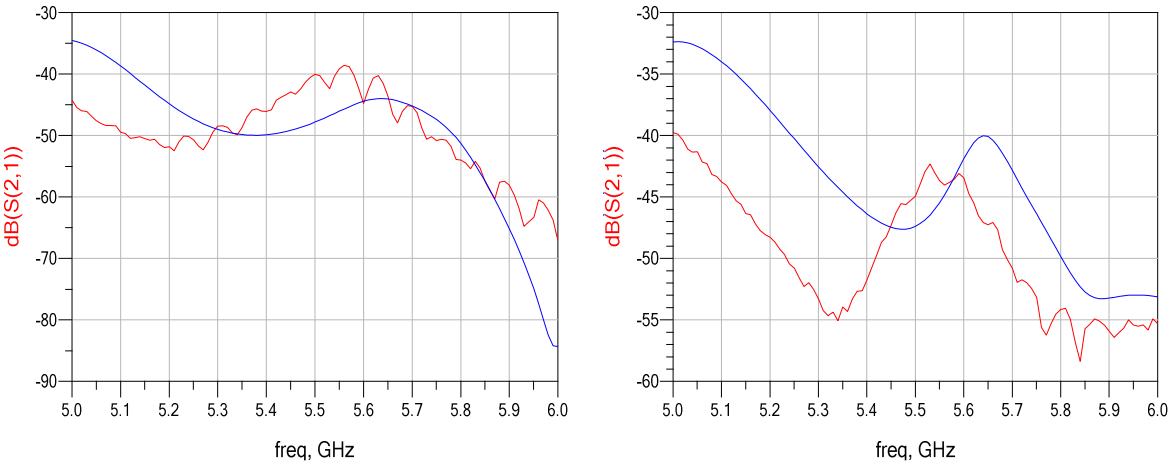

a) b)

Figure 5.31: Mutual coupling through simulation (blue curve) and measurement (red curve): a) oriented along E-plane, b) oriented along H-plane.

Two Element patch antenna array	**3D Simulation (S_{12})**	**Realization (S_{12})**
Conventional patches$_{(E\text{-plane})}$	-21.03dB	-21.56dB
Conventional patches$_{(H\text{-plane})}$	-27.45dB	-29.53dB
Pin loaded patches$_{(E\text{-plane})}$	-26.04dB	-
Pin loaded patches$_{(H\text{-plane})}$	-31.64dB	-
Pin loaded patches with walls$_{(E\text{-plane})}$	-44.89dB	-39.18dB
Pin loaded patches with walls$_{(H\text{-plane})}$	-42.14dB	-44.06dB

Table 5.5: Summarized comparative analysis on the reduction of mutual coupling among conventional patch antennas, pin loaded patch antennas and pin loaded patch antennas with metallic wall barrier in E and H-plane configurations.

It can be observed that the proposed design in E-plane and H-plane improves isolation (realized value) by 19 dB and 15 dB, respectively as compared to conventional patch antenna arrays. The screen shot of the measurement setup is shown in Figure 5.32.

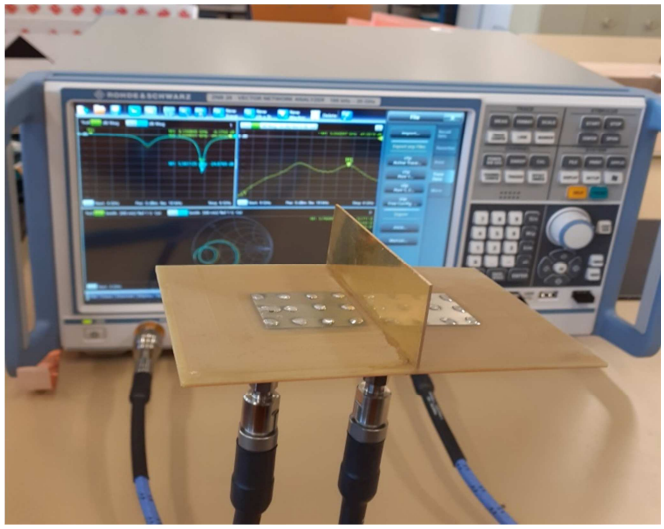

Figure 5.32: Screen shot of measurement setup.

5.8.4 Parametric analysis of the effect of mutual coupling with respect to height of the metallic wall

A parametric analysis of the variation in level of mutual coupling with respect to height of the wall has been carried out in both E and H-planes. It has been observed that a variation in height of the wall (W_h) produces a linear shift in transmission coefficient for this particular design. As the height of the wall is increased, a tendency of lower mutual coupling is observed. S-parametric analysis of mutual coupling variation along E-plane and H- plane with respect to height of the metallic wall is illustrated through Figure 5.33.

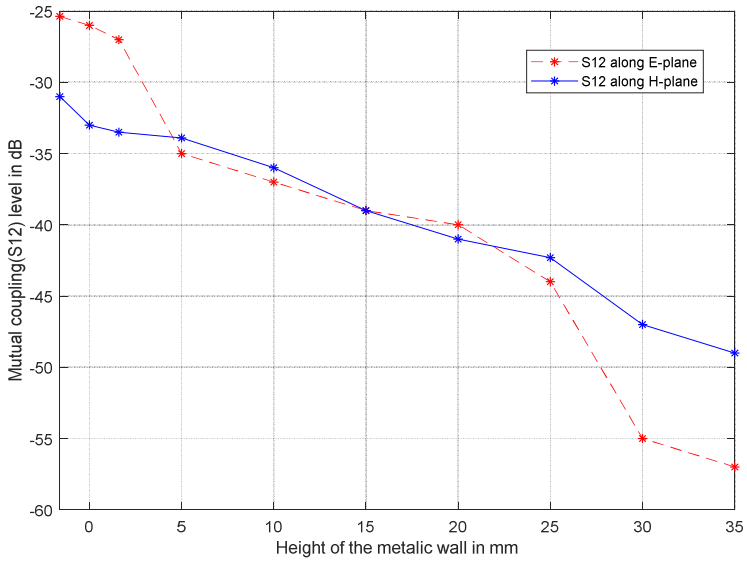

Figure 5.33: Parametric analysis of mutual coupling variation with respect to the wall height (W_h) in E and H-plane orientations in pin loaded patch antenna arrays.

In addition to how mutual coupling gets affected with the size of the metallic wall in between two antennas, Figure 6.23 relates also three other cases in both E and H-plane orientations briefed below:

- Case (a): In Figure 5.33, height of the wall (-1.6*mm*) refers to Figure 5.34(a) where there is continuous substrate involved.
- Case (b): In Figure 5.33, height of the wall (0*mm*) refers to Figure 5.34(b) where there is an air cavity involved (with cavity of 1 *mm* width).
- Case (c): In Figure 5.33, height of the wall (1.6*mm*) refers to Figure 5.34(c) where there is metallic cavity involved (with cavity of 1 *mm* width).

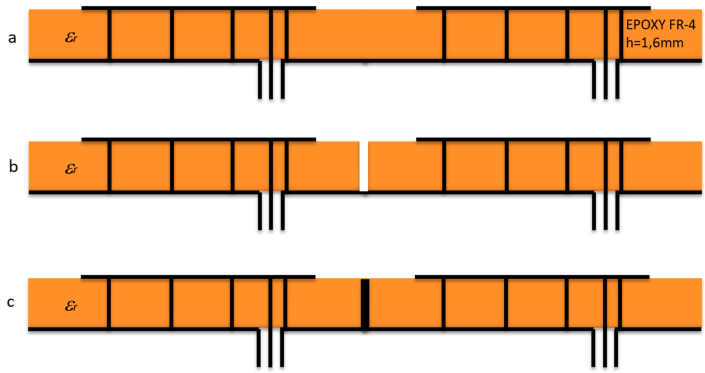

Figure 5.34: Side view of two pin loaded patch antennas: a) Two patches on a continuous substrate, b) Two patches with partially removed substrate (air cavity), c) Two patches with metallic wall in substrate (metallic cavity).

The effect on mutual coupling in all three cases (a-c) in E-plane and H-plane has been summarized in Table 5.6.

Two pin loaded patch antennas	**E-plane coupling (S_{12})**	**H-plane coupling (S_{12})**
Case (a)	-26.04dB	-31.64dB
Case (b)	-26.5dB	-33dB
Case (c)	-27dB	-33.5dB

Table 5.6: Comparison of isolation level among three cases in two pin loaded patch antenna elements oriented along E-plane and H-plane; a) on a continuous substrate, b) with partially removed substrate (air cavity), c) with metallic wall in substrate (metallic cavity).

Here, case (a) shows the highest level of mutual coupling. Case (b) with air cavity exhibits around 0.5 dB and 1.5 dB reduction of mutual coupling in E and H-plane, respectively with reference to case (a). While case (c) shows around 1 dB and 2 dB coupling reduction in E and H-planes with reference to case (a). It implies that the pin loaded patch antennas present least quantity of surface waves. That is the reason; introducing air cavity and metallic cavity in such antennas do not reduce much of mutually coupled power through surface waves.

5.9 Four element pin loaded patch antenna array with metallic walls oriented along E-plane.

In previous sections, it has been observed that an isolation of about 39 dB (Measured value) in between two elements is attained in E-plane. This decoupled power is quite negligible. In this section, we would build four element E-plane decoupled array to see whether active S-parameters present same values to that of simple S-parameters and compare those results. Here, it is important to recall that the theoretical results obtained in chapter 3 are based on conventional patch antenna and cannot be related with pin loaded patch antenna since both represent different models. Cavity model of pin loaded patch antennas is part of future studies and is not incorporated in this thesis.

5.9.1 3D simulation of four patch antenna array

The four element pin loaded patch antenna array with metallic wall structure oriented along E-plane has been simulated (Figure 5.35) and their corresponding S-parameters are shown in Figure (5.36). It can be observed that the maximum coupled power shared between inner two antenna elements is -34.88 dB as shown in Figure 5.36. The denormalised input impedance of each antenna has been recorded in Table 5.7.

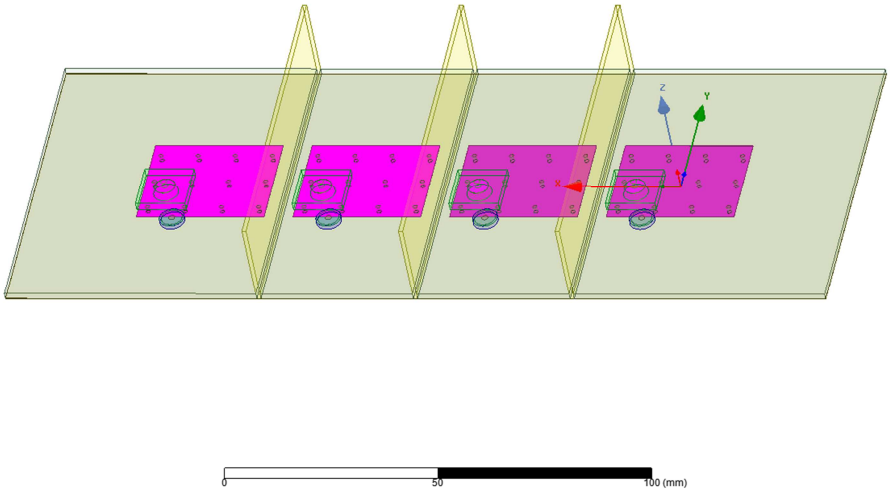

Figure 5.35: Four pin loaded patch antenna elements with metallic walls oriented along E-plane.

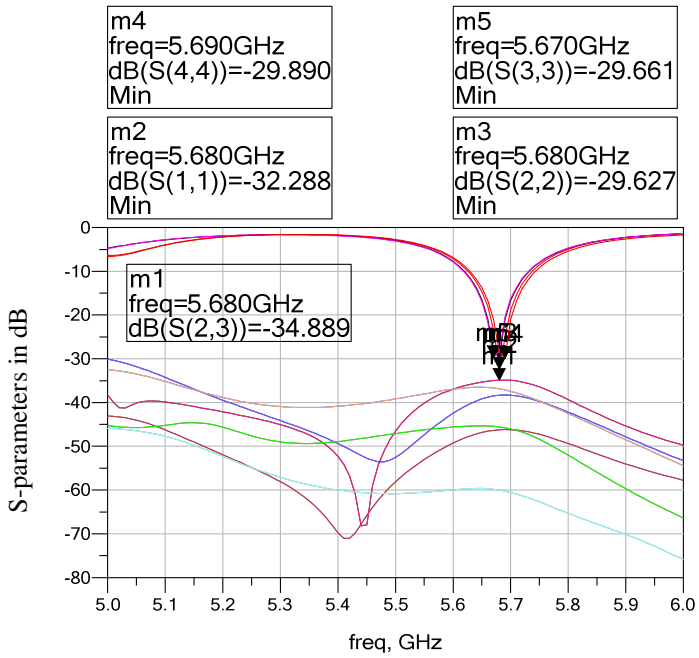

Figure 5.36: Simulated S-parameters of four pin loaded patch antenna elements with metallic walls oriented along E-plane.

Input impedance in Ω @ 5.69 GHz	**A) Zin passive**	**B) Zin active from HFSS**
Antenna 1	(54.86+j0.38) Ω	(54.09-j0.53) Ω
Antenna 2	(58.58+j1.48) Ω	(56.29-j0.82) Ω
Antenna 3	(59.31+j1.86) Ω	(57.15-j1.22) Ω
Antenna 4	(53.30-j0.30) Ω	(52.91-j1.62) Ω

Table 5.7: Input impedance evaluated via HFSS for four pin loaded patch antenna elements with metallic walls oriented along E-plane.

Table 5.7(column A) shows the values obtained according to passive S-parameters. Here, the antennas present a different value than 50Ω and it is probably due to the proximity of the antenna elements. The antennas (1 and 4) and antennas (2 and 3) present also a slightly different value which is due to the introduced mesh. Column B shows the results of active S-parameters according to equation 4.3. It can be observed that both antennas 1 and 4 present almost same values in column A and B (edge elements) and antenna 2 and 3 present a difference of almost 2 Ω which is due to the present coupled power (-34.88 dB). According to passive typical calculation from equation 4.3, it has been shown that a coupling factor as small as -34.88 dB seems small enough to let the input impedance of antennas in the array similar to these obtained by a passive analysis. This leads us to consider that a coupling factor less than 34.88 dB remains a targetable objective when focusing only on reducing coupling phenomenon.

5.9.2 Measurement analysis of four elements

Four pin loaded patch antenna elements arranged along E-plane with metallic wall barriers has been fabricated as shown in Figure 5.37. The array is put under test for S-parametric analysis. The S-parameters have been shown in Figure 5.38 with inner element (antenna 2 and 3) coupling of -37 dB which is about 2 dB better than that of simulation and also consistent with the previous analysis which leads us to consider a coupling better than -34.88 dB. The denormalised input impedance of all four antennas has been recorded in Table 5.8 from their corresponding smith charts.

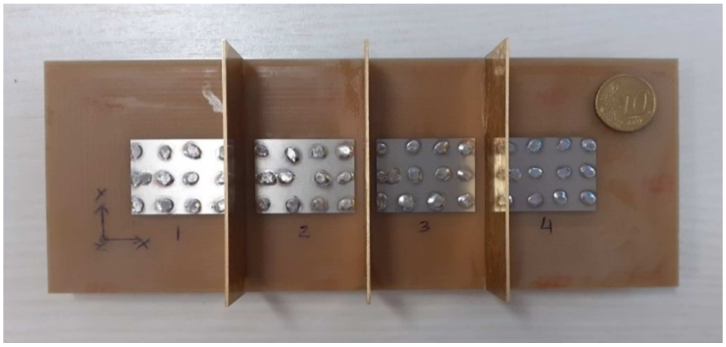

Figure 5.37: Fabricated pin loaded four patch antenna elements with metallic walls oriented along E-plane.

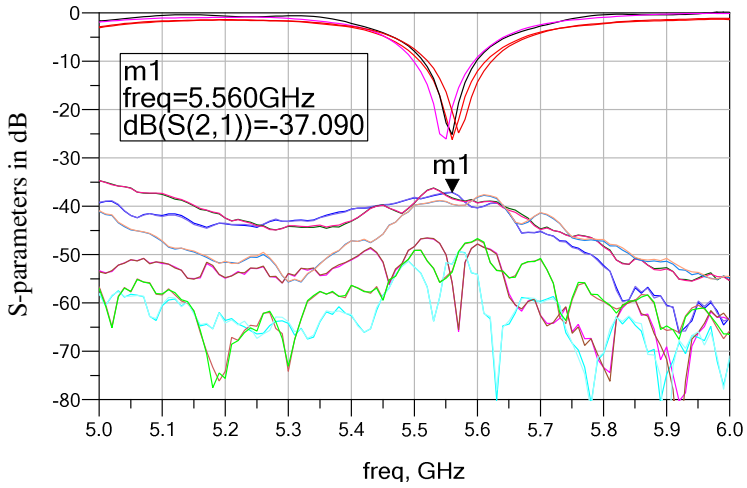

Figure 5.38: Measured S-parameters of pin loaded four patch antenna elements with metallic walls oriented along E-plane.

Because of the manufacturing tolerance, a slight shift in frequency is observed (5.56 GHz). This slight change in frequency will not affect the observance of our results in terms of input impedance analysis.

Here, Table 5.8 (column A) shows the denormalised impedance evaluated through passive S-parameters obtained from their smith chart (Figure 5.39). Column B shows

active S-parameters evaluated according to equation 4.3. It can be observed that the obtained results in column A and B present almost the same values in all antennas. It means that -37 dB coupled power does not alter the impedance evaluated through active S-parameters (equation 4.3). It is of interest to note that the values obtained through coherent mode of VNA (column C), where all antennas radiate simultaneously, present a decreased value despite having negligible coupling. It can be further observed from Table 5.8(column C) that as every element of the array is powered on simultaneously, not only the real part of impedance changes at the frequency of interest, the reactive part changes also.

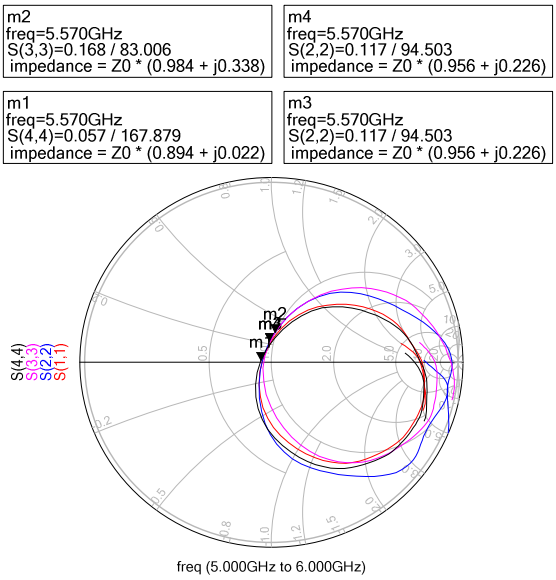

Figure 5.39: Smith chart of pin loaded four patch antenna elements with metallic walls oriented along E-plane.

Input impedance in Ω @ 5.56GHz	**A) One antenna is powered on**	**B) Zin active according to equation 4.3**	**C) All antennas are powered on simultaneously**
Antenna 1	(49.2+j16.9) Ω	(49.05+j14.75) Ω	(46.5+j19.35) Ω
Antenna 2	(47.8+j11.4) Ω	(48.15+j8.95) Ω	(44.6+j14.17) Ω
Antenna 3	(47.8+j11.4) Ω	(48.15+j8.95) Ω	(44.6+j14.18) Ω
Antenna 4	(44.7+j1.1) Ω	(44.96+j0.4) Ω	(41.7+j5.23) Ω

Table 5.8: Input impedance of pin loaded four patch antennas with metallic walls evaluated through measurement.

It can be inferred from above discussion that despite having negligible coupling, the effect of total radiation cannot be ignored. We observe through Table 5.8 (column C) that when all antenna elements radiate simultaneously, the impedance of proposed antenna elements decrease as compared to their standalone values.

These findings thus lend support for the hypothesis that the decreased values (in true active S-parameters) is perhaps the result of total radiation caused by the antenna array elements. This leads us to assume that perhaps four antenna elements is not enough to characterize fully the effect of total radiation. Most importantly we need to test practically bigger array (more than 16 elements at least) to consolidate the proposed hypothesis. Nevertheless, it has been shown that simultaneously excited antenna array exhibits different values as compared to standalone values of antenna elements in presence of practically negligible coupling.

5.10 Conclusion

In the first part of this chapter, the impact of mutual coupling in microstrip antenna arrays parameters is studied and discussed. A theoretical background about antenna mutual coupling was presented where several useful concepts were revised. A literature review about the different decoupling techniques was cited precisely, along the ones that were simulated and analyzed.

A two element patch antenna array oriented along E-plane with novel DGS (μ-shaped) design was simulated. This technique has the advantage of simple execution and improves the isolation between the microstrip antenna elements upto -33 dB. A parametric analysis of coupling with respect to width (W1) of the DGS was carried out. It was found that a variation in the width of the DGS produces a shift in the cutoff frequency for this particular design. As a limitation, we could find a narrow bandwidth of the stop band filter.

In the second part of this chapter, a pin loaded patch antenna has been shown to outperform a conventional patch antenna in terms of suppressing surface waves and radiation in horizontal directions resulting in better directivity. Moreover, when these pin loaded patch antennas are set in arrays, at a separation distance of $0.7\lambda_0$ between their feed points, they share -5 dB and -4 dB less coupled power (simulated value) as compared to conventional patch antenna array arranged along E-plane and H-plane orientations, respectively. For further reduction of coupling, pin loaded patch antennas arrays are complemented with metallic walls erected in between the antenna elements to reduce the effect of free space waves coupling. When a combination of pins and metallic wall is utilized, a reduction of -19 dB and -15 dB in E-plane and H-plane, respectively, has been observed (measured value) at the resonant frequency. It has also been shown that apart from suppression of mutual coupling, this technique presents a wide band rejection characteristic of transmission coefficient along both E and H-plane orientations.

The third part of this chapter further highlights the importance of simultaneous excitation of antenna elements when there is negligible mutual coupling. It has been observed that -37 dB (measured value) of coupled power presents same values as that of passive S-parameters and active S- parameters (based on passive scattering). However, in addition to that it has been observed that when all antennas are excited simultaneously according to coherent mode of excitation of VNA, the true active S-parameters present decreased values as compared to so called active S-parameters based on passive scattering. Even if the model of pin loaded patch antenna has not been develop yet, the results obtained tend to prove that the passive scattering approach to evaluate the active one is not

accurate enough as a shift is always observed when comparing the true active S matrix and its approximate value through equation 4.3 using measured values.

Chapter 6

Conclusion & Perspectives

6.1 Conclusion

The objective of this thesis is to propose and clarify input impedance evaluation from the effect of total radiation.

In chapter 1, an introduction about antenna and antenna arrays has been presented. In addition to that a background study about different antenna analysis methods has been presented along with motivation, thesis contribution and thesis structure.

In chapter 2, we have developed the basic concepts related to antenna radiating field regions and antenna analysis parameters. These basic concepts are used frequently to define and characterize antenna and antenna array performance.

A model to evaluate input impedance of individual antenna elements in an array based on total radiation has been proposed in chapter 3. In this regard, we have built a theoretical model to evaluate input impedance of different antennas (short dipole, resonant half wave length dipole, patch antenna) in different combinations (linear and planar). It has been demonstrated that by arraying the antennas the input impedance of each element in the array changes compared to that of single element which is not arrayed. In other words input impedance changes versus antenna number and position. In this approach, we do not take into account mutual coupling. However, the results suggest that even though there is no mutual coupling, the input impedance of individual antenna elements varies in an array inferring the cause being the total radiation. In our approach, we have considered free space combination as a probable contributor so we tried to investigate this part by isolating this contributor considering the others as null. Nevertheless, it will be interesting to have a deeper approach of all other possible contributors which in terms could explain the impedance shift on antenna array. It's also highly likely that some aspects are not taken into account in the array calculations.

Further, in order to consolidate the theoretical aspect of the effect of total radiation, an array of patch antennas has been manufactured in chapter 4. In this part, the problem to address is to excite all antennas simultaneously. This is done with the help of existing four ports VNA. The used VNA (R&S ZVA24) is capable of providing two coherent signals out of four ports. Thus, a novel method of exciting any number of antenna elements is introduced with the help of power splitter. This work further proposes an important aspect of the evaluation of active S-parameters in antenna arrays. It has been observed that the active S-parameters obtained by using the passive scattering matrix do not correspond to the actual values obtained during a simultaneous excitation of all the elements.

Since the theoretical code does not include the effect of mutual coupling, hence to verify the effect of total radiation practically, we need to decouple an antenna array to a

level where mutual coupling presents no change of active S-parameters as compared to passive S-parameters. In this context, in the first section of chapter 5, a novel DGS (**μ** shaped) has been introduced. This work reduced coupling upto -33 dB in two E-plane oriented patch antenna arrays with limitation of narrow band rejection characteristics of transmission coefficient (S_{12}).

To have even better rejection in coupled power and wide band rejection characteristics, a method of loaded pins with metallic walls has been introduced in the second section of chapter 5. A method of loaded patch antennas with shorting pins and erected walls in between patch antenna arrays is introduced to reduce surface waves and free space wave coupling in both E and H-plane, respectively. This simple technique works equally well in both orientations by reducing coupling upto -39 dB and -44 dB (measured value) in E-plane and H-plane, respectively, as compared to conventional patch antenna array. Apart from mutual coupling reduction, this technique presents wide band rejection characteristics of transmission coefficient (S_{12}). This section further highlights that coupling less than -34.88 dB is fully negligible if we consider active scattering through passive matrix as the impedance does not change much.

Further, a four element patch antenna array in E-plane with -37 dB of coupled power, in between two inner antennas, has been manufactured and put under test. It has been shown that despite having negligible mutual coupling, the active S-parameters evaluated through passive scatterings do not correspond to same values when all antennas radiate simultaneously according to coherent mode of VNA. Finally, input impedance of measured four element antenna array, evaluated through the true active S-parameters is analyzed. These findings lend support for the hypothesis that the decreased values (in true active S-parameters) are perhaps the result of total radiation caused by the antenna array elements.

6.2 Perspectives

The work in this thesis correlates the theory of the effect of total radiation on the impedance value of an array. Apart from this, it has been observed that active s-parameters evaluated through passive scattering matrix do not correspond to actual values obtained through simultaneously excited antenna array (through coherent mode of excitation of VNA). In light of this, the research has also opened a horizon for carrying out further analysis starting from the observations carried out in this work. Even though these techniques do not result in the desired end-state of implementation in operational arrays, still they can be useful in laboratory and simulation set-ups to facilitate and enhance greater understanding of total radiation from an array and its corresponding effects on different antenna types and array arrangements.

Thus, further research can be focused on;

- To address the aspect of the physical explanation behind the change in input impedance of individual antenna elements due to the effect of total radiation.
- To test and verify bigger arrays through measurements (more than 16 elements) to verify and consolidate further the effect of total radiation.

- To develop cavity like model for shorted pin loaded patch antenna to evaluate its input impedance. The model should be consistent with that of the measured one when coupling is observed negligible.
- To verify the effect of total radiation in other types of antenna elements (wide band and non-resonant antennas).
- The research can also be focused on this issue of mismatch which has not been apprehended so for. Development of equations or physical solutions may still be taken into account to propose so that the effect of mismatch may properly be understood and overcome.

References

[1] "Heinrich Hertz."

[Online]. Available: https://en.wikipedia.org/wiki/Heinrich_Hertz.

[2] "Guglielmo Marconi."

[Online].Available: https://en.wikipedia.org/wiki/Guglielmo_Marconi.

[3] "Luis Alvarez."

[Online]. Available: https://en.wikipedia.org/wiki/Luis_Walter_Alvarez.

[4] R. Mailloux, *Phased Array Antenna Handbook*, 2nd ed., vol. 16, no. 4. Artech House, 2011.

[5] R. W. Bickmore, "Adaptive antenna arrays," *IEEE Spectr.*, vol. 1, no. August, pp. 78–88, 1964.

[6] R. F. Harrington, *Field Computation by Moment Methods*. New York: Macmillan Publishing Company, 1993.

[7] C. A. Balanis, "Antenna theory: a review," in *Proceedings of the IEEE*, 1992, vol. 80, no. 1, pp. 7–23.

[8] F. M. Kahnert, "Numerical methods in electromagnetic scattering theory," *J. Quant. Spectrosc. Radiat. Transf.*, vol. 80, pp. 775–824, 2003.

[9] C. A. Balanis, *Antenna Theory: Analysis and Design*, 3rd ed., vol. 38, no. 6. John Wiley & Sons, 2005.

[10] H. T. Hui, "Mutual Coupling in Antenna Arrays," *Int. J. Antennas Propag.*, vol. 2010, pp. 1–2, 2010.

[11] D. F. Kelley and W. L. Stutzman, "Array Antenna Pattern Modeling Methods That Include Mutual Coupling Effects," *IEEE Trans. Antennas Propag.*, vol. 41, no. 12, pp. 1625–1632, 1993.

[12] D. F. Kelley, "Relationships between Active Element Patterns and Mutual Impedance Matrices in Phased Array Antennas," in *IEEE Antennas and Propagation Society International Symposium (IEEE Cat. No.02CH37313), San Antonio, TX, USA*, 2002, pp. 524–527.

[13] D. F. Kelley, "Embedded element patterns and mutual impedance matrices in the terminated phased array environment," in *2005 IEEE Antennas and Propagation Society International Symposium, Washington, DC*, 2005, no. 1, pp. 659–662.

[14] D. M. Pozar, "The active element pattern," *IEEE Trans. Antennas Propag.*, vol. 42, no. 8, pp. 1176–1179, 1994.

[15] D. M. Pozar, "A relation between the active input impedance and the active element pattern of a phased array," *IEEE Trans. Antennas Propag.*, vol. 51, no. 9, pp. 2486–

2489, 2003.

[16] Q. Li, W. Shao, and H. Li, “Scattering Pattern Calculation for Large Finite Arrays using the Element-Varying Active Element Factor Method,” *Appl. Comput. Electromagn. Soc. J.*, vol. 26, no. 11, pp. 893–898, 2011.

[17] R. Mittra, C. H. Chan, and T. Cwik, “Techniques for Analyzing Frequency Selective Surfaces-A Review,” in *Proceedings of the IEEE*, 1988, vol. 76, no. 12, pp. 1593–1615.

[18] A. K. Bhattacharyya, *Phased Array Antennas: Floquet Analysis, Synthesis, BFNs, and Active Array Systems*. Hoboken, NJ, USA: John Wiley & Sons, 2006.

[19] Y. Liu, X. Huang, K. Da Xu, Z. Song, S. Yang, and Q. H. Liu, “Arrays Including Mutual Coupling Using Iterative FFT via Virtual Active Element Pattern Expansion,” *IEEE Trans. Antennas Propag.*, vol. 65, no. 8, pp. 3950–3958, 2017.

[20] H. Marder, Michael and . Aubert, “the Concept of Scale-Changing Network in the Global Electromagnetic Simulation of Complex Structures,” *Prog. Electromagn. Res. Electromagn. Res. B*, vol. 16, no. May, pp. 127–154, 2009.

[21] A. K. Bhattacharyya, “Accuracy of floquet model in predicting performances of finite arrays,” *IEEE Antennas Wirel. Propag. Lett.*, vol. 13, pp. 19–22, 2014.

[22] A. Maati, C. Menudier, M. Thevenot, F. Torres, and T. Monediere, “Determination of the scattering matrix of large periodic antenna arrays,” *2016 10th Eur. Conf. Antennas Propagation, EuCAP 2016*, pp. 1–3, 2016.

[23] B. Lesur *et al.*, “Development and validation of modelling techniques for large periodic arrays in Ka-band,” *2017 11th Eur. Conf. Antennas Propagation, EUCAP 2017*, pp. 3728–3732, 2017.

[24] S. M. Mikki and Y. M. M. Antar, “Near-Field Analysis of Electromagnetic Interactions in Antenna Arrays Through Equivalent Dipole Models,” *IEEE Trans. Antennas Propag.*, vol. 60, no. 3, pp. 1381–1389, 2012.

[25] P. Kabacik, “Active microstrip array for satellite communication applications,” in *Proceedings of 1995 SBMO/IEEE MTT-S International Microwave and Optoelectronics Conference, Rio de Janeiro, Brazil*, 1995, pp. 626–631.

[26] A. Harrabi, “Conception et réalisation d’une antenne plate pour la réception satellite, Thèse de Doctorat, Université de Nantes, Nantes, France,” 2015.

[27] “Antenna Polarisation.”

[Online].Available:https://www.electronicsforu.com/resources/learn-electronics/antenna-polarisation.

[28] “Antenna impedance.”

[Online]. Available: http://www.antenna-theory.com/basics/impedance.php.

[29] “Omni-directional antenna.”

[Online]. Available: https://en.wikipedia.org/wiki/Omnidirectional_antenna.

[30] G. Augustin, P. C. Bybi, V. P. Sarin, P. Mohanan, C. K. Aanandan, and K. Vasudevan, “A Compact Dual-Band Planar Antenna for DCS-1900/PCS/PHS,

WCDMA/IMT-2000, and WLAN Applications," *IEEE Antennas Wirel. Propag. Lett.*, vol. 7, pp. 108–111, 2008.

[31] H. Wang, X. B. Huang, and D. G. Fang, "A Single Layer Wideband U-Slot Microstrip Patch Antenna Array," *IEEE Antennas Wirel. Propag. Lett.*, vol. 7, pp. 9–12, 2008.

[32] A. D. Yaghjian, S. R. Best, and S. Member, "Impedance , Bandwidth , and Q of Antennas," *IEEE Trans. Antennas Propag.*, vol. 53, no. 4, pp. 1298–1324, 2005.

[33] S. De Silva, L. Belostotski, and M. Okoniewski, "Modeling and Measuring of Antenna Array S-parameters and Radiation Efficiency," *2017 IEEE Int. Symp. Antennas Propag. Usn. Natl. Radio Sci. Meet.*, pp. 2293–2294, 2017.

[34] K. Kurokawa, "Power Waves and the Scattering Matrix," *IEEE Trans. Microw. Theory Tech.*, vol. 13, no. 1, pp. 194–202, 1964.

[35] "The short dipole antenna." [Online]. Available: http://www.antenna-theory.com/antennas/shortdipole.php.

[36] R. Pokuls, J. Uher, and D. M. Pozar, "Dual-Frequency and Dual-Polarization Microstrip Antennas for SAR Applications," *IEEE Trans. Antennas Propag.*, vol. 46, no. 9, pp. 1289–1296, 1998.

[37] A.G Deschamps, "Microstrip antennas," in *Third USAF Symposium on Antennas*, 1953, p. 1.

[38] R. E. Munson, "Conformed Microstrip Antennas Microstrip Phased Arrays.," *Antennas Propagation, IEEE Trans.*, vol. 22, pp. 74–78, 1974.

[39] K. R. Carver, "A Leaky Wave Analysis of the High-Gain Printed Antenna Con guration.," in *Proceedings of the Workshop on Printed Antenna Technology*, 1979, pp. 1–4.

[40] D. C. Chang, "Conformed Microstrip Antennas Microstrip Phased Arrays," *Spec. Issue. Antennas Propagation, IEEE Trans.*, vol. 29, pp. 1–4, 1981.

[41] I. J. B. Bhartia., *Microstrip Antennas. Norwood, MA : Artech House,*. 1980.

[42] D. M. Pozar, "Microstrip antennas," *Proc. IEEE*, vol. 80, no. 1, pp. 79–91, 1992.

[43] "The basics of patch antennas." [Online]. Available: https://its-wiki.no/images/c/cf/The_Basics_Of_Patch_Antennas.pdf.

[44] P. Bhartia, K. V. S. Rao, and R. S. Tomar, *Millimeter-wave microstrip and printed circuit antennas*. Bostan, MA: Artech House, 1991.

[45] C. R. Keith and J. W. Mink, "Microstrip Antenna Technology," *IEEE Trans. Antennas Propag.*, vol. AP-29, no. 1, 1981.

[46] Girish Kumar and K. P. Ray, *Broadband Microstrip Antennas*. Artech House, 2003.

[47] Chen Zhang et al, "Measurement of Active S-Parameters on Array Antenna Using Directional Couplers," in *2017 IEEE Asia Pacific Microwave Conference (APMC)*, 2017, pp. 1167–1170.

[48] M. Kalfa and E. Halavut, "A Fast Method for Obtaining Active S-Parameters in Large Uniform Phased Array Antennas," in *IEEE International Symposium on*

Phased Array Systems and Technology, Waltham, MA, 2013, 2013, pp. 684–688.

[49] A. R. Djordjevic and M. M. Nikolic, "Microstrip Antennas With Suppressed Radiation in Horizontal Directions and Reduced Coupling," *IEEE Trans. Antennas Propag.*, vol. 53, no. 11, pp. 3469–3476, 2005.

[50] F. LINOT, "Apport des Surfaces à Hauteb Impédance à la conception d'antennes réseaux compactes et d'antennes réseaux à très large bande passante," Doctoral thesis, Paris Tech, Paris, 2011.

[51] S. Gmbh and C. Kg, "Vector Network Analyzers Operating Manual." [Online]. Available:https://cdn.rohdeschwarz.com/pws/dl_downloads/dl_common_library/dl_manuals/gb_1/z/zva_2/ZVA_ZVB_ZVT_OperatingManual_en_30.pdf.

[52] I. Gupta and A. Ksienski, "Effect of Mutual Coupling on the Performance of Adaptive Arrays," *IEEE Trans. Antennas Propag.*, vol. 31, no. 5, pp. 785–791, 1983.

[53] G. J. Foschini and M. J. Gans, "On Limits of Wireless Communications in a Fading Environment when Using Multiple Antennas," *Wirel. Pers. Commun.*, vol. 6, no. 3, pp. 311–335, 1998.

[54] Y. Urzhumov and D. R. Smith, "Metamaterial-enhanced coupling between magnetic dipoles for efficient wireless power transfer," *Phys. Rev. B*, vol. 83, no. 20, 2011.

[55] H. M. Aumann, A. J. Fenn, and A. J. Fenn, "Phased array antenna calibration and pattern prediction using mutual coupling measurements," *IEEE Trans. Antennas Propag.*, vol. 37, no. 7, pp. 844–850, 1989.

[56] H. Zhang, Y. Mahe, and T. Razban, "Ku-band Dual-polarized Patch Antenna Array Arrangement Using Patch Sharing Technique," in *Proceedings of the 44th European Microwave Conference*, 2014, pp. 390–393.

[57] J. Hannula, A. Lehtovuori, R. Luomaniemi, T. O. Saarinen, and V. Viikari, "Beneficial Interaction of Coupling and Mismatch in a Two-Antenna System," in *13th European Conference on Antennas and Propagation*, 2019, no. EuCAP, pp. 1–4.

[58] H. Lui, H. T. Hui, and M. S. Leong, "A Note on the Mutual-Coupling Problems in Transmitting and Receiving Antenna Arrays," *IEEE Antennas Propag. Mag.*, vol. 51, no. 5, pp. 3–8, 2009.

[59] G. Dubost, "Influence of surface wave upon efficiency and mutual coupling between rectangular microstrip antennas," in *International Symposium on Antennas and Propagation Society, Merging Technologies for the 90's, Dallas, TX, USA*, 1990, pp. 660–663.

[60] D.M.Pozar and P. R. Haddad, "Anomalous Mutual Coupling Between Microstrip Antennas," *IEEE Trans. Antennas Propag.*, vol. 42, no. 11, pp. 1545–1549, 1994.

[61] M. A. Khayat, S. Member, J. T. Williams, S. Member, D. R. Jackson, and S. A. Long, "Mutual Coupling Between Reduced Surface-Wave Microstrip Antennas," *IEEE Trans. Antennas Propag.*, vol. 48, no. 10, pp. 1581–1593, 2000.

[62] D. R. Jackson, J. T. Williams, A. K. Bhattacharyya, R. L. Smith, S. J. Buchheit, and S. A. Long, "Microstrip Patch Designs That Do Not Excite Surface Waves," *IEEE*

Trans. Antennas Propag., vol. 41, no. 8, pp. 1026–1037, 1993.

[63] D. R. Jackson, "Fundamental Superstrate (Cover) Effects on Printed Circuit Antennas," *IEEE Trans. Antennas Propag.*, vol. 32, no. 8, pp. 807–816, 1984.

[64] J. Yook and L. P. B. Katehi, "Micromachined Microstrip Patch Antenna With Controlled Mutual Coupling and Surface Waves," *IEEE Trans. Antennas Propag.*, vol. 49, no. 9, pp. 1282–1289, 2001.

[65] Y. Liu and X. Zhao, "Perfect Absorber Metamaterial for Designing," *IEEE Antennas Wirel. Propag. Lett.*, vol. 13, pp. 1473–1476, 2014.

[66] Q. Zhang, Y. Jin, J. Feng, X. Lv, and L. Si, "Mutual Coupling Reduction of Microstrip Antenna Array Using Metamaterial Absorber," in *2015 IEEE MTT-S International Microwave Workshop Series on Advanced Materials and Processes for RF and THz Applications (IMWS-AMP), Suzhou*, 2015, pp. 8–10.

[67] F. Yang and Y. Rahmat-samii, "Microstrip Antennas Integrated With Electromagnetic Band-Gap (EBG) Structures : A Low Mutual Coupling Design for Array Applications," *IEEE Trans. Antennas Propag.*, vol. 51, no. 10, pp. 2936–2946, 2003.

[68] R. Coccioli, F.-R. Yang, K. Ma, and T. Itoh, "Aperture-Coupled Patch Antenna on," *IEEE Trans. Microw. Theory Tech.*, vol. 47, no. 11, pp. 2123–2130, 1999.

[69] Z. Iluz, R. Shavit, S. Member, and R. Bauer, "Microstrip Antenna Phased Array With Electromagnetic Bandgap Substrate," *IEEE Antennas Wirel. Propag. Lett.*, vol. 52, no. 6, pp. 1446–1453, 2004.

[70] M. Coulombe, S. F. Koodiani, C. Caloz, and S. Member, "Compact Elongated Mushroom (EM) -EBG Structure for Enhancement of Patch Antenna Array Performances," *IEEE Trans. Antennas Propag.*, vol. 58, no. 4, pp. 1076–1086, 2010.

[71] D. Guha, S. Biswas, and C. Kumar, "Printed antenna design using defected ground structures: a review of fundamentals and state-of-the-art developments," in *Proceedings of the Forum for Electromagnetic Research Methods and Application Technologies (FERMAT '14),* 2014, no. 2, pp. 1–13.

[72] I. Nadeem and D. Choi, "Study on Mutual Coupling Reduction Technique for MIMO Antennas," *IEEE Access*, vol. 7, pp. 563–586, 2019.

[73] J. Zbitou, A. Tajmouati, M. Latrach, A. Errkik, and L. El Abdellaoui, "A New Design of a Miniature Microstrip Patch Antenna Using Defected Ground Structure DGS," in *2017 International Conference on Wireless Technologies, Embedded and Intelligent Systems (WITS)*, 2017, pp. 1–4.

[74] D. Hou, S. X. B. Wang, L. J. J. Wang, and W. Hong, "Elimination of scan blindness with compact defected ground structures in microstrip phased array," *IET Microwaves, Antennas Propag.*, vol. 3, no. 2, March 2009, pp. 269–275, 2009.

[75] S. X. M. Tang and Y. B. S. Gao, "Mutual coupling suppression in microstrip array using defected ground structure," *IET Microwaves, Antennas Propag.*, vol. 5, no. 12, September 2011, pp. 1488–1494, 2011.

[76] E. Rajo-iglesias, S. Member, Ó. Quevedo-teruel, S. Member, and L. Inclán-sánchez, "Mutual Coupling Reduction in Patch Antenna Arrays by Using a Planar EBG

Structure and a Multilayer Dielectric Substrate," *IEEE Trans. Antennas Propag.*, vol. 56, no. 6, pp. 1648–1655, 2008.

[77] E. Beiranvand, M. Afsahy, and V. Sharbati, "Reduction of the mutual coupling in patch antenna arrays based on EBG by using a planar frequency-selective surface structure," *Int. J. Microw. Wirel. Technol.*, vol. 9, no. 2, pp. 349–355, 2015.

[78] L. Qiu, F. Zhao, K. Xiao, S. Chai, and J. Mao, "Transmit – Receive Isolation Improvement of Antenna Arrays by Using EBG Structures," *IEEE Antennas Wirel. Propag. Lett.*, vol. 11, pp. 93–96, 2012.

[79] S. Farsi *et al.*, "Mutual Coupling Reduction Between Planar Antennas by Using a SimpleMicrostrip U-Section," *IEEE Antennas Wirel. Propag. Lett.*, vol. 11, pp. 1501–1503, 2012.

[80] A. Ali, L. Neyestanak, F. Jolani, and M. Dadgarpour, "Mutual coupling reduction between two microstrip patch antennas," in *2008 Canadian Conference on Electrical and Computer Engineering, Niagara Falls*, 2008, pp. 739–742.

[81] H. Qi, L. Liu, X. Yin, H. Zhao, and W. J. Kulesza, "Mutual Coupling Suppression Between Two Closely Spaced Microstrip AntennasWith an Asymmetrical Coplanar Strip Wall," *IEEE Antennas Wirel. Propag. Lett.*, vol. 15, pp. 191–194, 2016.

[82] B. A. Arand, A. Bazrkar, and A. Zahedi, "Design of a Phased Array in Triangular Grid With an Efficient Matching Network and Reduced Mutual Coupling for Wide-Angle Scanning," *IEEE Trans. Antennas Propag.*, vol. 65, no. 6, pp. 2983–2991, 2017.

[83] M. Kiani and H. R. Hassani, "Wide scan phased array patch antenna with mutual coupling reduction," *IET Microwaves, Antennas Propag.*, vol. 12, no. 12, pp. 1932 – 1938, 2018.

[84] X. Zhang, S. Member, and L. Zhu, "Gain-Enhanced Patch Antennas With Loading of Shorting Pins," *IEEE Trans. Antennas Propag.*, vol. 64, no. 8, pp. 3310–3318, 2016.

[85] S. Samanta, P. S. Reddy, and K. Mandal, "Cross-Polarization Suppression in Probe-Fed Circular Patch Antenna Using Two Circular Clusters of Shorting Pins," *IEEE Trans. Antennas Propag.*, vol. 66, no. 6, pp. 3177–3182, 2018.

[86] H. Sanad, "Effect of the shorting posts on short circuit microstrip antennas," in *Proceedings of IEEE Antennas and Propagation Society International Symposium and URSI National Radio Science*, 1994, no. 2, pp. 794–797.

[87] S.D Targonski and R. B. Waterhouse, "Performance of microstrip patches incorporating a single shorting post," *IEEE Antennas Propag. Soc. Int. Symp.*, no. 1, pp. 29–32, 1996.

[88] A. A. Kishk, L. Shafai, and A. Ittipiboon, "Single-element rectangular microstrip antenna for dual frequency operation," *Electron. Lett.*, vol. 19, no. 8, pp. 298–300, 1983.

[89] N.V Shuley and R. B. Waterhouse, "Dual frequency microstrip rectangular patches," *Electron. Lett.*, vol. 28, no. 7, pp. 606–607, 1992.

[90] D. Guha, S. Member, and Y. M. M. Antar, "Circular Microstrip Patch Loaded With

Balanced Shorting Pins for Improved Bandwidth," *IEEE Antennas Wirel. Propag. Lett.*, vol. 5, pp. 217–219, 2006.

[91] M. Abdullah, Q. Li, W. Xue, G. Peng, and Y. He, "Isolation enhancement of MIMO antennas using shorting pins," *J. Electromagn. Waves Appl.*, vol. 33, no. 10, pp. 1–15, 2019.

[92] W. Li, P. Li, and J. Zhou, "Control of Higher Order Harmonics and Spurious Modes for Microstrip Patch Antennas," *IEEE Access*, vol. 6, pp. 34158–34165, 2018.

Appendix A
Matlab Code

```
clear all;
clc;
tic;
warning('off','all')
format shortG
freq = 5*10^9;
c = 3*10^8;
lambda = c./freq;
k = (2.*pi)./lambda;
eta = 120.*pi;
d = lambda;
A=[1 4 16 64 ];
B=[1 2 4 8 16 64 ];


% ResonantWireAntenna

for i=A

Etot1=@(theta,phi)0.5.*sin(theta).*eta.*cos((pi./2).*cos(theta)).*
cos((pi./2).*cos(theta))./((2.*pi).*(2.*pi).*sin(theta).*sin(theta
)).*((sin(((sqrt(i)).*k.*d./2).*sin(theta).*cos(phi)).*sin(((sqrt(
i)).*k.*d./2).*sin(theta).*sin(phi))./sin((k.*d./2).*sin(theta).*c
os(phi))./sin((k.*d./2).*sin(theta).*sin(phi))).^2);
P1 = integral2(Etot1,0,pi,0,2*pi);
Zres(i) = P1.*2./((i));

end

for i=B
Etotx=@(theta,phi)0.5.*sin(theta).*eta.*cos((pi./2).*cos(theta)).*
cos((pi./2).*cos(theta))./((2.*pi).*(2.*pi).*sin(theta).*sin(theta
)).*((sin((i.*k.*d./2).*sin(theta).*cos(phi)).*sin((k.*d./2).*sin(
theta).*sin(phi))./sin((k.*d./2).*sin(theta).*cos(phi))./sin((k.*d
./2).*sin(theta).*sin(phi))).^2);
Etoty=@(theta,phi)0.5.*sin(theta).*eta.*cos((pi./2).*cos(theta)).*
cos((pi./2).*cos(theta))./((2.*pi).*(2.*pi).*sin(theta).*sin(theta
)).*((sin((k.*d./2).*sin(theta).*cos(phi)).*sin((i.*k.*d./2).*sin(
theta).*sin(phi))./sin((k.*d./2).*sin(theta).*cos(phi))./sin((k.*d
./2).*sin(theta).*sin(phi))).^2);
Px = integral2(Etotx,0,pi,0,2*pi);
Py = integral2(Etoty,0,pi,0,2*pi);
Zresx(i) = Px.*2./i;
```

```
Zresy(i) = Py.*2./i;

end

Zres = Zres(find(Zres>0));
Zresx = Zresx(find(Zresx>0));
Zresy = Zresy(find(Zresy>0));
resonantwire_planar = [A;Zres]'
resonantwire_XY = [B;Zresx;Zresy]'

% Short Dipole Antenna

dl = lambda./10;
for i=A
Etot1=@(theta,phi)(((k.*dl.*sin(theta)./(4.*pi)).^2).*eta.*sin(the
ta)./2).*((sin(((sqrt(i)).*k.*d./2).*sin(theta).*cos(phi)).*sin(((
sqrt(i)).*k.*d./2).*sin(theta).*sin(phi))./sin((k.*d./2).*sin(thet
a).*cos(phi))./sin((k.*d./2).*sin(theta).*sin(phi))).^2);
P1 = integral2(Etot1,0,pi,0,2*pi);
Zdip(i) = P1.*2./((i));

end

for i=B
Etotx=@(theta,phi)(((k.*dl.*sin(theta)./(4.*pi)).^2).*eta.*sin(the
ta)./2).*((sin((i.*k.*d./2).*sin(theta).*cos(phi)).*sin((k.*d./2).
*sin(theta).*sin(phi))./sin((k.*d./2).*sin(theta).*cos(phi))./sin(
(k.*d./2).*sin(theta).*sin(phi))).^2);
Etoty=@(theta,phi)(((k.*dl.*sin(theta)./(4.*pi)).^2).*eta.*sin(the
ta)./2).*((sin((k.*d./2).*sin(theta).*cos(phi)).*sin((i.*k.*d./2).
*sin(theta).*sin(phi))./sin((k.*d./2).*sin(theta).*cos(phi))./sin(
(k.*d./2).*sin(theta).*sin(phi))).^2);
Px = integral2(Etotx,0,pi,0,2*pi);
Zdipx(i) = Px.*2./i;
Py = integral2(Etoty,0,pi,0,2*pi);
Zdipy(i) = Py.*2./i;

end

Zdip = Zdip(find(Zdip>0));
Zdipx = Zdipx(find(Zdipx>0));
Zdipy = Zdipy(find(Zdipy>0));
shortdipole_planar = [A;Zdip]'
shortdipole_XY = [B;Zdipx;Zdipy]'


% Patch Antenna

h = 1.6*(10^-3);
k = (2.*pi)./(lambda);
```

```
w = (lambda./2).*(((er+1)./2).^-0.5) ;
eff = ((er+1)/2)+((er-1)/2).*((1+(10*h/w))^(-0.5));
delta = 0.412*h*(eff+0.3)*((w/h)+0.262)./((eff-
0.258)*((w/h)+0.813));
l = (lambda/(2*sqrt(eff)))-(2*delta);
d = (2*l)+(2*delta);
d2 = l+delta;

% Testing with single antenna aperture

G2 = (pi.*w.*(1-(((k.*h)^2)./24))./(eta.*lambda);
Zin1_with_single_aperture_test = 1/(G2);
E2=@(theta,phi)(2.*sin(theta).*sin(phi).*sin(phi).*sin((pi.*w./lam
bda).*sin(theta).*sin(phi)).*sin((pi.*w./lambda).*sin(theta).*sin(
phi)).*cos(pi.*cos(phi).*sin(theta)./(2.*sqrt(eff))).*cos(pi.*cos(
phi).*sin(theta)./(2.*sqrt(eff)))./(pi.*pi.*sin(theta).*sin(phi).
*sin(theta).*sin(phi));
P2 = integral2(E2,0,pi/2,0,2*pi)/eta;
Zin2_with_single_aperture_test = 1/(P2.*2);
patch_with_single_aperture_compare=[Zin1_with_single_aperture_test
;Zin2_with_single_aperture_test]'

% Arrays with single aperture

for i=A
Etot2=@(theta,phi)(2.*sin(theta).*sin(phi).*sin(phi).*sin((pi.*w./
lambda).*sin(theta).*sin(phi)).*sin((pi.*w./lambda).*sin(theta).*s
in(phi)).*cos(pi.*cos(phi).*sin(theta)./(2.*sqrt(eff))).*cos(pi.*c
os(phi).*sin(theta)./(2.*sqrt(eff)))./(pi.*pi.*sin(theta).*sin(ph
i).*sin(theta).*sin(phi)).*((sin(((sqrt(i)).*k.*d./2).*sin(theta).
*cos(phi)).*sin(((sqrt(i)).*k.*d./2).*sin(theta).*sin(phi))./sin((
k.*d./2).*sin(theta).*cos(phi))./sin((k.*d./2).*sin(theta).*sin(ph
i))).^2);
P2 = integral2(Etot2,0,pi/2,0,2*pi)/eta;
Zpatch2(i) = 1./(P2.*2./((i)));

end

for i=B
Etotx2=@(theta,phi)(2.*sin(theta).*sin(phi).*sin(phi).*sin((pi.*w.
/lambda).*sin(theta).*sin(phi)).*sin((pi.*w./lambda).*sin(theta).*
sin(phi)).*cos(pi.*cos(phi).*sin(theta)./(2.*sqrt(eff))).*cos(pi.*
cos(phi).*sin(theta)./(2.*sqrt(eff)))./(pi.*pi.*sin(theta).*sin(p
hi).*sin(theta).*sin(phi)).*((sin((i.*k.*d./2).*sin(theta).*cos(ph
i)).*sin((k.*d./2).*sin(theta).*sin(phi))./sin((k.*d./2).*sin(thet
a).*cos(phi))./sin((k.*d./2).*sin(theta).*sin(phi))).^2);
Etoty2=@(theta,phi)(2.*sin(theta).*sin(phi).*sin(phi).*sin((pi.*w.
/lambda).*sin(theta).*sin(phi)).*sin((pi.*w./lambda).*sin(theta).*
sin(phi)).*cos(pi.*cos(phi).*sin(theta)./(2.*sqrt(eff))).*cos(pi.*
cos(phi).*sin(theta)./(2.*sqrt(eff)))./(pi.*pi.*sin(theta).*sin(p
hi).*sin(theta).*sin(phi)).*((sin((k.*d./2).*sin(theta).*cos(phi))
```

```
.*sin((i.*k.*d./2).*sin(theta).*sin(phi))./sin((k.*d./2).*sin(thet
a).*cos(phi))./sin((k.*d./2).*sin(theta).*sin(phi))).^2);
Px2 = integral2(Etotx2,0,pi/2,0,2*pi)/eta;
Py2 = integral2(Etoty2,0,pi/2,0,2*pi)/eta;
Zpatchx2(i) = 1./(Px2.*2./(i));
Zpatchy2(i) = 1./(Py2.*2./(i));

end

Zpatch2 = Zpatch2(find(Zpatch2>0));
ZpatchE2 = Zpatchx2(find(Zpatchx2>0));
ZpatchH2 = Zpatchy2(find(Zpatchy2>0));
patch_planar_with_single_aperture = [A;Zpatch2]'
patch_EH_with_single_aperture = [B;ZpatchE2;ZpatchH2]'

% Testing with one antenna element with two apertures

G = (pi.*w.*(1-(((k.*h)^2)./24))).*(eta.*lambda);
Zin1_with_aperture_test = 1/(2.*G);
E=@(theta,phi)(2.*sin(theta).*sin(phi).*sin(phi).*sin((pi.*w./lamb
da).*sin(theta).*sin(phi)).*sin((pi.*w./lambda).*sin(theta).*sin(p
hi)).*cos(pi.*cos(phi).*sin(theta)./(2.*sqrt(eff))).*cos(pi.*cos(p
hi).*sin(theta)./(2.*sqrt(eff)))).*(pi.*pi.*sin(theta).*sin(phi).*
sin(theta).*sin(phi));
P = integral2(E,0,pi,0,2*pi)/eta;
Zin2_with_aperture_test = 1/(P.*2);
patch_with_aperture_compare =
[Zin1_with_aperture_test;Zin2_with_aperture_test]'

% Now for arrays

for i=A
Etot1=@(theta,phi)(2.*sin(theta).*sin((pi.*w./lambda).*sin(theta).
*sin(phi)).*sin((pi.*w./lambda).*sin(theta).*sin(phi)).*cos(pi.*co
s(phi).*sin(theta)./(2.*sqrt(eff))).*cos(pi.*cos(phi).*sin(theta).
/(2.*sqrt(eff))).*sin(phi).*sin(phi))./(pi.*pi.*sin(theta).*sin(ph
i).*sin(theta).*sin(phi)).*((sin(((sqrt(i)).*k.*d./2).*sin(theta).
*cos(phi)).*sin(((sqrt(i)).*k.*d./2).*sin(theta).*sin(phi))./sin((
k.*d./2).*sin(theta).*cos(phi))./sin((k.*d./2).*sin(theta).*sin(ph
i))).^2);
P1 = integral2(Etot1,0,pi,0,2*pi)/eta;
Zpatch(i) = 1./(P1.*2./((i)));

end

for i=B
Etotx=@(theta,phi)(2.*sin(theta).*sin(phi).*sin(phi).*sin((pi.*w./
lambda).*sin(theta).*sin(phi)).*sin((pi.*w./lambda).*sin(theta).*s
in(phi)).*cos(pi.*cos(phi).*sin(theta)./(2.*sqrt(eff))).*cos(pi.*c
os(phi).*sin(theta)./(2.*sqrt(eff)))).*(pi.*pi.*sin(theta).*sin(ph
i).*sin(theta).*sin(phi)).*((sin((i.*k.*d./2).*sin(theta).*cos(phi
```

```
)).*sin((k.*d./2).*sin(theta).*sin(phi))./sin((k.*d./2).*sin(theta
).*cos(phi))./sin((k.*d./2).*sin(theta).*sin(phi))).^2);
Etoty=@(theta,phi)(2.*sin(theta).*sin(phi).*sin(phi).*sin((pi.*w./
lambda).*sin(theta).*sin(phi)).*sin((pi.*w./lambda).*sin(theta).*s
in(phi)).*cos(pi.*cos(phi).*sin(theta)./(2.*sqrt(eff))).*cos(pi.*c
os(phi).*sin(theta)./(2.*sqrt(eff)))).^2./(pi.*pi.*sin(theta).*sin(ph
i).*sin(theta).*sin(phi)).*((sin((k.*d./2).*sin(theta).*cos(phi)).
*sin((i.*k.*d./2).*sin(theta).*sin(phi))./sin((k.*d./2).*sin(theta
).*cos(phi))./sin((k.*d./2).*sin(theta).*sin(phi))).^2);
Px = integral2(Etotx,0,pi,0,2*pi)/eta;
Py = integral2(Etoty,0,pi,0,2*pi)/eta;
Zpatchx(i) = 1./(Px.*2./i);
Zpatchy(i) = 1./(Py.*2./i);

end

Zpatch = Zpatch(find(Zpatch>0));
ZpatchE = Zpatchx(find(Zpatchx>0));
ZpatchH = Zpatchy(find(Zpatchy>0));
patch_planar_with_aperture = [A;Zpatch]'
patch_EH_with_aperture = [B;ZpatchE;ZpatchH]'

% Plotting

semilogx(A,Zres)
xlabel ('No.of Antennas')
ylabel('Impedence')
title('PlanarArray')
grid on
hold on
semilogx(A,Zdip,'k')
hold on
semilogx(A,Zpatch,'g')
hold on
semilogx(A,Zpatch2,'b')
hold on
legend('ResonantWireAntennaplanar','Short
DipoleAntennaplanar','Patch
Antennaplanarwithaperture','PatchAntennaplanarwithout aperture');
plot(A,Zres,'r*')
hold on
plot(A,Zdip,'r*')
hold on
plot(A,Zpatch,'r*')
hold on
plot(A,Zpatch2,'r*')
hold on
figure
semilogx(B,Zresx,'--')
xlabel('No.of Antennas')
ylabel('Impedence')
title('patch antenna-Eplane')
```

```
grid on
hold on
semilogx(B,Zresy,':')
hold on
semilogx(B,Zdipx,'r')
hold on
semilogx(B,Zdipy,'c')
hold on
semilogx(B,ZpatchE,'b')
hold on
semilogx(B,ZpatchH, 'b')
hold on
plot(B,ZpatchE,'r*')
hold on
plot(B,ZpatchH,'r*');
```

UNIVERSITE BRETAGNE LOIRE MATHSTIC

UNIVERSITÉ DE NANTES

Titre : Etude de l'adaptation d'impédance dans le réseau d'antennes.

Mots clés : Réseau d'antennes, rayonnement total, impédance d'entrée, couplage mutuel, paramètres S actifs.

Résumé : La désadaptation d'impédance dans les réseaux d'antennes est un problème important, en particulier lorsqu'un grand nombre d'éléments rayonnants sont placés côte à côte. Cette désadaptation est généralement due au couplage mutuel entre les éléments d'antenne. Le phénomène de couplage mutuel peut cependant provenir des ondes de surface, du rayonnement de champ proche ou du rayonnement de champ lointain. Le phénomène de désadaptation se révèle néanmoins important lorsque l'ensemble du réseau est réglé pour rayonner même temps même si le couplage est faible. Dans cette thèse, nous concentrons nos travaux sur l'effet du rayonnement total en champ lointain. En mettant les antennes en réseau, l'impédance d'entrée de chaque élément du réseau d'antennes change par rapport à celle de l'élément unique lorsqu'il n'est pas en réseau. En d'autres termes, la valeur de l'impédance d'entrée des éléments rayonnants individuels change en fonction du nombre d'éléments et de la position de l'antenne.

Ce travail propose en outre un aspect important de l'évaluation des paramètres S actifs dans les réseaux d'antennes. Il a été montré que les paramètres S actifs obtenus en utilisant la matrice de distribution passive ne correspondent pas aux valeurs réelles obtenues lors d'une excitation simultanée de tous les éléments.

Enfin, cette étude a fait un pas de plus vers deux nouvelles méthodes de découplage afin de valider la théorie du rayonnement total et l'évaluation des paramètres S actifs.

Les résultats théoriques sont complétés par des simulations 3D et des mesures.

Title : Study of impedance matching in antenna array.

Keywords: Antenna array, total radiation, input impedance, mutual coupling, active S-parameters.

Abstract: Impedance mismatching in antenna arrays is an important issue especially when a huge number of antenna elements are placed side by side. This mismatch is generally blamed to exist because of mutual coupling between antenna elements. The phenomenon of mutual coupling, however, may result due to surface waves, near field radiation or far field radiation. The phenomenon of mismatch, nevertheless, reveals itself strongly when the whole array is set to radiate even in presence of less significant coupling. In this thesis, we focus our work to the effect of total radiation due to far field radiation only. It says that by arraying the antennas the input impedance of each element of the antenna array changes as compared to that of the single element which is not arrayed. In other words, the value of the input impedance of individual antenna elements changes versus antenna number and position. This work further proposes an important aspect of the evaluation of active S-parameters in antenna arrays. It has been shown that the active S-parameters obtained by using the passive scattering matrix do not correspond to the actual values obtained during a simultaneous excitation of all the elements.

Finally, this study has taken a step further towards two novel decoupling methods in order to validate the theory of total radiation and evaluation of active S-parameters.

Theoretical results are complemented with 3D simulations and measurements.